Microplastic Deformation of Polycrystalline Silver Chloride Containing a Small Volume Fraction of Hard Inclusions

by

Robert Bensen Calhoun

B.S. Materials Science and Engineering
Massachusetts Institute of Technology, 1990

Submitted to the Department of Materials Science and Engineering
in Partial Fulfillment of the Requirements for the Degree of

Doctor of Philosophy in Metallurgy

at the

Massachusetts Institute of Technology

February 1998
[June 1998]

© 1998 Massachusetts Institute of Technology
All rights reserved

Signature of Author ..
Department of Materials Science and Engineering
January 9, 1998

Certified by ..
.....
Andreas Mortensen
Professor of Mechanical Metallurgy

Accepted by .....
Linn W. Hobbs
John F. Elliott Professor of Materials
Chairman, Departmental Committee on Graduate Students

Science

AUG 1 7 1998
LIBRARIES

Microplastic Deformation of Polycrystalline Silver Chloride Containing a Small Volume Fraction of Hard Inclusions

by

Robert Bensen Calhoun

Submitted to the Department of Materials Science and Engineering
on January 9, 1998 in Partial Fulfillment of the
Requirements for the Degree of
Doctor of Philosophy in Metallurgy

ABSTRACT

Silver chloride is a ductile ionic solid which has mechanical properties typically associated with metals. A new method is presented for making composites of silver chloride doped with 500 ppm copper chloride (CuCl) and 0.01 volume percent of 1 to 5 micron glass spheres and particles. After rolling, recrystallizing and tensile testing, composite samples are exposed to UV light. This "decorates" dislocations in the top 40 microns of a sample with metallic silver so they can be seen with an optical microscope.

Dislocation decoration is used to investigate the nucleation of dislocations in polycrystals. In one set of experiments, precisely determined thermal misfit strains are generated between the AgCl and spherical inclusions by quenching. The critical sphere diameter d_p required for punching compares favorably with the predictions of Ashby and Johnson (1969). For spheres larger than the critical diameter, the data are well-fit by a stochastic model for heterogeneous nucleation which predicts that the probability of one or more loops nucleating is $1 - \exp(-cd_p^2)$.

In other experiments, dislocation decoration is used to reveal dislocations and slip bands in samples loaded to strains of 90 to 250 microstrain. The equilibrium shape of prismatic loops under stress compares favorably to a dislocation-based model which incorporates the matrix friction stress and the orientation dependence of a dislocation's line energy. Additionally, the role that grain triple junctions and inclusions play in the nucleation of slip is considered. Statistical tests show slip is independent of inclusion location for diameters less than 5 microns. Conversely, triple junctions are positively correlated with slip (p-value= 0.00004). A simple model predicts 46% of slip bands should initiate at triple junctions, vs. 56% observed.

In conclusion, slip bands do not nucleate at inclusions in grain interiors but at grain boundaries and in the largest grains first. Preliminary results obtained by straining AgCl with an NaCl epilayer support the conclusion that elastic compatibility effects between large features are more important in determining the initial yielding behavior than a small volume fraction of 1–5 micron inclusions.

Thesis Supervisor: Andreas Mortensen
Title: Professor of Mechanical Metallurgy

Contents

Acknowledgements

I am happy to acknowledge support from the following sources:

NDSEG Fellowship Program of the DOD Dr. Dan Miracle, WPAFB Dr. Warren Peele, SCEEE	3 years
NSF DMR-9002558 and extension Dr. Bruce MacDonald	2 years plus all research funds
MIT DMSE, 3.091 TA and Loeb Fellowship Prof. Tom Eager	2 semesters
Alcoa Chair and other funds of Prof. Andreas Mortensen	2 semesters

I am also fortunate to have a long list of people to thank.

First, thanks go to my thesis committee for their helpful comments on the text and useful discussions over the years. Bob Balluffi encouraged me to study nucleation of dislocations from grain boundaries and heterophase interfaces, and his recent book, *Interfaces in Crystalline Materials* was an invaluable reference. David Dunand shared his expertise on silver chloride both in person and through his Ph.D. thesis on the same subject. Heather Lechtman was a source of excellent advice on a number of topics, and her faith in my abilities never wavered.

Special thanks go to my advisor Andreas Mortensen for putting up with a strong-headed (and occasionally wrong-headed!) student and for believing that I'd be able to make dislocation decoration work even when I didn't. Through the months of failure that lie hidden behind mundane phrases like "best results were obtained with a freshly opened bottle of CuCl," Andreas supported my decision to abandon the "tried and true" method in the literature. The experimental results presented are a testament to Andreas' unwavering vision of the silver chloride decoration technique as a unique tool for the study of plasticity.

I'd be remiss if I didn't point out the reasons I ended up at MIT in the first place—my parents. Bob and Sandy Calhoun always supported me and my interest in science. It took me decades to realize that most kids don't grow up in households with 3,000 books. Thanks for the Apple //e, for the telescope and for not yelling at me *too* much when I "fixed" some piece of malfunctioning equipment so severely it had to be landfilled. I also thank all of my family for supporting me financially in graduate school and for

their understanding; I have put my thesis work ahead of them for years and years, this Christmas being only the most recent example.

I am also thankful for the good teachers I had in the City of Alexandria school system, especially Dr. John Liebermann. Dr. Liebermann is notable for his continuing efforts to involve high school students in real chemistry research; I didn't make Westinghouse Top 40, but I did develop the mysterious skill known as "chemical intuition" that has been invaluable ever since. I guess I should also thank Dr. L. for getting me used to working on weekends.

Since coming to MIT in 1986, I've been helped by countless friends. In particular, thanks go to Brent Chambers, Elizabeth Earhart, John Lum, Brian "Schmooz" Lantz and Kohta "Batman" Ueno for their help in the lab or in threshing out ideas over coffee, to Earl Johns, Andrea Benco and Mike "Crusher" Ernst for their support, to the TEPs for (mostly) staying out of trouble, and to Jennifer Lantz, Pearl Renaker and John DeRoo for turning Elizabeth Wilmer and me over to the Fun Police once every couple of weekends.

One other group deserves credit for keeping me alive through graduate school, literally. I have cystic fibrosis and the last few years have been difficult. I deeply appreciate the advice and care of Dr. Allen Lapey at the MGH and Dr. David Diamond at MIT Medical. My thanks extend to the staff of the Inpatient Unit at MIT. My yearly "vacation" there was much improved by their good cheer, words of encouragement, and excellent food. Thanks also for bending the rules a bit and skipping the 6 AM blood pressure reading!

It is Elizabeth Wilmer, however, who gets the gold star. In addition to playing the role of the supportive spouse during my last years in graduate school and putting up with my Grinch-like personality during the last six months, Elizabeth had the unenviable task of teaching me all of the probability and statistics I never learned at MIT. She was a key sounding board for the models presented in the thesis. Nevertheless, as I have an engineer's reckless disregard for the proper uses of mathematics, I claim full credit for all mistakes.

—R.B.C.
Cambridge, MA
December 30, 1997

Dedication

Last August, I started receiving inquiries from people who wanted to know if I or anyone else had information on the whereabouts of Fred Fenning. Fred was flying from Boston to Seattle in a single engine plane, and he had not appeared as scheduled. As we found out in the days that followed, Fred's plane suffered some kind of mechanical failure and crashed into a lake on the Missouri river on August 9th, 1997. His death was a crushing blow.

An alumnus of MIT and of my fraternity, TEP, Fred was the best engineer I've ever known. Fred had seemingly limitless engineering skills—from fields requiring great precision like circuit design, digital recording, telephony and laser optics, to "hands-on" activities like machining, casting, welding, plumbing, and FredVan Science and Engineering (a field of one). Fred played an instrumental role my engineering education by bridging the gap between the idealized theoretical models taught at MIT and the "real world," something he could do because he knew them both so well.

I remember many good times with Fred: teaching me how to wire houses; rebuilding TEP's heating system after it literally fell apart one January night; coming into the foundry lab on a weekend and arc welding new pipes onto to my motorcycle; sketching out a fully functional optical detector for a musical stairwell I wanted to build without ever seeing the synthesizer it would drive; recording and mixing a short record together; building a flawlessly performing custom controller for the 30 year-old Instron in the End Lab. Fred had a razor-sharp understanding of technology and rich, cynical sense of humor. I learned more about engineering from Fred than from anyone else. I'll never forget him.

And so, I dedicate this thesis

to Fred

List of Figures

Chapter 3

Chapter 4

Chapter 5

Chapter 6

Chapter 8

CHAPTER 1

Introduction and Literature Survey

1. Introduction

The three fundamental qualities of a structural material are stiffness, toughness, and strength. The stiffness of a material is given by its elastic constants, functions of the interatomic potentials which are little changed by processing. Fracture toughness in brittle materials is highly dependent on the presence of flaws and is the limiting property of such materials. The theoretical treatment of fracture toughness derives from the work of GRIFFITH 1921. Strength, the subject of this thesis, is the ability of a material to withstand stress without irreversible shape change. This irreversible change is called plastic deformation and the point at which it begins, the yield stress. The ability to undergo plastic deformation before fracture is one of the characteristic properties of metals and the reason for their high fracture toughness.

As most engineered structures are designed so that the stresses encountered in normal service do not exceed the macroscopic yield stress, the yield stress of a metal is one of its most important properties. Additionally, very small amounts of plastic deformation can occur even in metals loaded to well below the macroscopic yield stress; this microplastic deformation can lead to fatigue damage under cyclic loading. As the behavior of a metal during the earliest stages of plastic deformation affects its yield and fatigue properties, the microplastic regime is an area of both theoretical and practical interest.

In what follows we investigate the microplastic behavior of a ductile polycrystalline solid which contains a low volume fraction of hard, non-deformable particles. The goal of the work is to understand where slip initiates in these materials.

The earliest attempts to model the strength of solids considered the stress required to shear one plane of atoms over another by displacing all atoms at the same time. At this stress, plastic deformation must occur; this upper bound is called the *theoretical strength* of a crystalline solid. FRENKEL 1926 estimated the theoretical shear strength to be on the order of $G/5$, where G is the elastic shear modulus.

Real crystals plastically deform at much lower stresses, from a stress of $G/10000$ to $G/50$. TAYLOR 1934, POLANYI 1934 and OROWAN 1934 rationalized this discrepancy by postulating the existence of dislocations—atomic scale, linear defects in crystalline solids that locally deform the lattice and displace it by one atomic spacing as they propagate across a crystal.

Taylor's seminal papers introduced the dislocation, presented a solution to the stress state around an edge dislocation,[1] developed a theory of work-hardening and compared predictions with experiment.

Today, the existence of dislocations and their role in slip has been irrefutably demonstrated. Dislocation theory forms the core of physical and mechanical metallurgy, and it has been widely applied to ceramics and electronic materials as well. Numerous books have been devoted to the subject: HIRTH AND LOTHE 1982 present a broad introduction to the field, and the ten volumes of NABARRO 1979 are notable for their comprehensive indexing of the primary literature. Other classic texts include READ 1953, WEERTMAN AND WEERTMAN 1964, and NABARRO 1967.

Nevertheless, many questions remain unanswered. Even in the low-temperature deformation of metals, debate continues in areas of practical interest such as the nature of work hardening (BAY ET AL. 1992, KUHLMANN-WILSDORF 1992), the development of texture during large strain deformation, and the mechanism of grain-size strengthening (HANSEN 1985). Nor are dislocation-based models the only approach to modeling the deformation of metals; the methods of continuum plasticity (see, for example, HILL 1950, CHAKRABARTY 1987 and HOSFORD 1993) are also widely applied. Efforts to unify dislocation theory and continuum plasticity (e.g. MURA 1968, WENG 1978, WENG ET AL. 1990) have just begun.

2. Sources of Dislocations

The concept of the dislocation explains why metals yield at stresses below the theoretical strength, but immediately raises questions about the origin of the dislocations. Topological considerations require that a dislocation end at a free surface, an interface, or another dislocation; hence, if a new dislocation is to nucleate in a region of perfect crystal, it must form a closed loop. Simple estimates of the critical stress required for the nucleation of such a loop, such as that of COTTRELL 1953, predict that a shear stress on the order of $G/30$ is required, much higher than is observed empirically.[2]

2.1. Glide and Multiplication of Pre-Existing Dislocations. One way around the nucleation problem is to assume that the dislocations created during solidification (FRANK 1949) multiply under stress. FRANK AND READ 1950 proposed a possible mechanism—now known as the Frank-Read source—by which an existing pinned dislocation could generate an unlimited number of shear loops. During the decade which followed, these "grown in" dislocation segments were frequently assumed to be the primary source of dislocations in stressed crystals (e.g., MOTT 1952, FISHER ET AL. 1953).

[1] Taylor was able to use one of Volterra's solutions to a set of continuum elasticity problems Volterra called "distorsioni," which were presented in LOVE 1927. Love anglicized "distorsioni" to "dislocations," which Taylor adopted.

[2] At extremely high strain rates, such as are encountered during shock-loading, or at extremely high stresses, such as can be obtained by bending nearly flaw-free metallic and ceramic whiskers, homogeneous nucleation may occur (MEYERS AND CHAWLA 1984).

Later evidence demonstrated that mobile dislocations multiply under stress even without pinning points. This process occurs more rapidly as the stress is increased—see, for example, JOHNSTON AND GILMAN 1959 or GILMAN 1994. The multiple cross slip mechanism of KOEHLER 1952 (see also ARGON 1952 and LI 1961), is most likely responsible. JOHNSTON AND GILMAN also demonstrated that freshly nucleated dislocations glide at a lower stress than aged dislocations, most likely because the aged dislocations are pinned by solute atoms via the mechanism of COTTRELL AND BILBY 1949. Such pinning makes it more difficult to activate the grown-in network in the bulk of the crystal. The bicrystal work of HOOK AND HIRTH 1967 demonstrated that shear stresses can be higher at grain boundaries than in the bulk, further weakening models which rely on bulk sources of dislocations.

For these reasons, in more recent years models of yielding and of the Hall-Petch relationship have shifted from theories based on grown-in sources and dislocation pile-ups (HALL 1951, PETCH 1953) to grain boundary sources (LI 1963 and LI AND CHOU 1970) and elastic compatibility considerations (ASHBY 1970, THOMPSON ET AL. 1973, and MEYERS AND ASHWORTH 1982). In these later models, grain boundaries and cell walls are assumed to be the source of dislocations.

2.2. Interfacial Sources of Fresh Dislocations. Forty years' observation of dislocations suggests that there is no single mechanism for dislocation nucleation; rather, dislocations can be created at a variety of inhomogeneities such as grain boundaries, heterophase interfaces and free surfaces. These inhomogeneities are characterized by the shape of the inhomogeneity, the nature of the interface and the degree of misfit.

The shape of the nucleation site affects its ability to generate dislocations in two ways. First, the shape determines the functional dependence of the stress concentration, which follows from classical elasticity theory. Second, because the dislocation cannot terminate in perfect crystal, the shape determines the boundary conditions for the emerging dislocation.

The nature of the interface is important because it affects the stress required to nucleate lattice dislocations. In particular, there is a clear distinction between the ability of coherent (dislocation free) and incoherent (dislocated) interfaces to generate dislocations, as is described in further detail below.

The degree of misfit can be quantified using the concept of a misfit strain, ϵ^T. This term was called the "stress-free strain" by ESHELBY 1957 and "eigenstrain" by MURA 1982. The misfit strain is a stress-free transformation strain: that is, the difference between the strain in one body and the strain in another if each were to deform independently. While the state of stress at an inhomogeneity can be complicated, so long as the deformation remains elastic the stress at a point will increase linearly with the misfit

strain. This makes the misfit strain a useful measure for discussing the relative efficiency of dislocation sources.

These sources of misfit can be characterized more quantitatively.

2.3. Thermal Misfit. Nearly all engineered materials are processed at a high temperature at some stage during their manufacture. Thermal expansion is isotropic in cubic solids (NYE 1964), but for non-isometric crystals or polyphase materials with dissimilar coefficients of thermal expansion (CTE), a change in temperature results in a misfit strain.

For the case of a two-phase material each with isotropic coefficients of thermal expansion, α_i, the misfit strain is

$$\epsilon^T(T) = \int_{T_1}^{T_2} (\alpha_2 - \alpha_1)\, dT.$$

In metals, these misfit stresses can exceed those required to nucleate dislocations (WEATHERLY 1968a), causing the metallic phase to deform plastically. In ceramics, they can cause cracking (TVERGAARD AND HUTCHINSON 1988).

2.4. Lattice Parameter Misfit. A misfit strain can occur at coherent interfaces, where there is a one-to-one correspondence between the lattices of the two phases. Coherent interfaces occur in the earliest stages of second-phase precipitation (CHRISTIAN 1975) and in the epitaxial growth of thin films (MATTHEWS 1977). For this case, following HULL AND BEAN 1992, if a_i is the lattice parameter of material i, then

$$\epsilon^T = \frac{a_2 - a_1}{a_1}.$$

The resulting strain energy affects the kinetics of a phase transformation and limits the dislocation-free thickness of a mismatched epilayer. The strain energy of ellipsoidal coherent particles was determined by ESHELBY 1957, and the mathematical technique he presented widely adopted.

2.5. Elastic Inhomogeneity. When two phases having different elastic constants are subjected to an applied stress, a misfit strain is generated. The general case is complicated; see MURA 1982 for details. The simple case of a sphere under hydrostatic pressure is given in NABARRO 1940 and MOTT AND NABARRO 1940:

$$\epsilon^T(P) = -\frac{P}{3}\left(\frac{1}{K_p} - \frac{1}{K_m},\right)$$

where P is the pressure and K_p and K_m are the bulk moduli of the particle and matrix. Dislocations were observed by ASHBY ET AL. 1969 in Cu containing SiO_2 particles pressurized in this manner.

2.6. Growth of a Precipitate. Growth of a precipitate due to a phase transformation can result in a misfit strain. This can be treated as an elastic inhomogeneity under pressure, as described in Section 2.5 above.

One form of precipitation which results in the formation of dislocations directly is the condensation of vacancies formed high temperature. HIRSCH ET AL. 1958 observed these in aluminum; more recent results were reported by SATO ET AL. 1983. WEERTMAN 1957 noted that vacancies can condense heterogeneously onto an existing dislocation, turning it into a helix.

3. Nucleation at Inclusions

The formation of dislocations around isolated inclusions due to a uniform misfit strain is one of the best studied areas of dislocation nucleation. This is because the calculation of the stress state around spherical particles is relatively simple and because the dislocations tend to remain close to their point of nucleation. The latter effect allows these systems to be studied at high magnification with TEM. Consequently, the nucleation of dislocations around inclusions of diameter less than 0.5 μm has been well characterized experimentally.

3.1. Formation of the First Loop. The dislocations formed under this kind of misfit are frequently of the prismatic type (SEITZ 1950). A prismatic loop has its Burgers vector $\vec{b}$ parallel to the loop normal $\hat{n}$, whereas in a shear loop $\vec{b}$ is perpendicular to $\hat{n}$. These prismatic loops were first observed by JONES AND MITCHELL 1958 in the silver halides as a result of thermal misfit between the ductile halide matrix and hard glass particles; subsequently they have been observed in many other systems (see MATTHEWS 1977 and LI 1980).

These systems can be divided into two rough groups: coherent particles and incoherent particles. Coherent particles form in alloy systems which have similar lattice parameters but which are nevertheless insoluble at room temperature. During precipitate growth, the interface is initially dislocation-free. BROOKS 1952 suggested that these particles could lose coherency by nucleation of dislocation loops at the particle-matrix interface. WEATHERLY 1968b calculated the stress required for several particle morphologies. Classic experimental studies include work on Cu-Co (LIVINGSTON 1959, BROWN ET AL. 1968) and Cu-Fe (WOOLHOUSE AND IPOHORSKI 1971, MATSUURA ET AL. 1975). In these systems, very high stresses are required to nucleate dislocations, although coherency loss is easily achieved when a strained particle is cut by a lattice dislocation, as noted by MATTHEWS 1971, or when the system is subject to radiation damage.

Dislocation nucleation at incoherent particles requires lower stresses than at coherent particles. Unlike the case of coherent particles, the critical stress is radius-dependent. GULDEN AND NIX 1968 studied dislocations around silicon particles in quenched aluminum alloys; WEATHERLY 1968a studied quenched Cu-SiO_2 and Fe-NbC systems; ASHBY ET AL. 1969 pressurized

Cu-SiO_2; DAS AND RADCLIFFE 1969 pressurized W-ThO_2, W-HfC, and Cu-He; MAKENAS AND BIRNBAUM 1980 studied precipitation in the Nb-H system.

ASHBY AND JOHNSON 1969, in a widely adopted result, presented a simple energy balance model which accounted for the radius dependence of dislocation nucleation from particles with incoherent interfaces. A point noted by both ASHBY AND JOHNSON and BROWN AND WOOLHOUSE 1970 is that nucleation seems to occur at coherent particles at stresses close to that required for homogeneous nucleation, while at incoherent particles nucleation seems to occur whenever it becomes energetically feasible for a dislocation to be emitted. This is a much less stringent requirement; incoherent interfaces seem to act as a "perfect source" of dislocations.

3.2. Plastic Zone Predictions. After these studies had clarified the role of the interface in the nucleation of dislocations around misfitting particles, attention turned to quantifying the size of the resulting plastic zone.

LEE ET AL. 1980 calculated the radius of the plastic zone in a perfectly plastic matrix around a hard sphere, incorporating ASHBY AND JOHNSON'S nucleation criterion. KIM ET AL. 1990 extended this work and compared the predictions with experimental measurements of dislocation density in Al-SiC and Al-TiC. JOHNSON AND LEE 1983 developed a model in which tangled loops could move only by climb. DUNAND AND MORTENSEN 1991a used a dislocation-based work hardening model to predict the plastic zone radius and compared the predictions to measurements made on the AgCl-glass system.

In metal matrix composites (MMCs), significant dislocation generation occurs during cooling as a result of the large magnitude of $\Delta\alpha$, the high inclusion volume fraction V_f, and the large particle size. ARSENAULT AND FISHER 1983 proposed that these dislocations are the major contributor to the increased strength of MMCs; the *in situ* TEM study of VOGELSANG ET AL. 1986 proved that misfit dislocations were indeed responsible for the high dislocation density in MMCs. For more discussion on this issue, see ARSENAULT 1991.

3.3. Long-Range Effects. Incoherent inclusions have often been suggested as an important source of slip. In studying the stress-dislocation velocity relationship in silicon iron, STEIN AND LOW 1960 noted that slip seemed to begin with the motion of dislocations near inclusions. SUITS AND CHALMERS 1961 studied the deformation of polycrystalline silicon iron below its upper yield point and proposed a model where slip initiates on inclusions in the crystal. PRANGNELL ET AL. 1994 conducted a careful study of the yielding behavior of Al-SiC composites, finding that in many cases the yield stress of the composite was lowered by the presence of the reinforcement. They found this effect depended on the reinforcement size.

The role of hard particles in the work hardening rate of metals above their yield stress has been extensively studied; see, for example HIRSCH AND HUMPHREYS 1970, or BARLOW 1991.

4. Nucleation at Grain Boundaries

The study of interfaces in materials is an extremely broad topic; HIRTH 1972 noted that if one excluded work on single crystals, essentially all of metallurgy could be related to interfacial properties. The recent book of SUTTON AND BALLUFFI 1995 illustrates the breadth and complexity of the topic. Below, we review a few of the macroscopic compatibility requirements that can lead to stress concentrations—and therefore possibly dislocation generation—at grain boundaries, without going into detail about the exact mechanism operative on the atomic level. Some of the Hall-Petch theories which rely on grain boundary emission are also briefly noted.

4.1. Compatibility Stresses. While the thermal expansion properties of cubic solids are isotropic, their elastic properties are not. When grains of different orientation are forced to deform together, a misfit strain is generated.

Work on compatibility stresses in bicrystals (largely Fe-3% Si) by LIVINGSTON AND CHALMERS 1957, HAUSER AND CHALMERS 1961, HOOK AND HIRTH 1967, CHEN AND MARGOLIN 1989 and SITTNER AND PAIDAR 1989, among others, has shown that compatibility stresses can introduce secondary glide in the grain boundary region. Margolin and co-workers (MARGOLIN AND STANESCU 1975, HASHIMOTO AND MARGOLIN 1983a, HASHIMOTO AND MARGOLIN 1983b, WANG AND MARGOLIN 1984, MARGOLIN ET AL. 1984, CHEN AND MARGOLIN 1989, HU AND MARGOLIN 1990 and SAHIN AND MARGOLIN 1991) have studied compatibility effects in bicrystals, multicrystals and polycrystals by comparing the appearance of slip bands with the stresses in each grain as predicted by finite element modeling (FEM). They find the resolved shear stress is inhomogeneously distributed and a good predictor of yield. A similar study was made by YAO AND WAGONER 1993. CARRINGTON AND MCLEAN 1965 and MARGOLIN AND STANESCU 1975 found that slip bands started at grain boundaries. A theory of work hardening based on compatibility stresses was proposed by THOMPSON ET AL. 1973, based on the concept of geometrically necessary dislocations of ASHBY 1970 and the grain boundary dislocation source proposals of LI 1963 and LI AND CHOU 1970. A similar model, applied to the Hall-Petch relationship, has been developed by MEYERS AND ASHWORTH 1982.

4.2. Stress Concentrations at Triple Junctions. The stress at a triple junction (the intersection of three grains) can be higher than in a grain interior. ABE 1972 used FEM to analyze the stress at square grains, showing stress concentrations at the boundary range from about 0.2 to five times the far-field stress. MALIS AND TANGRI 1978 presented quantitative results on the sources of slip in high purity pre-macroyield copper using transmission

electron microscopy (TEM). They found that in the earliest stages of plastic deformation, the dominant mode is the generation of dislocations at grain boundaries. Citing ABE'S work, they noted that triple junctions are a potential source of high elastic incompatibility stresses, possibly explaining the preponderance of dislocation activity at triple junctions that they observed at lower strains.

Microcracking in ceramics shows grain-size dependence. Several researchers determined the stress at triple junctions due to elastic or thermal anisotropy and then applied techniques of fracture mechanics to the problem. EVANS 1978 analyzed grain boundary stresses in isotropic grains due to thermal expansion anisotropy and found the stress exhibited a singularity at triple junctions. FEM analysis by TVERGAARD AND HUTCHINSON 1988 of cubic grains in a honeycomb arrangement showed that the stress can be either higher (rising to a singularity) or lower (decaying to zero) at grain triple points than in the bulk. More recent studies by GHAHREMANI ET AL. 1990, PICU AND GUPTA 1997, and PICU 1997 suggest that the stress state at a triple junction can take the form of a supersingularity, i.e., the stress increases faster than the $1/\sqrt{a}$ (where a is a crack length) relationship found at crack tips.

That the emission of dislocations from compatibility-generated stress concentrations can be compared to the emission of dislocations from crack tips has been suggested by CHEREPANOV 1997 and, more tentatively, by SUTTON AND BALLUFFI 1995. Crack-tip emission is a much more widely studied problem; see RICE AND THOMSON 1974 and the review in LI 1980. Given that the stress concentration at triple junctions can exhibit a supersingularity, it seems likely that these sites can efficiently nucleate dislocations in ductile materials. In these cases, dislocation emission seems more likely than crack nucleation, a possibility suggested by WU 1997.

5. Nucleation at Other Sites

5.1. Grown-In Dislocations. As mentioned above, the grown-in network of dislocations can act as a source of lattice dislocations via the Frank-Read mechanism. Another possible mechanism is that of GRILHÉ 1963, in which existing prismatic loops and helices become Frank-Read sources under the influence of an applied stress. Prismatic loops can be formed by quenching, irradiation (AVERBACK AND GHALY 1996), or thermal mismatch and are a potentially significant source of dislocations. We consider this possibility in detail in Chapter 5.

5.2. Free Surfaces and Surface Damage as Dislocation Sources. Surface damage is a well-documented source of dislocations. (See, for example, JOHNSTON AND GILMAN 1959 or STEIN AND LOW 1960.) Small steps in free surfaces have also been proposed as a source of dislocations; recent work in this area is by JUNQUA AND GRILHÉ 1997.

5.3. Elastically Inhomogeneous Thin Films. While this area of research is active because of its relevance to semiconductor fabrication, it is beyond the scope of the present work. The reader is referred to review articles by MATTHEWS 1977, HULL AND BEAN 1992 and JAIN ET AL. 1997.

6. Continuum Plasticity Models for Flow Around Spheres

In the above sections we discussed models which used dislocation theory to model plastic deformation around spheres. While such models are commonly applied to submicron particles, they represent only a fraction of the literature devoted to the study of deformation around rigid spheres. Many other models are based on continuum elasticity and plasticity theories. In linear elasticity theory, solving for the stress is equivalent to solving for the strain, since the two are linearly related. This is not true in plasticity, where assumptions must be made about the constitutive relations and loading path. Hence, many techniques yield bounds on behavior instead of "exact" solutions.

A disadvantage of these continuum plasticity models is that they rarely predict the (observed) dependence of mechanical properties on inclusion size. Advantages of these models are that they can predict the modulus of a composite and, often, the overall stress-strain response.

As the literature in this area is extensive, this review is not exhaustive.

6.1. Eshelby Methods. The Eshelby equivalent inclusion method (see ESHELBY 1957, ESHELBY 1959, and ESHELBY 1961) is the basis for many analytical theories. MORI AND TANAKA 1973 extended the Eshelby theory to determine the mean stress in a body containing multiple inclusions. Many problems in the mechanics of solids can be solved with these methods; MURA 1982 reviews this work. WITHERS ET AL. 1989 demonstrated empirically that the technique is appropriate for modeling stresses in an elastic matrix, even when the inclusion is not an ellipsoid. MASSARDIER ET AL. 1995 used a combination dislocation-Eshelby model to explain results on Al-Al_2O_3. ISUPOV 1996 used an averaging method to evaluate plastic strains in a hardening matrix.

The monograph of CLYNE AND WITHERS 1993 when used in conjunction with that of MURA 1982 provides a relatively straightforward explanation of how to apply the equivalent inclusion method to ductile matrix composites with a finite volume fraction of inclusions. Since localized plasticity is not incorporated, these models provide an upper bound on the stress state in the composite.

6.2. Finite Element Models. FEM has been used to study the development of plasticity around hard spheres and particles. A strength of the finite element technique is the ability to incorporate multiple effects, such as thermal residual stresses or spatially variable matrix properties, into a single model. This can result in a much better fit to empirical results. A disadvantage of the technique is the loss of generality associated with the

need to specify boundary conditions and constitutive equations numerically. Notable FEM work includes that of CHRISTMAN ET AL. 1989, SHI ET AL. 1992 and SHEN ET AL. 1995.

Recently, researchers have tried to incorporate the effect of polycrystalline plasticity on the deformation of composites (MCHUGH ET AL. 1993) and polycrystals (e.g., DAO AND ASARO 1996a, DAO AND ASARO 1996b.) These models can predict some of the slip inhomogeneity which is observed experimentally.

6.3. Other Continuum Plasticity Methods. One common technique is to bound the behavior of a problem by finding one solution which satisfies strain compatibility requirements. Velocity field solutions based on the work of GURSON 1977 include ZHU AND ZBIB 1993b, ZHU AND ZBIB 1993a and VAN HOUTTE 1995. These provide a lower bound estimate on the stresses in the matrix.

7. Summary of Existing Literature

Theoretical and empirical results suggest that homogeneous dislocation nucleation is not a significant mechanism under normal circumstances. The Frank-Read source provided an early possible mechanism for multiplication of existing dislocations; later, interfaces were considered as a possible source of lattice dislocations. Many yield strength and work hardening theories have been developed which incorporate a dislocation source into the model. Early theories tended to assume nucleation from sources in the grain interiors, while later theories tend to emphasize sources in grain boundaries or cell walls.

Empirical studies using TEM have confirmed the ability of spherical inclusions to generate dislocations and demonstrated the difference between inclusions with coherent and incoherent interfaces. Agreement with simple analytical models is good. TEM observations around hard particles in deformed materials have revealed a variety of dislocation reactions that result in accentuated cross-slip and matrix rotation in the area near the inclusion.

Continuum mechanics models predict high stress concentrations at grain triple junctions, although the problem is less well-defined than the the case of misfitting spheres. Limited evidence suggests that these are important sources of slip during the earliest stages of yielding.

Continuum plasticity models of ductile matrix composites generally do not address the issues of dislocation nucleation and have only just begun to incorporate grain effects. In these models, the highest strain rates and highest stresses are predicted to lie near the spherical inclusion. These models can predict the bulk mechanical behavior of high volume fraction composites with reasonable accuracy.

CHAPTER 2

Goals of the Thesis

1. Introduction

In the previous chapter, prior work on dislocation nucleation and plastic flow around hard spherical particles was reviewed. While many aspects of this problem have been studied in great detail, there is a paucity of data in other areas. In particular:

- There are few experimental data on the nucleation of dislocations from spherical particles with a diameter of more than 0.5 μm.
- There are few empirical data on dislocation arrangements around large (> 0.5 μm) particles from methods other than TEM. Since the thinning of TEM samples can, as described below, introduce artifacts when the inclusion size is larger than the TEM sample thickness, it is important to corroborate TEM observations with other techniques.
- There are few experimental data on how and, specifically, where plastic flow begins in real inclusion-containing solids. Continuum plasticity models predict that the highest levels of plastic deformation occur near hard inclusions and, presumably, that plastic deformation should initiate at these locations. At the same time, high stresses are predicted at grain boundaries and triple junctions, and plastic deformation has often been observed to begin at these locations in unreinforced materials.
- As the volume fraction of inclusions V_f increases, the mechanical behavior of a composite should be increasingly different from that of the unreinforced matrix material. There is little experimental data on where this transition occurs.
- Micromechanical models are very popular for predicting the behavior of materials, yet virtually all quantitative experimental studies report only bulk properties such as stress-strain curves. There is a real need for quantitative experimental measurements made on a micromechanical level.

In order to address these issues, we have focused our attention on the earliest stages of plastic deformation of a polycrystalline material containing non–deformable inclusions. We use an optical microscopy–based decoration technique. This method allows dislocations to be observed over a large sample area to a depth of 40 μm.

2. Selection of the Model Material

The model material used in this study is silver chloride containing 0.5 μm to 5 μm glass spheres and particles. Silver chloride is a ductile, polycrystalline solid with an elastic modulus about 40% that of aluminum. High purity forms of the two materials have comparable yield strains and normalized rates of work hardening. Unlike metals, silver chloride is transparent to visible light, allowing the interior of relatively thick samples to be investigated with an optical microscope. Exposure to UV light forms metallic silver which precipitates heterogeneously on defects on the surface and in the bulk of the material. The former effect is responsible for the photographic process; the latter can be used to "decorate" grain boundaries, dislocations, and precipitates in the bulk of the solid, rendering them visible with a high resolution transmission optical microscope.

3. Advantages and Disadvantages of the Technique

The dislocation decoration technique was developed by J. W. Mitchell and co-workers at the University of Bristol in the 1950's (See MITCHELL 1980 for a review of this work.) Mitchell's group made some of the earliest direct observations of dislocations in solids. With the invention and refinement of the TEM, decoration and other indirect methods for observing dislocations (such as etch pitting) became less widely used.

TEM has many advantages: the resolution and contrast are excellent, dislocations can be imaged dynamically, it provides crystallographic information, and it works on nearly all materials which can be thinned to the required thickness of about 1 μm or less. However, when studying plastic flow around large particles, the dislocation decoration technique has important advantages over TEM.

First, the decoration technique allows the top 40 μm of a sample to be imaged without removing the imaged section from the test coupon. This allows dislocations around particles up to about 10 μm in diameter to be observed in an environment which is similar to that of a bulk material. Preparation of a TEM disk requires chemical or mechanical thinning which can change the state of stress in the sample and allow dislocations to escape. This is particularly problematic around the large particles in particulate reinforced MMCs, which are typically larger in diameter than the foil is thick. ARSENAULT ET AL. 1991 reported that the dislocation density measured in a 0.9 μm thick region with a 1 MV TEM was about three times greater than in a 0.3 μm thick region of the sample sample imaged at 100 kV; it is likely that still thicker samples would have an even higher dislocation density.

The work of PRANGNELL ET AL. 1994, who decorated dislocations in aluminum alloys with θ' precipitates before TEM disk thinning, avoided this problem. A limitation of their technique is that a heat treatment is needed for the decoration process to work, and some dislocation rearrangement may occur during the heat treating process.

The second advantage of the decoration technique is that, as with etch-pit techniques, large areas of a sample can be investigated. This is useful in the study of the plastic deformation of well-annealed polycrystals, where slip can propagate across a grain that is far larger than the electron-transparent area of a TEM sample.

The advantages of decoration over etch-pitting are better resolution and the ability to image the interior of the sample. The latter is an important advantage, as it is difficult to interpret the arrangement of dislocations in the interior from their surface intercepts. Furthermore, these dislocations are necessarily influenced by the presence of the free surface.

Finally, the stress state in a decorated sample can be well characterized. The decoration process requires no thermal treatment and "freezes" dislocations in their stressed configuration; subsequent handling damage has no influence on the dislocation structures observed.

There are a few disadvantages to the technique in addition to its specificity to the silver halides. First, the resolution and contrast limitations of optical light microscopy limit the utility of the technique to regions of low dislocation density. Second, the classical method for preparing samples is unreliable and potentially dangerous. We address the sample preparation issues in the thesis.

4. Outline of the Thesis

The remaining chapters of the thesis can be summarized as follows:

In CHAPTER 3, we discuss the methods used for producing the AgCl composites used in the research. The method is significantly different from the method developed by Mitchell and allows substantially pore-free decorable material to be produced in a highly reliable and reproducible manner. We report stress-strain curves for pure silver chloride and the doped, inclusion-containing material. Chapter 3 also discusses some experiments and calculations which shed light on the chemical physics of the decoration process.

In CHAPTER 4, we consider the formation of thermal misfit dislocations. Results from the nucleation of dislocations around 1 to 5 μm spheres are compared with the theory of ASHBY AND JOHNSON 1969 and a new stochastic model is presented. Thermal misfit dislocations are shown to make up nearly all of the lattice dislocations visible after annealing.

In CHAPTER 5, we consider the nucleation of slip from prismatic dislocation loops by deriving the shape of a loop under an applied tensile strain. We show that the loop should be able to expand into a slip line at a stress of around Gb/r, where b is the magnitude of the Burgers vector and r the loop radius. Predicted loop shape is compared with experimental measurements on the shape of the outermost thermal misfit loops.

In CHAPTER 6, we consider the relative importance of inclusions and grain boundaries as dislocation sources in polycrystals. We find that the number of inclusions found in slipped regions is consistent with what one

would expect from random chance alone. We present data which suggest that grain triple junctions constitute an important source of slip at the earliest stages of plastic deformation and conclude that, at least in these samples, the inclusions do not play an important role.

In CHAPTER 7, we summarize the results of the present work.

In CHAPTER 8, we suggest some areas of future research.

APPENDIX A contains some *Mathematica* code for computing the elastic moduli of AgCl and critical diameters for thermal dislocation punching.

CHAPTER 3

Fabrication of Composites of Silver Chloride and Glass Suitable for Decorating Dislocations

1. Introduction

In order to study the sources of slip in polycrystals which contain hard inclusions, we turned to the silver halide dislocation decoration technique originally developed by J. W. Mitchell and co-workers. This technique induces the precipitation of metallic silver on dislocations in the top 40 μm of a flat sample, rendering these dislocations visible to an optical microscope.

In this chapter, we briefly review the history of the silver halide decoration technique and describe a new method for making samples. The classical technique is based on casting thin sheets of material, while the new method uses conventional metallurgical methods to reduce the thickness of an initially larger casting. This produces a material with uniform doping levels, well-distributed reinforcements, few solidification voids and a low density of lattice dislocations. In contrast to our experience with the classical technique, dislocations in samples prepared with the new technique can be decorated reliably. The new technique also avoids the use of chlorine gas, improving safety.

2. The Classical Technique

Driven by a desire to understand the scientific basis of the photographic process, J.W. Mitchell and co-workers engaged in a thorough study of the light sensitivity of silver halides. Because the small silver halide grains in film emulsion were difficult to study, Mitchell and co-workers worked with the bulk material. This work was presented in HEDGES AND MITCHELL 1953a, CLARK AND MITCHELL 1956 and MITCHELL 1957. HEDGES AND MITCHELL 1953b developed a process for casting thin sheets of silver bromide, exposing them to light, and observing the resulting latent image (precipitated silver) under an optical microscope. HEDGES AND MITCHELL 1953a found that the internal latent image formed preferentially on subgrain boundaries and individual dislocations in the solid, decorating these defects and rendering them visible with an optical microscope. These observations comprised some of the earliest direct evidence of crystal dislocations; MITCHELL 1980 reviews this work.

2.1. Purification. HEDGES AND MITCHELL 1953a developed the techniques generally used by later researchers. CLARK AND MITCHELL 1956

purified freshly prepared silver halides by melting the powders in Pyrex crucibles under an atmosphere of the hydrogen halide plus the halogen—HCl and Cl_2 for AgCl and HBr and Br_2 for AgBr. The oxidizing atmosphere was removed with a cold finger and the molten salt filtered by passing it through a series of fine glass capillaries. Next, excess halogen was removed by purging the molten salt with inert gas. When a change in the wetting behavior of the liquid salt was observed, the purification process was stopped. It is difficult to achieve the desired chlorine activity with this technique; see DUNAND 1991 and DUNAND AND MORTENSEN 1991b for details.

2.2. Doping. Proper doping, or "sensitization," of the silver halide proved to be a critical issue both for dislocation decoration and in photographic emulsions. After realizing that light sensitivity reported in their earlier work was highly dependent on the presence of certain impurities, Mitchell's group explored a variety of doping strategies to maximize sensitivity. These included adding oxygen by MITCHELL 1957, AgI by BARTLETT AND MITCHELL 1960, $AuCl_3$ by BARTLETT AND MITCHELL 1958, and CuCl and $CuCl_2$ by PARASNIS AND MITCHELL 1959 and PARASNIS ET AL. 1963. The goal of adding the dopant is to make the interior of the silver halide more conducive to silver precipitation while adding as few artifacts, such as insoluble precipitates, as possible. DUNAND AND MORTENSEN 1991b found silver chloride doped with approximately 500 ppm CuCl to be the most suitable system for decorating dislocations. The present study corroborates this finding.

2.3. Solidification Processing. Hedges and Mitchell's technique for making thin sheets consists of melting a small amount of silver halide and casting it between two polished, heated Pyrex disks separated by 250 to 380 μm spacers. Several important observations were made using composites of glass spheres and AgBr; these samples were made by placing a drop of a suspension of 0.5–5 μm glass spheres in distilled water onto the upper glass plate, as described by JONES AND MITCHELL 1958. DUNAND 1991 used a similar technique to disperse spheres, particles, and chopped fibers. The casting technique yields samples with an excellent surface finish and, as reported by JONES AND MITCHELL 1958, a strong texture in which the planar surfaces are very close to (001). This orientation of the grains simplifies photomicrography and provides useful crystallographic information.

2.4. Thermal Treatment. Because of the CTE difference between the silver halide and glass, the thin sheets of silver halide obtained are highly stressed and must be annealed before use. JONES AND MITCHELL 1958 annealed for 8 hours at 643 K in an atmosphere of the appropriate halogen. DUNAND AND MORTENSEN 1991b found that 2 hours at 673 K under a nitrogen atmosphere also worked well.

2.5. Mechanical Testing. Mitchell's group performed a few tests in which the silver halide samples were mechanically deformed. This was done by pressing a stylus into the surface, indenting it in a manner similar to a hardness test. These experiments demonstrated that the decoration process works on dislocations created by mechanical deformation after the annealed samples are cooled. Thus AgCl can be used, as it is in the present work, to investigate the effects of an external stress on dislocations.

2.6. Limitations. The classical technique described above yields samples with excellent surface finish but which are in other ways unsuitable for mechanical testing. Macrosegregation during casting produces an inhomogeneous distribution of the required sensitizing agent, and a large number of voids appear during solidification. (These are due to solidification shrinkage and, possibly, to chlorine gas evolution.) Additionally, the considerable run-to-run variability in the casting process makes it difficult to compare the mechanical behavior of different samples.

The process described below produces more homogeneous samples which are suitable for mechanical testing.

3. The New Experimental Technique

3.1. General Considerations. In the presence of visible or UV light, AgCl slowly decomposes into metallic silver and chlorine gas. The resulting finely dispersed metallic silver alters the color of AgCl from nearly colorless to dark purple with increasing exposure. To minimize this reaction, all material processing and handling was performed under red safelights.

Silver chloride reacts slowly with commonly used metals such as aluminum, iron, and stainless steel. When the use of metal tools was unavoidable, the tools were cleaned with a weak ammonia solution and the silver chloride treated as described below. Razor blades, frequently used for shaping and trimming, were discarded after use.

To avoid particulate contamination from airborne dust, textile and paper fibers, all but the melting steps were performed in a Class 1000 cleanroom, following standard cleanroom dressing protocols and using cleanroom grade wipers and solvents.

We used plastic tweezers for material handing, cleaned glass microscope slides as cutting surfaces and mounting substrates, polystyrene petri dishes wrapped in aluminum foil for storage, and a sharpened quartz "knife" as a non-reactive sharp edge. Glass-reinforced plastic tweezers were found to shed glass fibers and were not used.

3.2. Raw Material Preparation.

3.2.1. *Silver Chloride:* Optical grade AgCl was obtained from the Harshaw Crystal Optics division of Bicron Corporation (Solon, OH). The thickest rolled stock available ($\sim$ 6 mm) was found to be most suitable for melting. This material needed to be cut and cleaned before use. We used the following procedure:

1. Cut AgCl pieces to suitable size with clean metal shears.
2. Mix regular laundry bleach (0.7 M Na_2ClO_4) with an equal volume of 0.7 M HCl in a well-ventilated fume hood. This creates a supersaturated solution of Cl_2 in water; the solution will turn yellow and slowly evolve bubbles of chlorine gas.
3. Place AgCl cuttings in the solution for 15 minutes. This will oxidize any metals present on the surface.
4. Rinse AgCl in DI water. Neutralize chlorine water with NaOH solution and discard.
5. Place silver chloride in 18 M HCl for 15 minutes to remove salts.
6. Rinse AgCl pieces in four successive rinses of boiling DI water, with a final rinse in hot HPLC grade DI water.
7. Allow AgCl to dry in a clean, dark place.

Material cleaned in this way had a rough, deeply etched finish because some of the AgCl is dissolved in the acid bath.

3.2.2. *Dopant:* High purity (99.999%) cuprous chloride (CuCl) was obtained from Strem Chemical Corporation (Newburyport, MA). CuCl reacts with air and moisture; best results were obtained with a freshly opened bottle of CuCl.

3.2.3. *Inclusions:* Corning 7070 glass[1] microspheres and particles of nominal diameter 1-5 μm were obtained from Mo-Sci Corporation (Rolla, MO). The spheres are manufactured by passing glass frit through a high temperature flame. As a result, some spheres had asperities, and a few were welded together into clusters.

3.3. Solidification Processing.

3.3.1. *Master Alloy:* Quartz tubing of 13 mm O.D. obtained from Quartz Plus (Concord, MA) was cleaned with DI water, cleanroom grade acetone, and HPLC grade DI water. The tubes were shaped into the hourglass crucible shown in Figure 1 using a methane/oxygen torch. Using a 100 μl micropipette, approximately 20 μl of glass microspheres and 70 mg CuCl per 100 g of AgCl were deposited in the lower part of the hourglass. Quartz wool (also obtained from Quartz Plus) was rolled into a yarn, folded in half, and inserted in the tube with the loose fibers facing up to form a filter. After charging with AgCl, the system was evacuated. The AgCl was melted with the torch; bubbles of chlorine form due to the decomposition reaction:

$$AgCl_{(l)} \rightarrow Ag_{(s)} + \frac{1}{2}Cl_{2(g)}$$

After the AgCl had become fully molten, nitrogen gas of around 0.1 MPa pressure was applied. This forced the molten salt through the quartz wool filter. The AgCl did not de-wet, so some was lost at this step. As the solubility of silver in molten AgCl is very low (SCHUSTER ET AL. 1979) and

[1]Corning 7070, a lithia-potash-borosilicate glass, is no longer available. (CORNING TECHNICAL STAFF 1997)

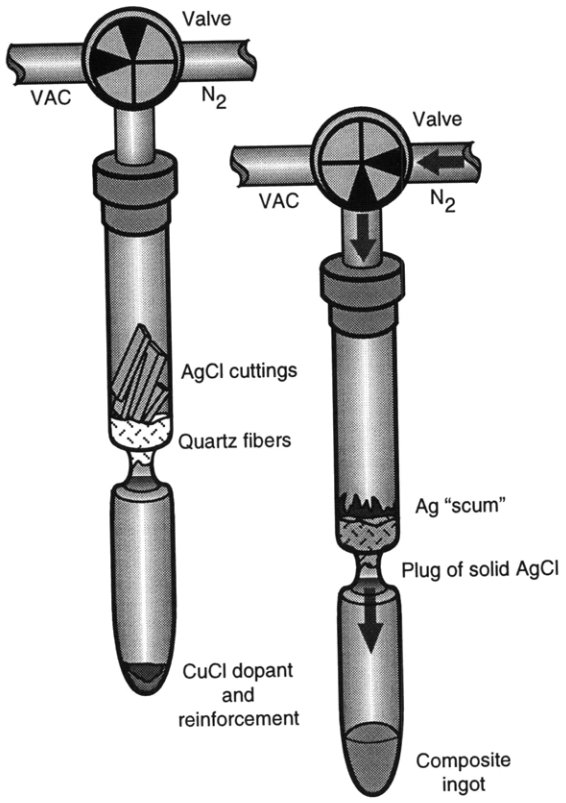

FIGURE 1. Method used for making doped silver chloride composites.

metallic silver appeared to stick to quartz, the filtration process was very effective at stripping metallic silver from the melt. After filtration, the melt was solidified using an external water quench. A vacuum was again applied to the system and the neck of the hourglass sealed, encapsulating matrix, dopant, and reinforcement in a quartz capsule.

Mixing of the three components was accomplished by remelting the contents of the capsule in a tube furnace at 873 K and then repeating a cycle of vigorous mechanical shaking, quenching in a water ultrasound bath and reheating until the glass microspheres appeared to be fully mixed. The purpose of the ultrasound bath was to aid in the deagglomeration and wetting of the glass microspheres and to decrease macrosegregation and shrinkage porosity. (The role of ultrasound on the solidification of metals was studied by ABRAMOV 1993.) Because of the poor thermal conductivity of the quartz, three to four seconds of ultrasonic mixing can be accomplished before solidification begins.

After the final solidification step, the master alloy was homogenized by soaking at 693 K (0.95 T_M) for 24 hours to reduce macrosegregation. Next, the master alloy was broken out of the quartz capsule, cooled to 77 K and fractured into smaller pieces.

Samples of the master alloy were extracted from three different locations on the ingot. These samples were sent to Luvak Corporation (Boylston, MA) where they were dissolved in ammonium hydroxide and analyzed for Cu/Ag ratio. The results were as follows:

TABLE 1. Results from chemical analysis of master alloy ingot.

Sample Location	Cu:Ag ratio, ppm atomic
Near top of ingot	1465 ppm
1/3 from top of ingot	1465 ppm
2/3 from top of ingot	1398 ppm

3.3.2. *Purified AgCl:* Undoped AgCl composites were made using a substantially identical process. These were used to dilute the master alloy to the target doping concentration. The above process was followed, except that no CuCl dopant was added and no solutionization treatment performed. AgCl treated in this manner was colorless, indicating that much of the colloidal silver had been removed.

3.3.3. *Standard Alloys:* An ingot of target composition 500 ppm CuCl was prepared by encapsulating under vacuum 16.8 g of master alloy and 38.2 g of purified AgCl. The mixing process used for the master alloy was repeated; final solidification was performed with the capsule upright, leaving a thick, dense shell with a porous core. We were unable to prevent these casting defects, most likely because of the large (about 7.9%[2]) change of volume on solidification. The ingot was solutionized for 120 hours at 673 K; from the reported diffusivity data on Cu^+ in AgCl of BATRA AND SLIFKIN 1972, $\sqrt{Dt} \approx 2$ cm, roughly twice the width of the ingot. After cooling, the ingot was broken out of the quartz capsule, cooled to 77 K and broken into pieces. The core of the ingot, which contained most of the shrinkage voids, was not used to make samples.

Material at this stage was stored in the dark at room temperature and used over a period of more than six months without noticeable loss of sensitivity. The remaining steps in the process were found to be time-sensitive, so only the amount needed for a particular experiment was processed at any one time.

3.4. Deformation Processing. Samples were formed into an appropriate shape for mechanical testing and microscopy by rolling. In addition, the rolling process broke down the coarse-grained structure of the original ingot and imparted a significant amount of cold work to the sample, allowing it to be readily recrystallized. We found that a hand-powered rolling mill was most suitable for this task. Silver chloride composites were rolled between polished 254 μm (10 mil) tungsten plates. Samples were rolled in one

[2]Based on $\rho_s = 5.257$ and $\rho_l = 4.871$ g/cm^3, determined by extrapolation of the X-ray data of FOUCHAUX AND SIMMONS 1964 and tabulated values of LYNCH 1989 to the melting point of 728 K.

direction to around half the total reduction in area, then cross-rolled to the final thickness of 120–200 μm. (This is a true strain of about 3.) Thicker samples could be decorated, but image quality was reduced due to light scattering. Thinner samples, on the other hand, were too easily damaged in handling.

For each experiment, two samples were cut to the desired shape of 3 mm $\times$ 37 mm using a clean razor blade. One sample was used in mechanical testing; the other was a reference sample which was identically prepared but left unstrained. To reduce sample bowing and improve surface finish, samples were cold-pressed against glass microscope slides. The top surface of the sample was placed face down against the glass and covered by a protective layer of Saran Wrap™ and a large piece of 1.6 mm thick silicon rubber sheet. This sandwich was loaded to 7×10^5 N between polished aluminum blocks.

After pressing, the samples were dipped first in 18 M HCl and then in three successive beakers of DI water. This treatment desensitizes the surface layer, increasing the quality of decoration in the bulk material.

3.5. Thermal Treatment. Deformation processing was followed by an annealing step. This re-solutionizes the CuCl dopant and forces nucleation of new, nearly dislocation-free grains.

Samples were placed top surface up on either Macor™ flats or an NaCl single crystal on top of a quartz slide inside an aluminum foil-wrapped quartz tube. These substrates were chosen to reduce the possibility of plastic deformation due to thermal mismatch between sample and substrate; while quartz substrates resulted in sample deformation, no damage was noted with either of the above substrates. The aluminum foil suppresses convection during cooling and lowers the cooling rate.

Most samples were annealed in air at a temperature of $T_{\text{rx}} = 623$ K for 20–45 minutes. After annealing, samples were cooled in their foil-wrapped tube in still room air. A cooling curve from a thermocouple embedded in an empty NaCl substrate that was equilibrated at $T_{\text{rx}} = 553$ K was fit to the Newtonian cooling curve

$$T = T_{\text{rx}} e^{-kt} + T_{\text{room}}$$

yielding $k = 0.094$ sec^{-1} with $R^2 = 0.995$. The goodness of the fit indicates that the cooling rate was limited by heat transfer from tube to room air. This implies that the temperature of the AgCl samples during cooling was reasonably uniform.

In some experiments, samples were decorated at this stage. Following the technique of DUNAND 1991, the decoration process consists of exposing the sample to light from an unfiltered Xenon bulb strobe lamp at 60 Hz for 2 to 2 1/2 hours. Good results were obtained when decoration immediately followed cooling and also when the sample was allowed to sit overnight. If several days passed between annealing and decoration, the quality of decoration diminished. Some samples were annealed at temperatures much

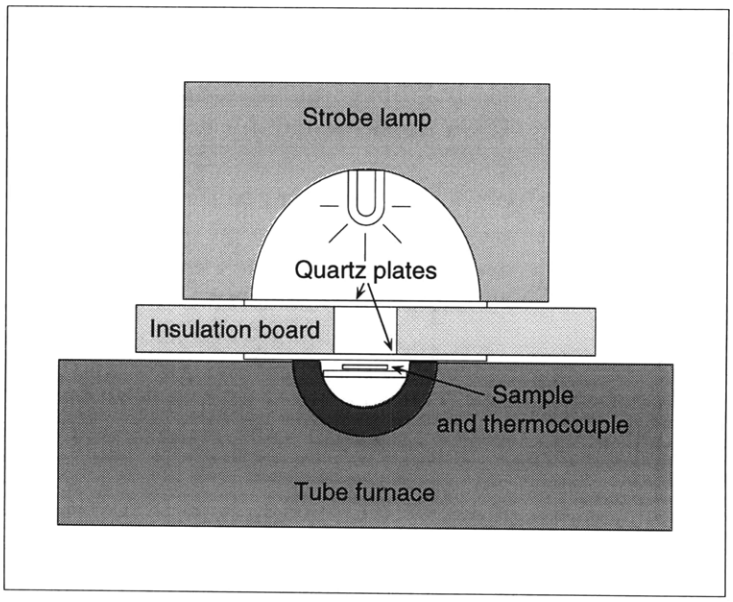

FIGURE 2. Apparatus for decorating samples at temperatures above ambient.

lower than 623 K. In a series of experiments, samples were recrystallized at temperatures from room temperature to 403 K. Recrystallization was not complete after several months at room temperature T_{room} although some recrystallized grains were found. At 348 K and 403 K, samples were partially and fully recrystallized, respectively, although the density of lattice dislocations was much higher in both samples than in samples annealed at 623 K. Best low-temperature recrystallization results were obtained by resolutionizing the material before rolling.

In another experiment, samples were annealed in the usual manner, but were cooled to 398 K and decorated at that temperature using the apparatus illustrated in Figure 2. Decorated dislocations were obtained at this temperature.

3.6. Sample Mechanical Testing. In order to apply small (less than 250 $\mu\epsilon$) tensile strains accurately, a beam-bending technique was used. The ends of freshly annealed samples were glued with a catalyzed cyanoacrylate adhesive onto the top surface of a stiff beam, made by bonding together five layers of fiberglass-epoxy printed circuit and one 6.35 mm layer of 2024 Al. The cyanoacrylate glue wets AgCl; 3M Scotchguard™ (St. Paul, MN) was used as a stop layer. The glue was allowed to cure overnight before testing. Samples were strained in tension by loading the beam in three-point bending as shown in Figure 3 and measuring the total applied strain using two strain gauges, ϵ_1 and ϵ_2, affixed to the beam on either side of the sample. Figure 4 shows a typical plot of ϵ_1 and ϵ_2 vs. t. The samples were decorated as described above while under load. (During decoration, the strobe lamp rests

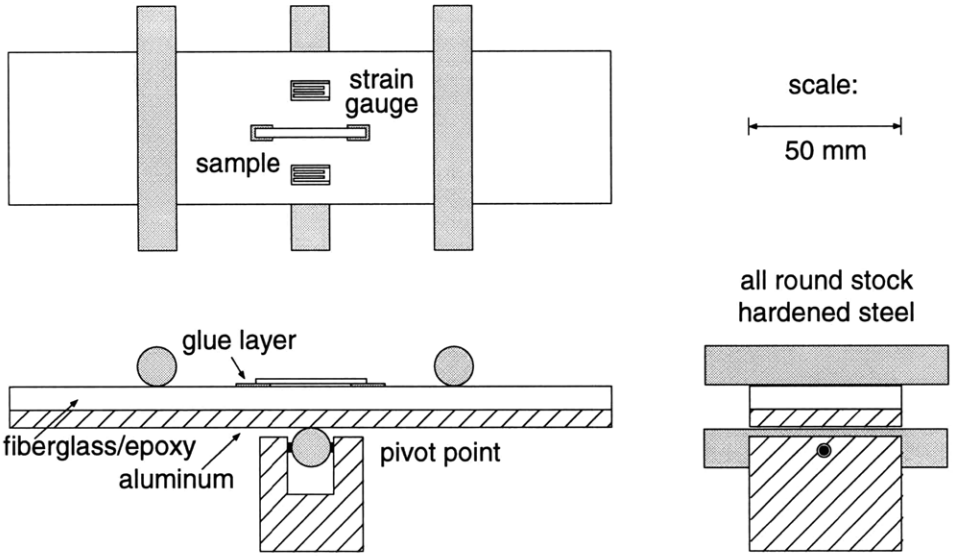

FIGURE 3. Tensile testing rig used with decoration samples. Sample dimensions approximately 37 mm×3 mm×0.15 mm. Glued regions on each end approximately 3 mm × 3 mm.

on the steel round stock shown in Figure 3.) The load dropped off slowly over the course of the test due to machine creep; we assume dislocations were pinned early in the decoration process.[3]

The reference sample was decorated at the same time to determine the initial state of the sample. The measurements on unstrained samples in Chapter 4 were made on these samples.

In one experiment, a "null-strain" sample was glued to the beam and decorated without loading. It was indistinguishable from an unglued reference sample, demonstrating that unintentional deformation due to glue shrinkage, handling damage, etc. was insufficient to generate dislocations.

After decoration, the center section of the sample (where the stress state most closely approximates uniaxial tension) was cut off and mounted along with the reference sample using No. 1 cover slips. As the samples faded with time, especially when exposed to the light of the microscope, measurements were made as soon as possible after decoration. Samples were stored in the dark in a freezer when not under observation.

3.7. Bulk mechanical testing. The above technique does not provide the stress applied to the sample; this had to be determined indirectly from a stress-strain curve. Unfortunately, strain gauges could not be used to determine the stress-strain curve; Figure 5 shows a typical plot of ϵ_1 and ϵ_3 vs. t, where ϵ_3 was the signal from a strain gauge glued directly to the

[3]From estimates of the silver precipitate size and spacing, on the order of 1-10 silver atoms are deposited per second per length b of dislocation.

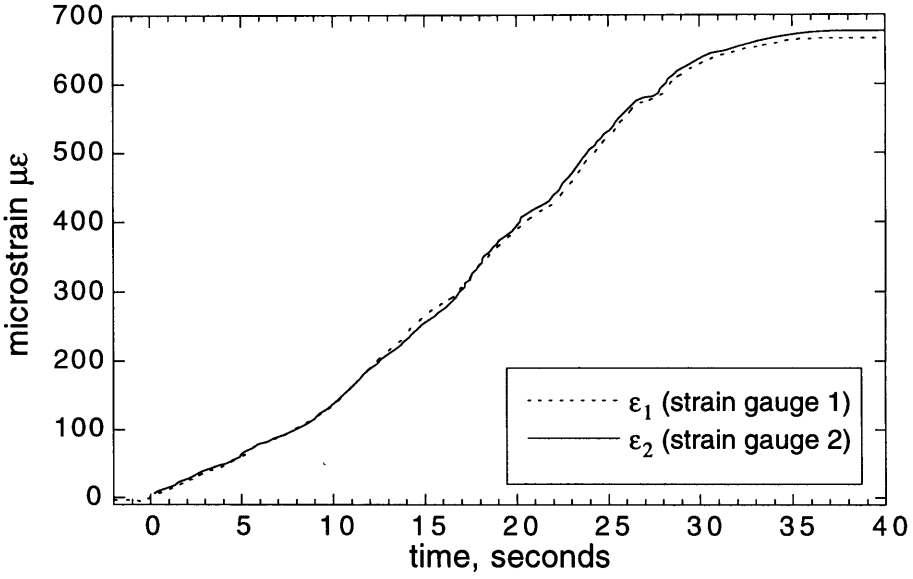

FIGURE 4. Plot of ϵ_1 and ϵ_2 vs. t showing that beam strain is relatively uniform and therefore that the mean of ϵ_1 and ϵ_2 is a good measure of sample strain. (Scanned and digitized strip-chart recorder output.)

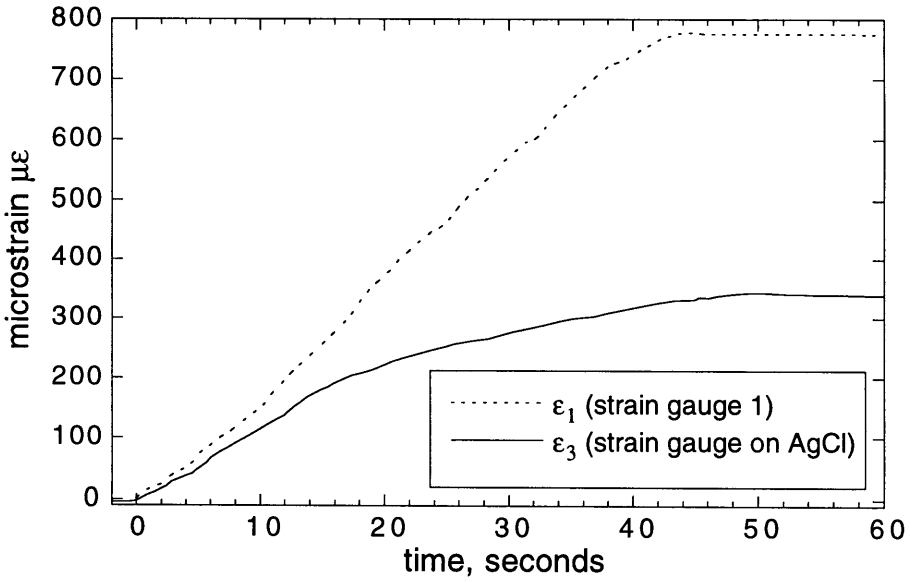

FIGURE 5. Plot of ϵ_1 (beam) and ϵ_3 (AgCl) vs. t. If gauge compliance were negligible, $\epsilon_1 \approx \epsilon_3$. Since they diverge, strain gauges cannot be used on these samples.

sample. The two signals diverge beyond the yield strain of the sample. This indicates that the stiffness of the strain gauge (one of the smaller available) was too great for use with the thin, soft samples used in the present study.

To work around this problem, load-crosshead displacement curves were measured to estimate the bulk stress-strain properties. This is a low-precision technique because the elongation of the sample must be inferred from the overall displacement.

The tensile stage used by EARHART 1997 (a fine-pitch screw driven stage) was used for the bulk tensile testing. A few modifications were made to increase sensitivity in the low strain regime:

- The load cell was replaced with a 45 N load cell.
- The stage motion was provided by low-speed motor, which provided a strain rate of about 200 $\mu\epsilon$/sec.
- Samples were glued directly onto the platforms with the catalyzed cyanoacrylate resin used in the micromechanical studies.
- The LVDT was positioned so as to measure platform-to-platform displacement, so that load cell displacement was not included.
- The lead screws were pre-loaded with a rubber band so that they were initially in tension before the sample was glued down; this reduced mechanical backlash. The load applied to the load cell by the rubber band was assumed to be constant over the duration of the test (approximately 20 μm total displacement) and the initial load simply subtracted from the measured load.

The LVDT signal was amplified by a factor of 500 using a Stanford Research Systems (Sunnyvale, CA) SR560 low noise preamplifier. Displacement and load signals were recorded vs. t at 120 Hz using the *LabVIEW* data acquisition system described in BYSTRICKY 1997. The quantized load levels are digitization artifacts of the (unamplified) load signal. Load-displacement curves were converted to stress-strain curves by setting zero displacement to the position at which the load just began to increase from its initial value.

4. Results and Discussion

4.1. Microstructure. Despite the high strain applied to the samples during rolling, voids were not observed around spheres or particles. Figure 6 shows three spheres in a doped sample after rolling but before annealing.

In samples annealed at 575 K or higher, full recrystallization occurred and very few lattice dislocations (other than those around misfitting inclusions) were observed. A low magnification photo of a typical unstrained decorated sample is given in Figure 7. Samples recrystallized at high temperature had a large grain size, on the order to 100 to 800 μm. Since the average grain size was usually larger than the sample thickness, the microstructure resembled a "honeycomb," composed of grains approximately the shape of right rectangular prisms. In computing the grain cross-sectional

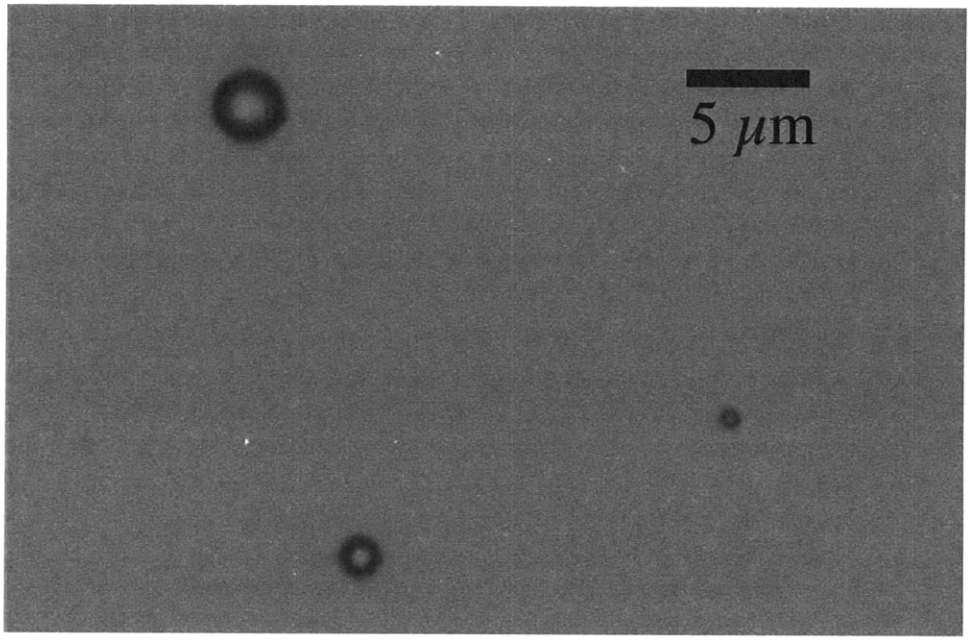

FIGURE 6. Spheres in rolled, unannealed AgCl. No voids are visible after rolling to a true strain of around 3. From the 1500 ppm master alloy.

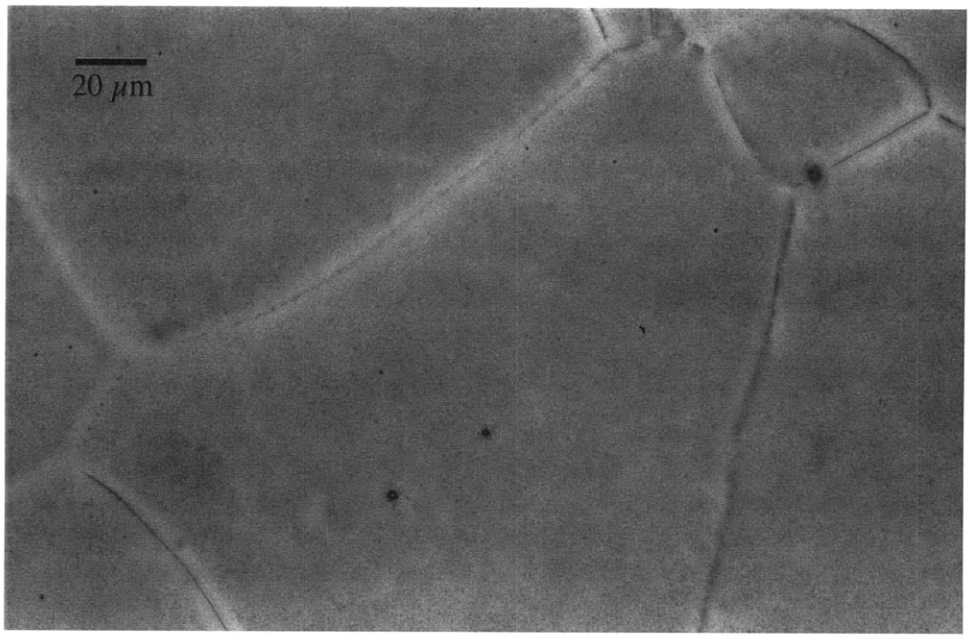

FIGURE 7. Typical microstructure after annealing and dislocation decoration. Misfit dislocations are present around glass spheres but otherwise few dislocations can be found.

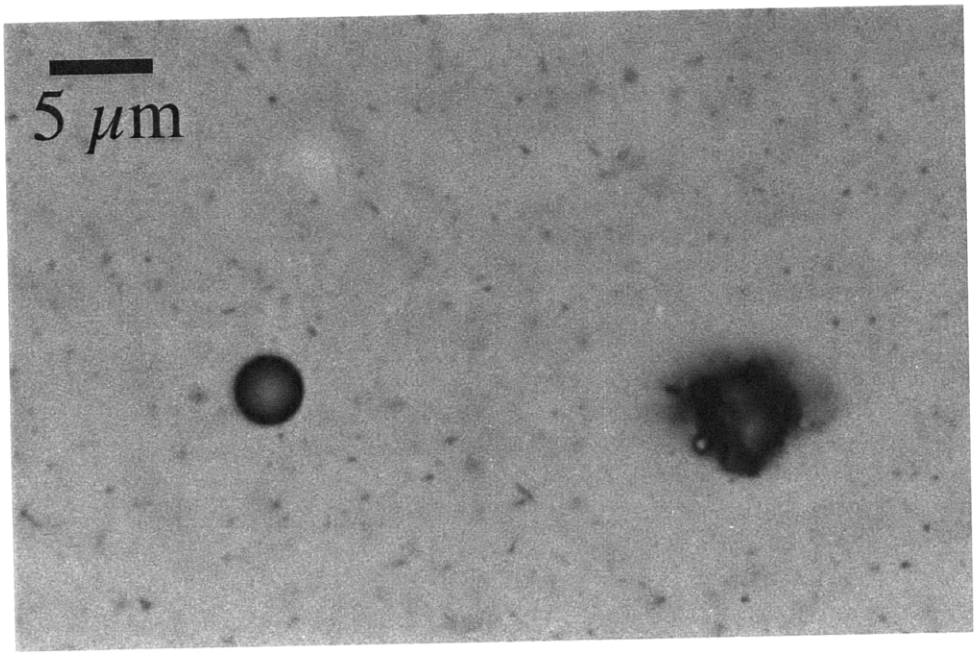

FIGURE 8. Sphere and particle in pure, undoped AgCl exposed to strobe illumination for 2 hours. No decorated dislocations are visible.

areas, perimeters and volumes used in Chapter 6, we assume invariance of the grain shape through the sample thickness.

Some samples had blistered regions caused by gaseous inclusions left over from the casting process; samples with significant blistering were rejected for use in tensile studies.

4.2. Effect of Doping Levels. Proper doping levels were found to be essential for the dislocation decoration technique to work. No dislocations were visible in exposed, undoped AgCl, although some metallic silver formed. An example of this is given in Figure 8.

In correctly doped samples, such as the approximately 500 ppm CuCl sample shown in Figure 9, dislocations were visible to a depth of greater than 40 μm, the limit of microscope travel at 1000×. Decoration contrast decreased with depth due to scattering and reduced silver density. Grain boundaries decorated heavily, creating precipitate-free zones in the adjacent material. The "random" precipitation which appears in Figure 9 was typical and has been noted by other researchers (PARASNIS AND MITCHELL 1959, PARASNIS ET AL. 1963, DUNAND AND MORTENSEN 1991b) using CuCl as a sensitizing agent.

Overdoped samples, such as the 1440 ppm CuCl master alloy shown in Figure 10, darkened five to ten times faster than correctly doped samples. At this concentration of CuCl, precipitates were observed at grain boundaries,

on thermal misfit dislocations, and in the interior of grains. These precipitates are not visible prior to decoration. Secondary precipitates in the shape of an asterisk surround each central, larger precipitate. Similar observations were made on 700 ppm CuCl-AgCl by PARASNIS AND MITCHELL 1959, who suggested that the secondary precipitates signal mismatch dislocations which form as photolytic silver deposits heavily on the primary precipitate. The sample in Figure 10 was loaded to a total strain of around 200 $\mu\epsilon$ after an overnight glue-curing step. Since thermal dislocations are surrounded by a cloud of secondary precipitates and dislocations freshly formed by the applied stress are not, the two types of dislocations can be differentiated in this sample. Some freshly formed dislocations are visible in the precipitate-free zone at "A." Thermal misfit dislocations punched around the sphere at "B" during cooling appear to have acted as heterogeneous nucleation sites for CuCl precipitation and are heavily decorated with secondary precipitates.[4]

By comparing Figures 9 and 10, we can speculate that the "random" precipitation encountered in correctly doped materials was also the result of CuCl precipitation. The effect of such precipitates on later deformation of the solid was unclear; however, in contrast to the overdoped sample, it was not possible to distinguish between thermal mismatch dislocations and applied stress dislocations. Furthermore, thermal mismatch dislocations have been observed to move under stress, so the dislocations are not pinned to the same extent that they are in Figure 10. We assume that the presence of Cu^+ ions—and any other impurities—affects the mechanical behavior of the matrix; for this reason, all tests were done using material from a single ingot so as to reduce the run-to-run variability in the friction stress.

Samples prepared from the correctly doped ingot could be decorated across their entire width, 100% of the time. The apparent robustness of the decoration technique allowed the dislocation nucleation experiments in Chapter 4 to be performed; if no dislocations were seen around a sphere, it was assumed that none was present.

4.3. Decoration Chemistry and Physics. The photographic process is generally assumed to proceed as follows. Photoelectron-photohole pairs are generated at the surface by an incoming photon. Electrons and holes diffuse through the solid, the mobility of the electron being high (HAYNES AND SHOCKLEY 1951). In the Gurney-Mott theory, the electron becomes trapped at a heterogeneity; the highly mobile Ag^+ ion diffuses interstitially to the trap and is reduced, neutralizing the trap. If a hole should recombine with the trapped electron first, no reduction occurs. It takes four silver atoms to form a stable silver nucleus (MEES AND JAMES 1966).

MALINOWSKI 1972 demonstrated that Cu^+ increases the photosensitivity of AgBr by acting as a hole trap. (The antihalation compounds added

[4]This type of accelerated precipitation is frequently observed in metal matrix composites made with precipitation-hardening alloys; see SURESH AND CHAWLA 1993.

FIGURE 9. Typical sphere from correctly doped material. A grain boundary with a precipitate-free zone is visible at the bottom of the picture.

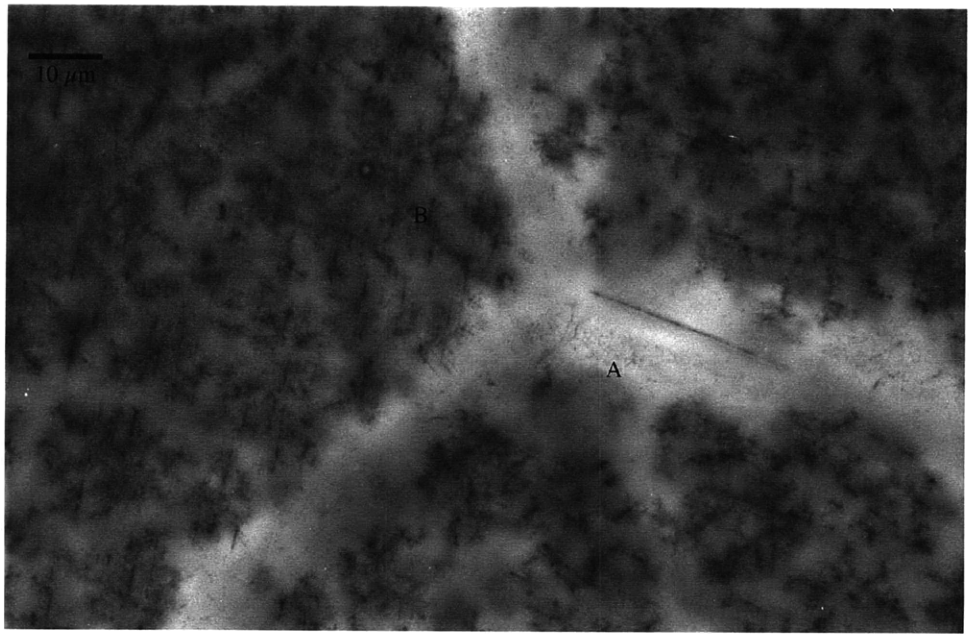

FIGURE 10. Sample doped to approximately 1500 ppm CuCl and strained to $\epsilon_t \approx 200\ \mu\epsilon$; a few dislocations created by the application of the external stress are visible at "A", and thermal misfit dislocations at "B."

to photographic film emulsion play a similar role.) The relevant reactions for the electron are:

$$\left.\begin{array}{rcl} e^-_{\text{trap}} + \text{Ag}^+_i & \rightarrow & \text{Ag}_s \\ e^-_{\text{trap}} + h^+ & \rightarrow & \text{null} \end{array}\right\} \text{competing reactions}$$

For the holes,

$$\begin{array}{rcll} h^+ + \text{Cu}^+ & \rightarrow & \text{Cu}^{++} & \text{hole trap, bulk crystal} \\ h^+ + \text{Cl}^- & \rightarrow & \frac{1}{2}\text{Cl}_2 & \text{hole trap, surface only} \end{array}$$

Without Cu^+, holes can only be trapped at the surface, so the amount of silver formed in the bulk is minimal. Cu^{++}, which acts as a hole source (GOLDENBERG ET AL. 1992), would not help with interior decoration. Better understanding of the CuCl-$CuCl_2$ equilibrium might be helpful in explaining the decoration process.

JACOB AND JEFFES 1972 report activity data for liquid mixtures of CuCl and AgCl. HILDENBRAND AND LAU 1996 report data for gaseous mixtures. No data for solid CuCl and $CuCl_2$ in AgCl were found. If we assume the activity coefficients of CuCl and $CuCl_2$ in AgCl are similar, then

$$\ln \frac{a_{\text{CuCl}_2}}{a_{\text{CuCl}}} = -\frac{\Delta G_{\text{rxn}}}{RT} + \frac{1}{2} \ln a_{\text{Cl}_2},$$

which is the usual dependence on a_{Cl_2}. Using thermodynamic data from BARIN 1993, we explore two regimes: $a_{Cl_2} = 1$, which corresponds to Cl_2 at atmospheric pressure, and a_{Cl_2} set by the decomposition of AgCl. This depends on temperature but is many orders of magnitude lower. The log of the CuCl:$CuCl_2$ ratio for these two values of a_{Cl_2} are given in Figure 11. At $a_{Cl_2} = 1$, $CuCl_2$ is favored just below the melting point of 728 K. If the melt is purged with Cl_2 gas at atmospheric pressure, oxidation of the CuCl can easily occur. In contrast, the new method relies on the AgCl decomposition reaction to set the Cl_2 activity; in this case CuCl is heavily favored.

We note that this calculation implies that Ag/$CuCl_2$ in AgCl is thermodynamically unstable with respect to AgCl/CuCl in AgCl. This might explain why samples doped with CuCl decorate well but fade with time.

4.4. Bulk Mechanical Testing. Figures 12 and 13 shows the stress-strain curves of pure AgCl and of the doped, reinforced material used in the micromechanical studies. Both materials were annealed at 623 K. The reinforced material had a higher yield stress (1.62 MPa) than pure AgCl (0.65 MPa), probably due more to the presence of CuCl than to the reinforcement.

The low precision of these curves was problematic in analyzing plastic behavior. Rather than average the results, we took what we believed to be

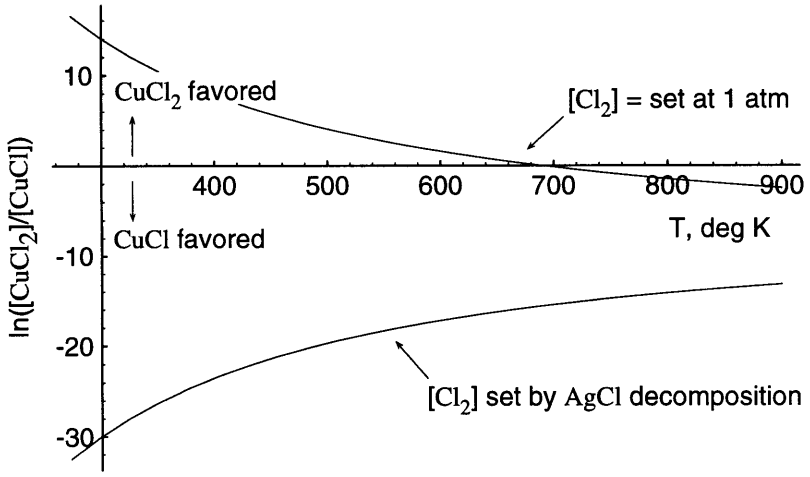

FIGURE 11. Effect of chlorine activity on the relative stability of CuCl and $CuCl_2$. Purging the AgCl/CuCl mixture with pure Cl_2 can easily result in oxidation of the CuCl.

the most precise[5] measurement, "Doped AgCl run 8." After adjusting the intercepts and dropping the very low strain data, we fit:

$$\sigma = 28.5 \text{ GPa} \cdot \epsilon_t \quad \text{for } \epsilon_t < \epsilon_{yp} \quad R^2 = 0.964 \tag{1}$$

to the elastic portion of the data, and

$$\sigma = 3.98 \text{ MPa} + 0.187 \text{ MPa} \cdot \ln(\epsilon_t - \epsilon_{yp}) \quad \text{for } \epsilon_t > \epsilon_{yp} \quad R^2 = 0.970 \tag{2}$$

to the plastic portion. The elastic limit is $\sigma_{yp} = 1.62$ MPa, $\epsilon_{yp} = 56.9$ $\mu\epsilon$. The fit to the elastic portion of the curve (28.5 GPa) is in reasonable agreement with the literature value of the Young's modulus of 21.9–24.0 GPa.[6] A fit to the elastic region of Figure 12 yielded a modulus of 25.6 GPa for pure AgCl, also in reasonable agreement with literature values.

5. Conclusions

A new method for preparing decorable AgCl composites was developed. This method has several advantages over the classical technique of Mitchell and co-workers. It is relatively easy, takes advantage of commercially available high purity materials, and is less dangerous. The microstructural uniformity is good and decoration is very reliable. The classical technique, on

[5]Testing techniques improved with each sample as the measurement techniques improved; best precision was obtained by allowing the tensile stage to relax fully (about 20 minutes) after applying the rubber band preload but before gluing the sample in place. Further tests were not performed because each test used a large amount of material.

[6]Reuss and Voigt averages of temperature–corrected elastic constants from LOJE AND SCHUELE 1970.

the other hand, provides a better surface finish and might be more suitable for composites containing long fibers, which fracture during the rolling step used in this technique.

Compared with TEM, the AgCl decoration technique offers lower resolution but fewer sample thinning artifacts and a better defined stress state. Work on the present system indicates that thermal misfit dislocations can extend many particle diameters away from an inclusion; hence, the thinning of a TEM disk to a thickness less than one inclusion diameter will necessarily result in the loss of at least these dislocations, and most likely many others.

The decoration technique cannot be used on metals of engineering interest. However, experiments on ductile ionic solids, such as the etch-pit work on LiF of JOHNSTON AND GILMAN 1959, have historically provided some of the best data on the physics of plasticity. While the AgCl decoration technique is not suitable for the study of all problems in plasticity, there are many interesting questions which might be appropriately investigated with the AgCl system. With the increased reliability of the method presented here, these investigations are more feasible than in the past.

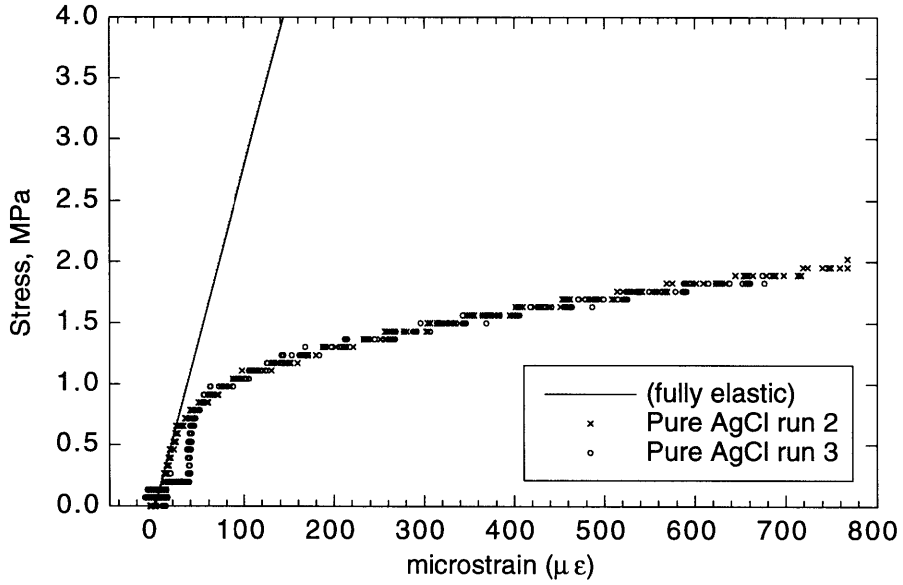

FIGURE 12. Stress-strain curves for pure AgCl. Yield stress $\sigma_y \approx 0.65$ MPa.

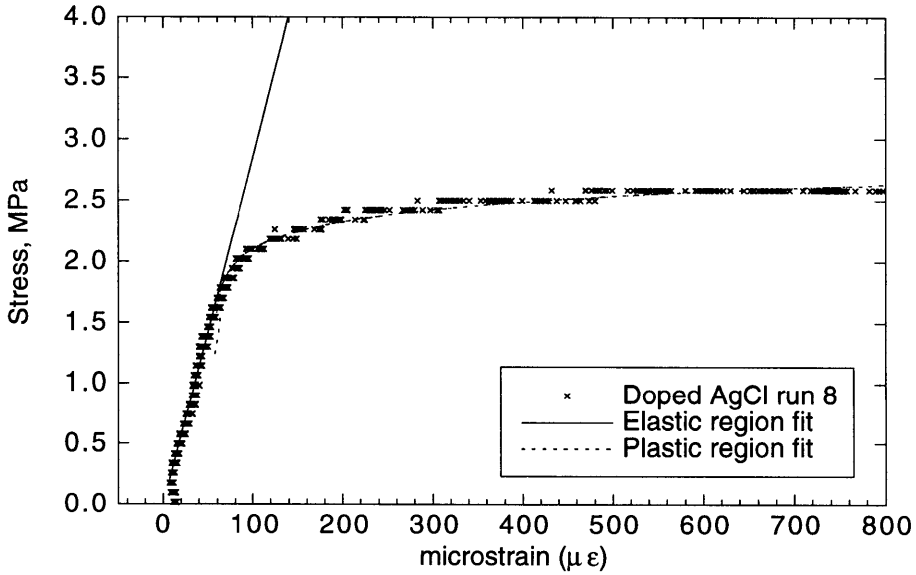

FIGURE 13. Stress-strain curve for reinforced AgCl with 500 ppm CuCl. Yield stress $\sigma_y \approx 1.65$ MPa

CHAPTER 4

Nucleation of Dislocations Around Hard Spheres in Silver Chloride due to Thermal Misfit

1. Introduction

As the mechanical properties of a plastically deforming solid depend on prior loading history, in order to study its tensile behavior we must first characterize the initial state. The sample preparation techniques of Chapter 3 generate polycrystalline samples with a very low density of lattice dislocations beyond those created by thermal mismatch. The thermal mismatch process creates large numbers of prismatic dislocation loops around the inclusions; since these dislocations are already extant at the point at which an external stress is applied to the solid, no nucleation event is necessary. For this reason, these loops play a potentially important role in the early stages of plastic deformation. In this chapter we attempt to characterize the number and distribution of thermal mismatch dislocations formed around glass particles in silver chloride so that we can estimate their importance to later deformation of the sample.

1.1. The Effective Plastic Temperature. Most samples used in this study were annealed at a temperature of 573 K or higher. Because of the large amount of cold work stored in the samples during the rolling process and because the recrystallization temperature T_{rx} is more than 80% of the absolute melting temperature T_M, these samples recrystallize rapidly.

The samples can be assumed to be free of stress and lattice dislocations at T_{rx}. As the temperature is lowered, thermal misfit forms between inclusion and matrix which is relieved via a series of overlapping processes—first diffusion, then creep plasticity and finally conservative dislocation glide. These processes are time and length scale dependent, so the boundaries between them are not absolute. However, since diffusion and creep rates decrease exponentially with temperature, for a given cooling rate the transition to fully conservative plastic deformation is frequently assumed to occur at a single temperature. We call this the effectively plastic temperature T_{ep}. The temperature change $T_{\text{ep}} - T_{\text{room}}$ along with the difference in CTE between phases determines the misfit strain ϵ^T. Because all nucleation and plastic zone size theories depend on ϵ^T, it is important to determine it as accurately as possible. T_{rx} places an upper bound on T_{ep}; in what follows, we estimate T_{ep} more accurately using measurements made on samples recrystallized at two different temperatures.

1.2. Loop Nucleation. A series of criteria must be met for nucleation to occur. The first, known as the Brooks criterion (BROOKS 1952), is that the misfit displacement must be larger than the Burgers vector b. Following LEE ET AL. 1980,

$$\epsilon^C \geq \frac{b}{r_p},$$

where ϵ^C is the constrained strain,

$$\epsilon^C = \left(\frac{3K_p}{3K_p + 4G}\right)\epsilon^T,$$

as given by ASHBY AND JOHNSON 1969. The second requirement is thermodynamic; the creation of a dislocation loop must lower the energy of the system. We adopt the calculation of ASHBY AND JOHNSON 1969, who compare the work done by the stress during the expansion of a shear loop (negative) with that due to the self-energy of the loop (positive). ASHBY AND JOHNSON assume that this step, the formation of the shear loop, is rate-limiting. The shear loop subsequently cross slips into a prismatic loop.

The work done by the stress as the loop expands is:

$$W = -6G\epsilon^C z r_p^3 b \int_{-r_l\sqrt{\pi}/2}^{+r_l\sqrt{\pi}/2} \int_c^{c+r_l\sqrt{\pi}/2} \frac{x}{(x^2+y^2+z^2)^{5/2}}\, dx\, dy.$$

where r_l is the loop radius and $c = z = r_p/\sqrt{2}$; this is the location of the maximum shear stress. The self-energy of the loop[1] is

$$E = \frac{Gb^2 r_l}{4}\left(\frac{2-\nu}{1-\nu}\right)\left\{\ln\frac{8r_l}{b} - 2\right\}.$$

The sum of W and E is the total change in the energy of the system[2] as a function of r_l. ASHBY AND JOHNSON note that for misfits which have been shown to nucleate dislocations at incoherent interfaces, the proposed path of the dislocation predicts energy barriers which are orders of magnitude larger than kT, the amount of energy available from statistical fluctuations. This suggests that dislocation nucleation at incoherent interfaces is not a thermally activated process, but one which depends on special features of the interface to catalyze the creation of the dislocation loop. They then propose that, while the actual path of the sub-critical loop is likely to differ from what is proposed, the model can be used to estimate the misfit required for a nucleated dislocation to lower the energy of the system. This provides a lower bound on the misfit needed.

Empirically, ASHBY AND JOHNSON found that data in the literature collected from systems with an incoherent interface, such as Cu-SiO_2, could be explained by assuming that dislocations are nucleated at this lower bound,

[1] One of the several simplifications in this model is that the effect of the elastic modulus of the particle on the stress field of the dislocation is ignored.

[2] There is an obvious sign error at this step in ASHBY AND JOHNSON 1969.

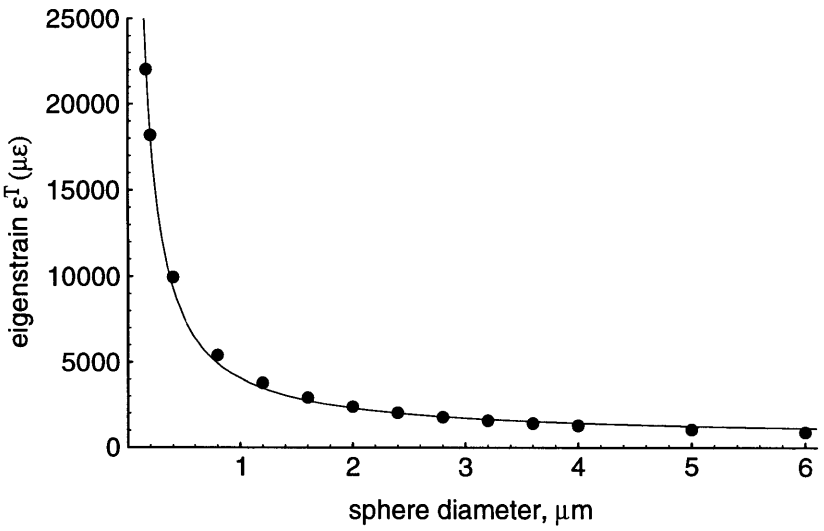

FIGURE 1. Predicted values of the critical misfit ϵ_*^T in the AgCl-glass system.

which is the value of ϵ^T were $W + E$ turns negative. This is the critical misfit ϵ_*^T.

Since the AgCl-glass interface must be incoherent, the Ashby-Johnson model is applicable. Using *Mathematica*, we determined ϵ_*^T numerically for this system. The results are given in Figure 1. The data can be approximated with a curve of the form

$$\epsilon_*^T = k_1 + k_2 {r_p}^{-1}$$

where $k_1 = 5.44 \times 10^{-4}$ and $k_2 = 1.76 \times 10^{-9}$ m.

ASHBY AND JOHNSON found reasonable agreement with experimental data on Cu-SiO_2, a system with an incoherent interface, for $d_p = 2\,r_p$ in the range 0.1 μm to 0.3 μm. It is of interest to see if the Ashby-Johnson model works for larger particles.

1.3. Free vs. Tangled Loops. Thermal misfit dislocations are often observed to form dense tangles around precipitates. As discussed in Chapter 1, such tangled regions are thought to play an important role in the deformation of inclusion-containing solids (e.g., ARSENAULT AND FISHER 1983), and several models have been proposed which predict the extent of the plastic zone as a function of the misfit strain, particle radius, and material parameters. Notable models include the perfectly plastic models of HILL 1950 and LEE ET AL. 1980, the creep model of JOHNSON AND LEE 1983 and the strain hardening models of KIM ET AL. 1990 and DUNAND AND MORTENSEN 1991a. KIM ET AL. 1990 and DUNAND AND MORTENSEN 1991a both presented experimental results in good agreement with their models.

One aspect of the thermal punching process which these models do not take into account is the presence of untangled loops outside of the tangled loop shell. These "free loops," while not necessarily important in high volume fraction composites, are a distinctive feature of samples with more widely spaced inclusions. These loops are not locked in place by reactions with neighboring dislocations and can expand across the crystal at a shear stress lower than that required to move the tangled loops. We consider this process in Chapter 5. At present, we define "free loops" to be all prismatic loops, figure-eight loops, helices, double helices, and shear loops with a diameter on the order of $d_p/\sqrt{2}$ where d_p is the inclusion diameter, since none of these configurations is tightly tangled. Figure 2 from MAKENAS AND BIRNBAUM 1980 illustrates the distinction between free and tangled loops.

The goals of this chapter are to determine the value of T_{ep} for samples recrystallized at a high temperature, to investigate the nucleation of dislocations from glass spheres in an AgCl matrix, and to characterize the number and distribution of free loops. We compare the results with some existing models and propose a simple stochastic model for the distribution of nucleation sites at incoherent interfaces.

2. Experiments Performed

DUNAND AND MORTENSEN 1991a calculated a value of $T_{ep} = 400 \pm 30$ K for AgCl-glass by fitting experimental data on the plastic zone radius as a function of the sphere radius to the work hardening model presented in that work.Using this result as a starting point, an experiment was performed to determine a lower bound for T_{ep}. Sample G30 was annealed at a high temperature, cooled to 398 K and decorated at this temperature. Numerous dislocations were found, demonstrating that T_{ep} must be above 398 K.[3] One sphere from this sample is shown in Figure 3. From the number of loops in this photo, $T_{ep} \approx 450$ K.

As the depth of decoration was poor (approximately 5–7 μm) in Sample G30 and the cooling rate low compared with the other samples used in the study, estimates of T_{ep} obtained from Sample G30 were not used in later analyses. Instead, the number of loops punched in two samples recrystallized at a temperature known to be below T_{ep} was compared with the number punched in a sample recrystallized at the normal temperature. The annealing and decoration temperatures used in these experiments are summarized schematically in Figure 4.

The two low-temperature samples were recrystallized at 403 K, cooled to room temperature at the standard cooling rate (see Chapter 3) and decorated. The number of loops around each isolated sphere was counted for 30 spheres in Sample G43 and 200 spheres in Sample G47. Sample G47

[3]We expect T_{ep} to be a function of cooling rate; see Appendix 6 of DUNAND 1991. The cooling rate of Sample G30 was roughly 20 times lower than normal because it was cooled in a hot furnace from the annealing temperature to the decoration temperature. Hence, the value of T_{ep} is rigorous lower bound for T_{ep} in the other samples.

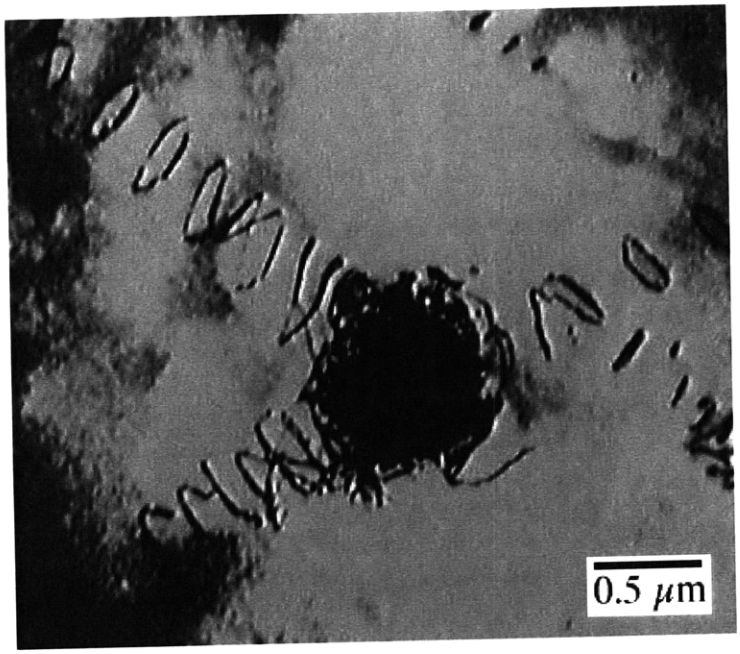

FIGURE 2. Tangled and free dislocation loops formed by precipitation of niobium hydrides in niobium. From MAKENAS AND BIRNBAUM 1980.

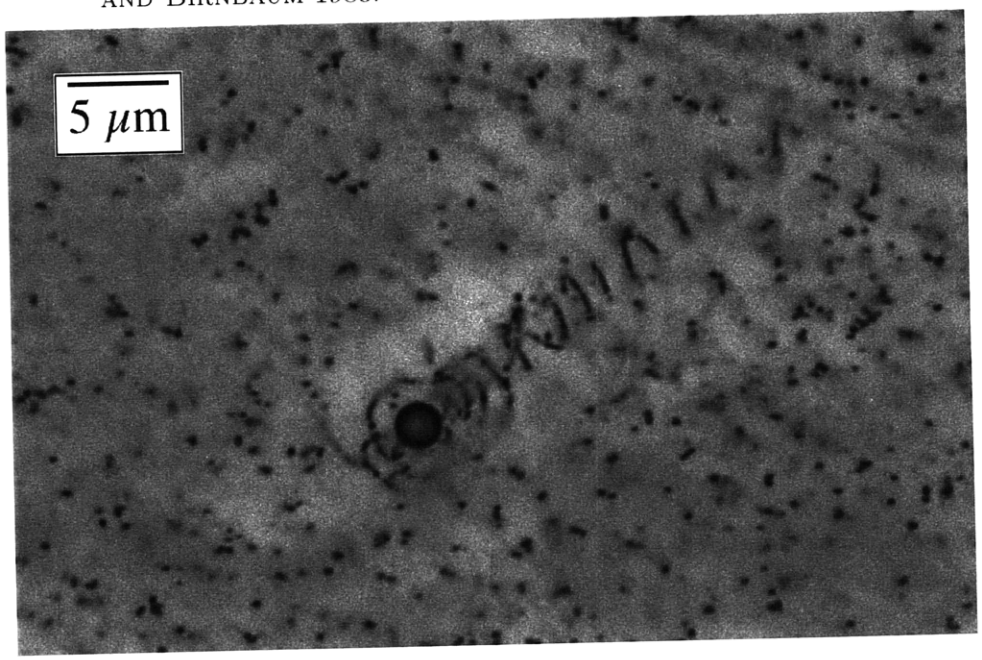

FIGURE 3. Dislocations around a sphere 2.4 μm in diameter, annealed at 570 K and decorated at 398 K. This proves that $T_{\mathrm{ep}} > 398$ K. From the number of loops visible, $T_{\mathrm{ep}} \approx 450$ K.

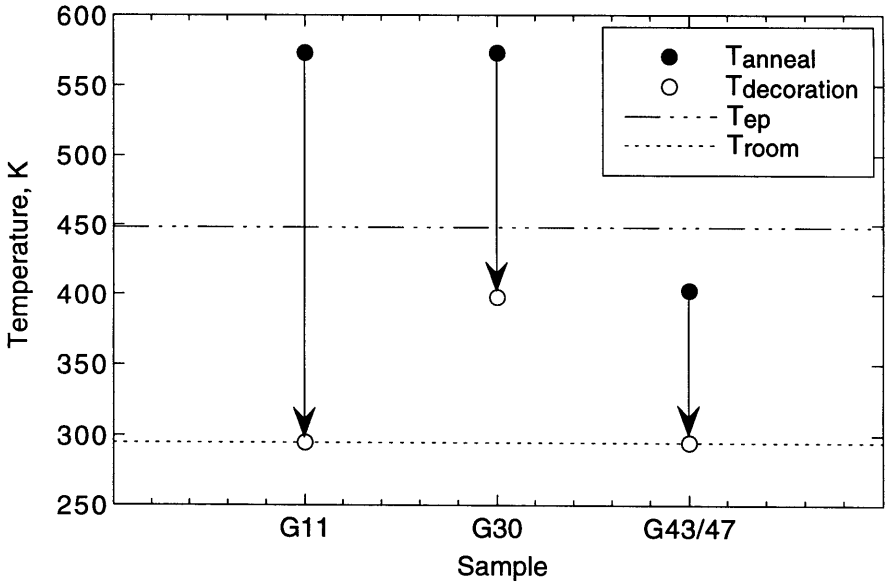

FIGURE 4. Schematic of annealing and decoration temperatures. All samples used in later studies were heat-treated on the same schedule as Sample G11.

was resolutionized before rolling; Sample G43 was not. Sphere diameters were measured by video-screen comparison with calibrated circles printed on transparency film in 0.5 μm increments; the absolute error in these measurements is estimated to be ± 0.25 μm. The number of loops was estimated by eye. While it is easy to tell the difference between "some loops" (Figure 5) and "no loops" (Figure 6), quantification of the number of loops is more difficult. For example, while the sphere in Figure 7 clearly has six loops, the estimate of the number of loops (30) in Figure 5 is more subjective.

High-temperature recrystallization data were collected from Sample G11, which was recrystallized at 573 K. Counts of the number of free loops were made by estimating upper and lower bounds on the number of loops in each cylinder; the reported values are the sums of means of these measurements on each sphere. Diameters were measured using the image analysis program *IPLabs* by applying the local minima of an intensity histogram to a thresholding function; this technique has an estimated relative error of 7.3%. Additional data on particles $d_p \leq 1.5$ μm were collected using the video technique described above. As these additional measurements were made after significant fading of the sample had occurred, no additional counts of the number of loops punched or the number of punching directions were taken. Spheres near grain boundaries or other inclusions were again excluded from the dataset.

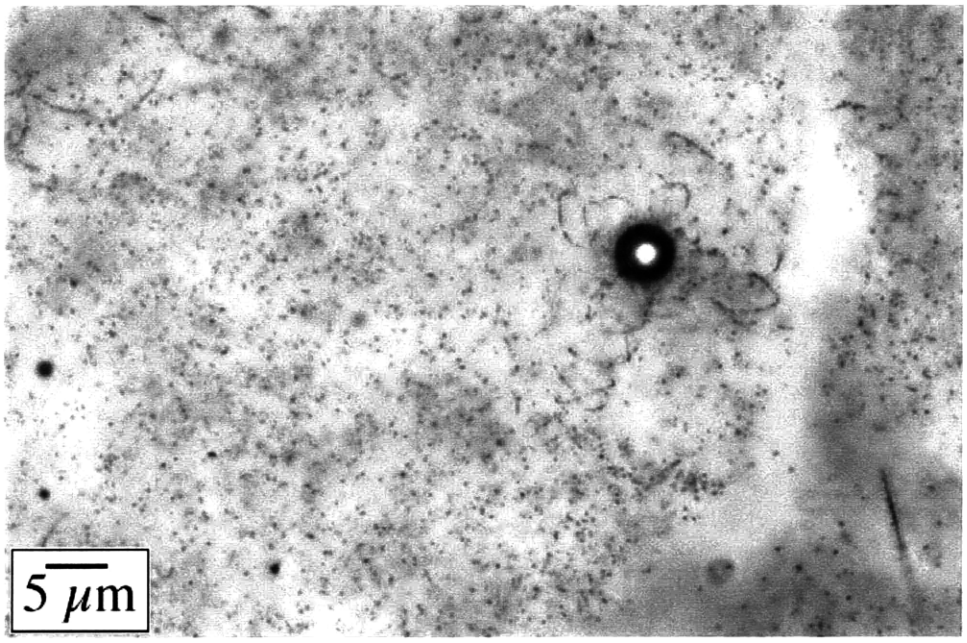

FIGURE 5. 4 μm sphere from Sample G47, recrystallized at 403 K. Loops are visible on several punching cylinders.

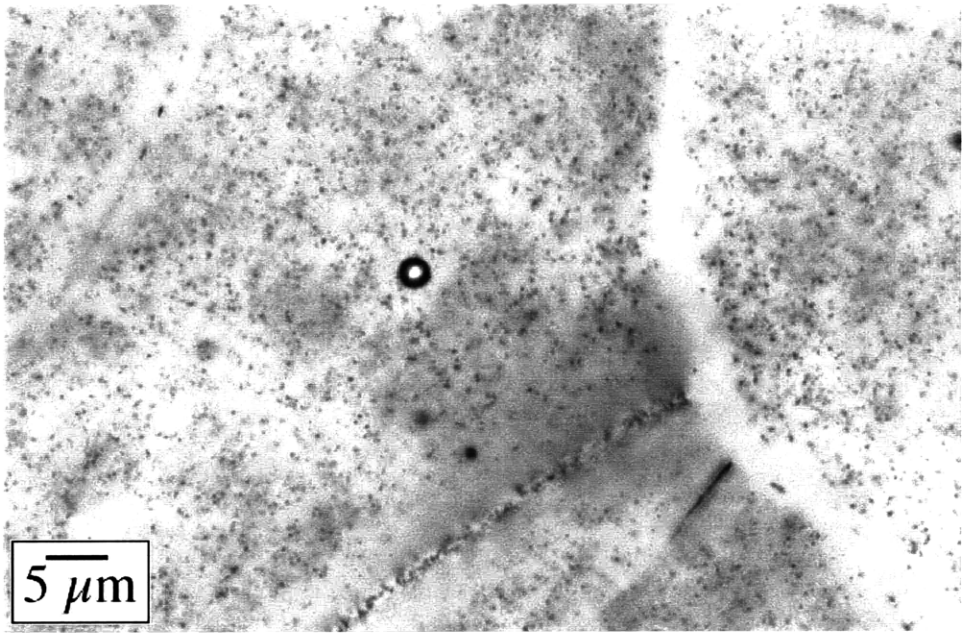

FIGURE 6. Sphere from Sample G47 which did not punch any loops. Sphere diameter is 2.5 μm.

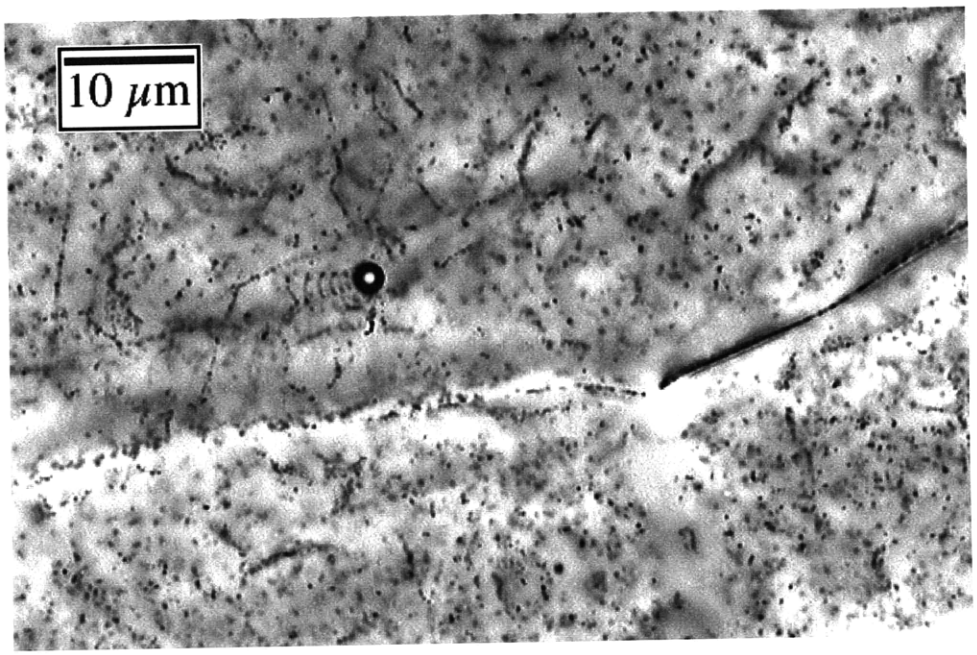

FIGURE 7. 2 μm sphere from Sample G43, recrystallized at 403 K. A total of 6 loops were punched on one cylinder.

3. Estimating T_{ep}

We adopt the common assumption[4] that all misfit dislocations are in the form of prismatic interstitial loops of radius $r_p/\sqrt{2}$, this being the loop radius at which the matrix shear stress is maximized at the sphere surface.

Let $\epsilon_r^T(r_p)$ be the radius-dependent residual misfit strain due to loop nucleation effects. The upper bound on the number of loops which can be punched (i.e., if no tangling were to occur) is

$$n(r_p) = \left\lfloor \frac{8r_p[\epsilon^T - \epsilon_r^T(r_p)]}{b} \right\rfloor .$$

If we approximate this as a continuous function, the difference between the upper bound on the number of loops punched at misfit strains ϵ_1^T and ϵ_2^T is

$$\Delta n(r_p) = \frac{8r_p}{b}(\epsilon_2^T - \epsilon_1^T). \tag{3}$$

Let the misfit strain of G43 and G47 be ϵ_1^T and that of G11 be ϵ_2^T. Figure 8 shows experimental data from Samples G43 and G47 ($T_{\text{rx}} = 403$ K) and G11 ($T_{\text{rx}} = 573$ K.) If we make the assumption that the highest points on

[4]Nearly all models which consider prismatic dislocations make this assumption. However, in the course of the present study, dislocations with radii approaching r_p were commonly observed. As the mechanism by which loops with $r > r_p/\sqrt{2}$ can form is not clear, this would be an interesting area for further theoretical and experimental investigation.

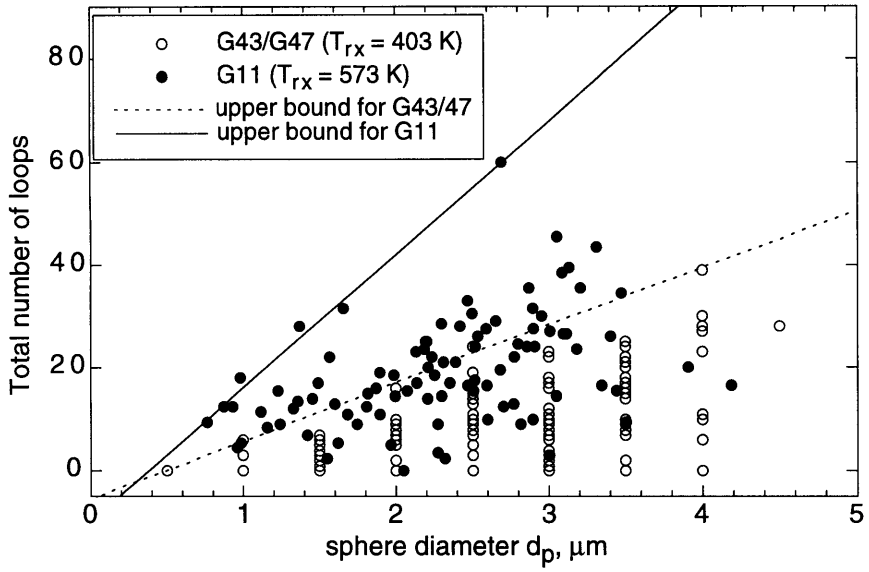

FIGURE 8. Measured number of loops vs. particle radius for samples recrystallized at two temperatures, 403 K and 573 K. Other experiments place the lower bound of T_{ep} at 398 K, so the strain relief effects of creep and diffusion can be neglected for the 403 K sample.

this plot represent the tangle-free upper bound, then we can use linear fits to these lines to solve for $\epsilon_2^T - \epsilon_1^T$ of (3). Obviously the choice of points to include in the fit is somewhat arbitrary. The results of these curve fits are

$$\begin{aligned} n_1 &= 2.25 \times 10^7 \cdot r_p - 5.56 \quad R^2 = 0.998, \\ n_2 &= 5.18 \times 10^7 \cdot r_p - 9.73 \quad R^2 = 0.991. \end{aligned}$$

Since $\Delta n = n_2 - n_1$, dropping the remnant intercept yields

$$\epsilon_2^T - \epsilon_1^T = \frac{2.93 \times 10^7 \cdot b}{8} = 1.44 \times 10^{-3}.$$

We can calculate ϵ_1^T by using the data of FOUCHAUX AND SIMMONS 1964 on the lattice parameter a_{AgCl} as a function of T and the known annealing and decoration temperatures $T_{ep} = 403.15 \pm 0.1$ K and $T_{room} = 294.6 \pm 0.5$ K. Once ϵ_1^T is known, ϵ_2^T and T_{ep} for Sample G11 are readily determined. The results are:

$$\begin{aligned} \epsilon_1^T &= (3.24 \pm 0.03) \times 10^{-3}, \\ \epsilon_2^T &= (4.69 \text{ or greater}) \times 10^{-3}, \text{ and} \\ T_{ep} &= 448+ \text{ K}. \end{aligned}$$

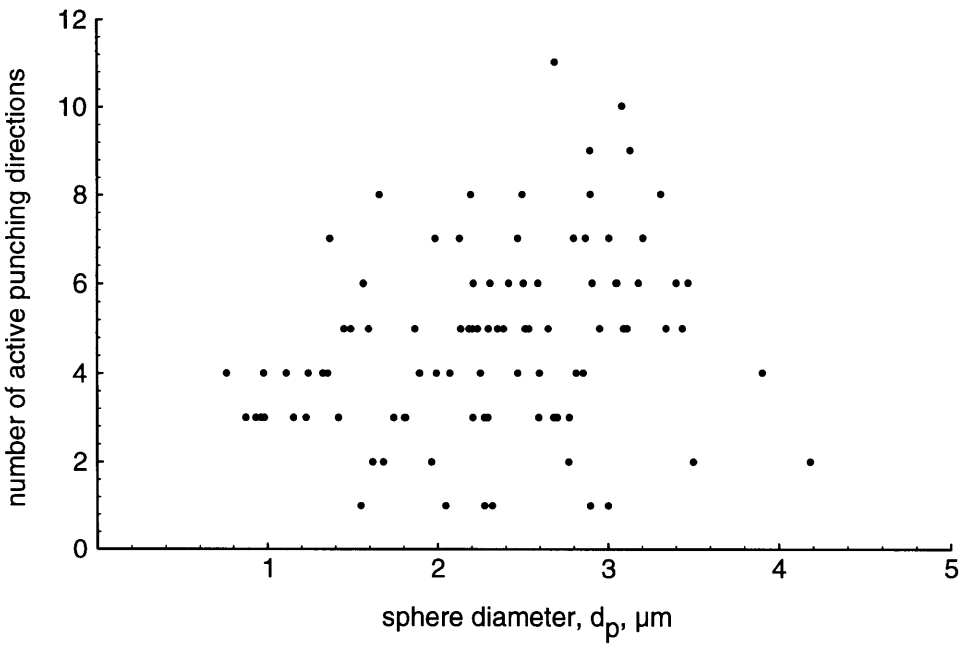

FIGURE 9. Number of active cylinders vs. sphere diameter from Sample G11.

The accuracy of ϵ_1^T is limited mostly by our value for the CTE of Corning 7070 glass[5]; overall it is quite good. The accuracy of ϵ_2^T is certainly much lower but difficult to quantify as our calculation depends on our assumption that the upper bounds of the data represent true tangle-free upper bounds. Since tangle-free punching is unlikely, it is reasonable to interpret 448 K as a lower bound on T_{ep}.

The value of T_{ep} calculated is a little higher than the 400 ± 30 K estimate of DUNAND 1991. Possible reasons are that Dunand's work hardening model did not include a nucleation barrier and that the experimental data in that reference were taken from spheres closer to the surface than in the present work, which would allow diffusion and creep to remain active to a lower temperature.

4. Number of Active Punching Cylinders

The number of active punching cylinders, out of a maximum of 12, increases with particle radius. Data from Sample G11 are given in Figure 9. There is a large amount of scatter in the data, which indicates that tangling is occurring.

[5] $\alpha = 32 \times 10^{-7}$ K^{-1} for "0–300 K" from CORNING TECHNICAL STAFF 1997. We assume an error of 5% over our temperature range.

5. Determination of the Friction Stress

The stress-strain curves presented in Chapter 3 suggest that the friction stress τ_f is low in AgCl. The value of τ_f can be estimated by measuring the spacing x and diameter d of isolated prismatic loops produced by thermal punching. (If τ_f were zero, thermal misfit dislocations would glide to infinite separation distance after nucleation.)

The loop spacing problem was treated theoretically by BULLOUGH AND NEWMAN 1960. They solved this problem in terms of dimensionless loop spacing ξ and dimensionless flow stress v, where

$$\xi = \frac{x}{d}$$

and

$$v = \frac{2\pi d(1-\nu)\tau_f}{Gb}.$$

DUNAND 1991 solved the elliptical integrals in BULLOUGH AND NEWMAN 1960 numerically for values of the spacing ξ_o between the penultimate loop and last loop. He found these expressions could be approximated by the function

$$\log v_o = 0.866 - 1.08\xi_o + 0.102\xi_o^2.$$

Eleven values of ξ_o were determined from Sample G11. Loop spacings were measured using *IPLab* and corrected for the position of the observer as described in Chapter 6. Loop diameters were taken to be the mean of the measured diameters of the two loops. The mean of the values of τ_f computed is

$$\tau_f = 0.36 \pm 0.06 \text{ MPa}.$$

We expect the friction stress to be similar in other freshly solutionized samples.

6. Nucleation of Thermal Misfit Dislocations

6.1. Threshold Values of Required Misfit.

6.1.1. *Testing Ashby and Johnson's model:* Once the value of T_{ep} is known, the nucleation model of Ashby and Johnson can be tested against experiment. For the purpose of testing the models, spheres were sorted by diameter into 0.5 μm-wide bins. The fraction X_i of spheres with loops is

$$X_i = \frac{m_i}{n_i} \pm \frac{1}{2\sqrt{n_i}}$$

where m_i is the number of spheres of size range i with one or more loops and n_i the total number of spheres. Errors are calculated assuming a binomial distribution[6] for which $\sigma = \sqrt{np(1-p)}$ with $p = 1/2$.

[6]The errors in the X_i are important in later curve-fitting calculations. STEINSALTZ 1997 has argued that in the absence of a theoretical basis for p, a value of $p = 1/2$ is most appropriate since it represents the worst case.

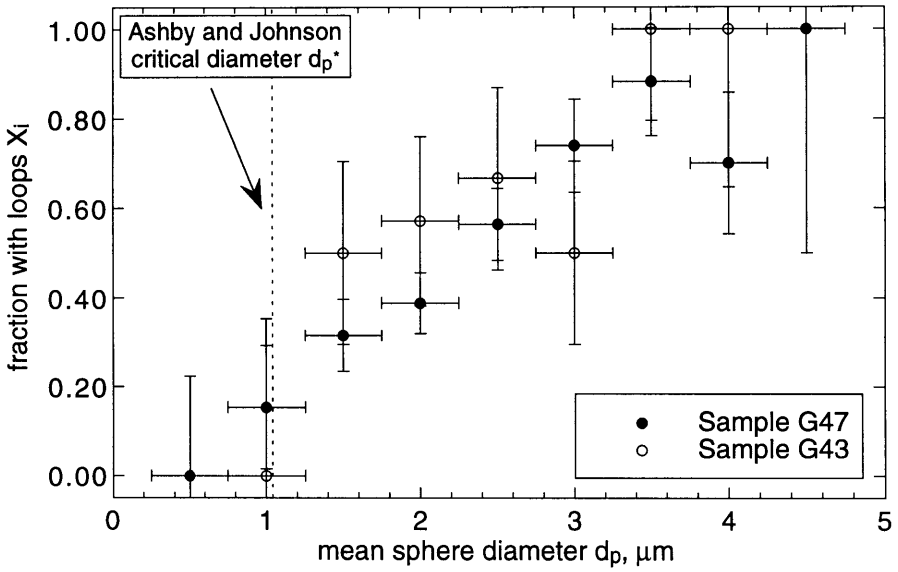

FIGURE 10. Fraction X_i of spheres with one or more loops. Ashby and Johnson's criterion gives a lower bound on the sphere diameter required for nucleation of 1.05 μm. (From Samples G43 and G47, $T_{ep} = 403$ K.)

A plot of the data from Samples G43 and G47 is given in Figure 10, and those from Sample G11 in Figure 11. Few measurements were made on Sample G43 because it had a visibly higher density of background precipitation, suggesting that CuCl which precipitated during storage was not resolutionized during the anneal. These precipitates would increase the flow stress over that of samples recrystallized at higher temperatures. The X_i calculated from the 30 spheres measured are neither consistently above nor consistently below the X_i from Sample G47. This suggests that small variations in the flow stress do not strongly affect nucleation behavior.

Given along with the data is the predicted critical (minimum) sphere diameter d_p^* required for dislocation nucleation, calculated using Ashby and Johnson's model.[7]

[7]Material parameters G, b and α are all functions of temperature. There is no obvious way to include this in Ashby and Johnson's model. We have taken the following approach. The misfit strains were determined using the best available, temperature-dependent data for the physical constants. The elastic moduli were determined at 294 K using a Voigt average of the temperature-corrected elastic constants of LOJE AND SCHUELE 1970. The Burgers vector (0.392 nm) was computed from $a_{AgCl}/\sqrt{2}$ at 294 K from the X-ray data of FOUCHAUX AND SIMMONS 1964. This choice of parameters corresponds to assuming that the sphere cools from T_{ep} to T_{room} in the fully elastic state, and dislocations either are or are not nucleated once the sample reaches T_{room}. While this is obviously non-physical, it is a reasonable approach for predicting nucleation because it yields the exact result for spheres which do not punch any loops during the cooling process and minimally incorrect

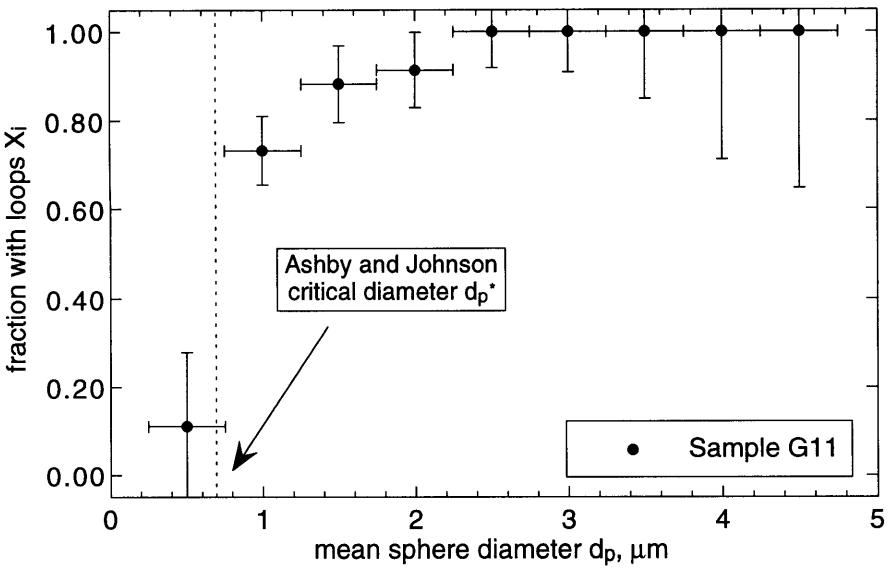

FIGURE 11. Fraction X_i of spheres with one or more loops. Ashby and Johnson's criterion gives a lower bound on the sphere diameter required for nucleation of 0.692 μm. (From Samples G11, $T_{ep} = 448$ K.)

We define the experimentally determined value of d_p^* to be the mean diameter of the first bin for which $X_i > 0$. The data are summarized in Table 1 below. Within experimental error, the agreement between theory and experiment is good.

TABLE 1. Comparison of predicted and observed values of d_p^*.

	Ashby-Johnson Model	AgCl Experiments
Sample G47	1.05 μm	1.0 ± 0.25 μm
Sample G11	0.69 μm	0.5 ± 0.25 μm

The Ashby-Johnson model does not predict the clear upward trend in the X_i with particle diameter which is seen in Figures 10 and 11. This is an interesting observation which, to our knowledge, has not been reported previously in the literature. We consider a possible explanation for this dependence in the next section.

6.1.2. *Comparison with other methods:* The misfit nucleation data obtained from Sample G47 are perhaps the best yet collected on this problem. A problem with the pressurization technique of ASHBY ET AL. 1969 is that emitted dislocations can potentially be reabsorbed into the particle-matrix interface during depressurization; a problem with most thermal misfit data

for spheres which punch only a few loops. Hence, this approach is most accurate for $d_p \approx d_p^*$ where accuracy is most important.

such as that of WEATHERLY 1968a is that ϵ^T is not known as precisely as in the present case. The reinforcements in the present case are also very nearly spherical. A further advantage of the AgCl system is that the spheres can be large and widely spaced yet still numerous enough to permit statistically significant measurements because of the large volume of material decorated.

Where the present data fall short is in the measurement of d_p. While the circle comparison method is quick and yields acceptable results for larger particles, the relative error for the 0.5 μm particles is as high as 50%. The small particle data are necessary at larger values of ϵ^T since $X_i \to 1$ for larger particles. Future work in this area should use image analysis and a magnifying extension tube to measure d_p so that the error is determined mostly by the diffraction limit.

6.2. A Stochastic Model for Nucleation Sites. Incoherent interfaces appear to act as "perfect," or zero activation energy sources from which dislocation loops are emitted as soon as it becomes energetically feasible to do so. ASHBY AND JOHNSON 1969 suggested that incoherent interfaces might contain line defects which bulge from the surface under misfit stresses, or possibly that the inevitable deviations from perfect sphericity cause stress concentrations at the sphere surface which lead to nucleation.

6.2.1. *Assumptions:* In what follows, we reject the latter mechanism, which is inconsistent with an experimental observation that larger defects do not have a strong influence on punching behavior. (The presence of a visible asperity on a sphere did not consistently lead to nucleation on the cylinder containing the asperity; furthermore, nucleation frequently occurred on cylinders which had no visible asperities.)

Data from Sample G41 (to which an additional macroscopic strain was applied) given in Table 2 show little difference between the nucleation behavior of spheres and equiaxed particles. Since the particles have many sharp corners, these data suggest that the shape of the inclusion has only a minor effect.

TABLE 2. Probability of one or more loops punched from Sample G41. ($T_{\text{ep}} \approx 448$ K, applied strain = 137 $\mu\epsilon$.)

bin	spheres	particles
0.5 μm	$X_{0.5} = 0.125 \pm 0.022$	$X_{0.5} = 0.194 \pm 0.038$
1.0 μm	$X_{1.0} = 0.118 \pm 0.036$	$X_{1.0} = 0.118 \pm 0.076$

Finally, since the stress around an inclusion of a given shape and misfit is independent of the size of the inclusion, a mechanism based solely on stress concentrations would not predict the sphere diameter dependence observed. For these reasons, we instead assume that there are some number of *potential* nucleation sites of unspecified nature which are randomly and independently distributed over the surface of a sphere. Thermal misfit results in a shear

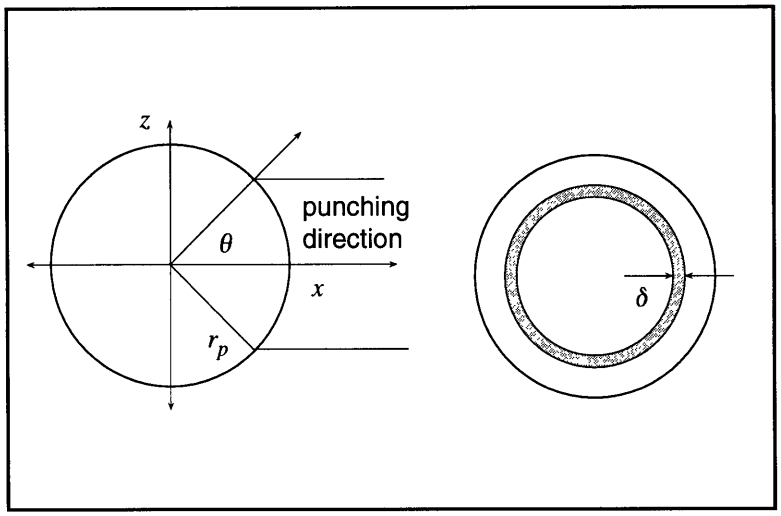

FIGURE 12. Definition of delta.

stress at the surface of the sphere; at a given shear stress some subset of the total number of nucleation sites is activated and able to emit a dislocation loop. In this way, irregularities in the shape of the inclusion do influence the number of active sites, but only to the extent that the number of special nucleation sites is changed.

The effects of the friction stress and any subsequent tangling are ignored in the model which follows. Since we are only interested in the appearance of the first loop, it is reasonable to ignore the influence of these factors.

6.2.2. *Derivation:* Let $N(\tau^*)$ be the number of nucleation sites per unit area of incoherent interface which are activated at a shear stress of τ^*. The stress in a particular <110> direction is given by ASHBY AND JOHNSON 1969 as

$$\tau_{xz} = \frac{-6Gxzr_p^3}{(x^2+y^2+z^2)^{5/2}}\epsilon^C.$$

Following Figure 12, we obtain the stress on the surface of the sphere as a function of θ, which is

$$\tau_{xz} = -3G\epsilon^C \sin 2\theta.$$

The width δ of the circular segment shown is then

$$\delta = r_p \cos^{-1}(-\tau^*/3G\epsilon^C).$$

There are 12 of these segments, each of radius $r_p/\sqrt{2}$. Hence, if we ignore overlap, the total surface area A which is at a stress of τ^* or higher is

$$A = 12\sqrt{2}\pi r_p \delta.$$

If δ is small, the stress τ does not vary too much across the width of δ. This can be seen by taking a Taylor series expansion around $\theta = \pi/4$, which

yields

$$\tau = -3G\epsilon^C \sin 2\theta \approx -3G\epsilon^C(1 - 2(\delta/2r_p)^2) \approx -3G\epsilon^C.$$

We assume δ is small. Then, since $N(\tau^*)$ is the density of *potential* sites, the mean number of *active* sites λ (those which are at stress τ^*) is

$$\lambda = AN(\tau^*),$$

or

$$\lambda = c\, d_p^2$$

where

$$c = 3\sqrt{2}\pi N(\tau^*) \cos^{-1}(-\tau^*/3G\epsilon^C).$$

We assumed that the potential nucleation sites were distributed randomly, independently, and with constant density over the sphere. The number of sites that fall within the high-stress area A can be described as a spatial Poisson process (p. 103 of McPherson 1990), which is fully characterized by a single parameter, its density c.

From the probability distribution of this Poisson process, we can compute the probability that a given sphere has k nucleation sites, where k is an integer. We are interested in knowing the probability that there are one or more nucleation sites in a sphere. This probability is

$$\Pr[k_i \geq 1] = \sum_{k_i=1}^{\infty} \frac{\lambda^{k_i}}{k_i!} e^{-\lambda}.$$

It is more convenient to compute the probability of a nucleation event via the probability of its complement, $\Pr[k_i = 0]$:

$$\begin{aligned} \Pr[k_i \geq 1] &= 1 - \Pr[k_i = 0] \\ &= 1 - e^{-\lambda} \\ &= 1 - e^{-c\, d_p^2}. \end{aligned} \tag{4}$$

In the limit as $n_i \to \infty$ (i.e., a large data set), $X_i \to \Pr[k_i \geq 1]$. Hence, we can test this model by curve-fitting a function of the form $X_i = 1 - e^{-c\, d_{p,i}^2}$ to the data in Figures 10 and 11.

Weighted curve fits, which place more emphasis on points with smaller error terms, were made using *KaleidaGraph* (Synergy Software, Reading PA). *KaleidaGraph* uses the Levenberg-Marquardt algorithm; for a discussion of this algorithm and the weighting process, see Bevington and Robinson 1992. The results are presented in Figures 13 and 14. For clarity, data from Sample G43 have been omitted.

The values of c determined are given in SI units in Table 3, which also contains τ_{max}, the highest value of the shear stress on the surface of a loopless sphere. This is independent of the particle radius.

This model is attractive because it automatically meets the boundary conditions $\lim_{d_p \to 0} X = 0$ and $\lim_{d_p \to \infty} X = 1$ and, with a single parameter,

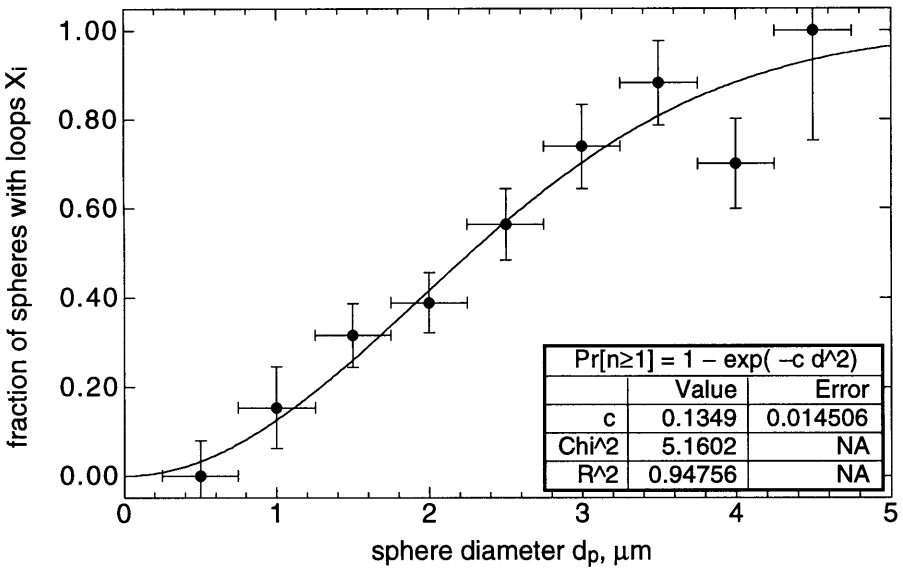

FIGURE 13. Fraction of spheres with loops and prediction of the stochastic model. Curve fits determined using a weighted Levenberg-Marquardt algorithm to d_p in μm.

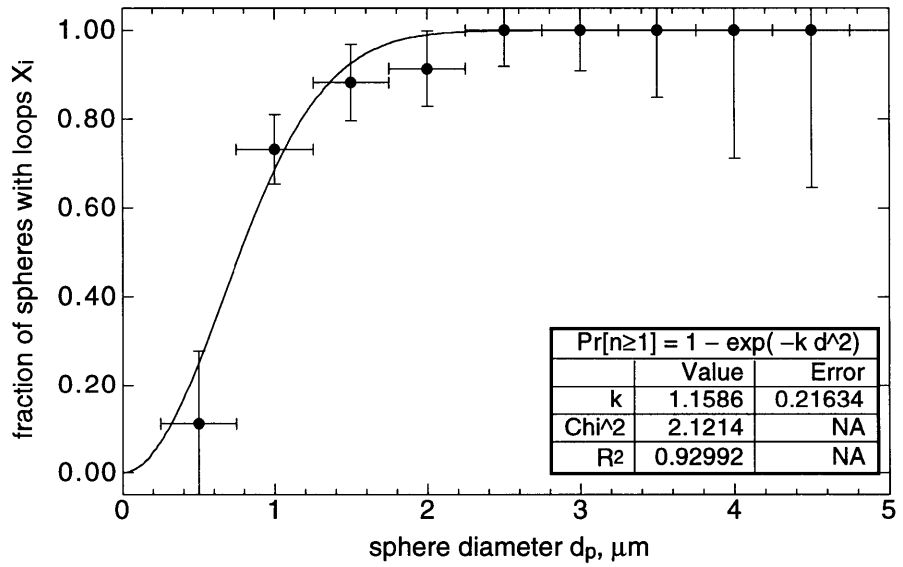

FIGURE 14. Fraction of spheres with loops and prediction of the stochastic model. Curve fits determined using a weighted Levenberg-Marquardt algorithm to d_p in μm.

generates a good fit to the data. The value of c appears to be strongly dependent on the maximum stress: a 44% increase in $\tau_{\max}$ increased c by over 800%. With only two values of c, it is not possible to make further

TABLE 3. Values of k determined for two values of ϵ^T.

Sample	$\tau_{\max}$	normalized $\tau_{\max}$	c
G47	60.3 MPa	$G/140$	$(0.135 \pm 0.014) \times 10^{12}$ m^{-2}
G11	87.0 MPa	$G/98$	$(1.16 \pm 0.22) \times 10^{12}$ m^{-2}

inquiries into the stress dependence of c. However, this is an attractive area for further research, as it would be relatively easy to repeat the experiments at $T_{\text{rx}} = \{390\text{ K}, 400\text{ K}, 410\text{ K}\ldots\}$, and, based on the results presented in this section, be relatively confident of the value of $\tau_{\max}$ determined from ϵ^T.

7. Conclusions

In this chapter, we presented data on the number of active cylinders and the number of free loops punched as a function of particle diameter d_p. The value of T_{ep} was estimated to be 448 K for samples annealed at high temperatures, and this result was used to determine the misfit strain ϵ^T for these samples.

The present results are in good agreement with the model of ASHBY AND JOHNSON. Additionally, the data are well characterized by a simple one-parameter probabilistic model. More experimental data would be helpful in clarifying some of the issues raised in this chapter, and these results would not be too difficult to obtain with the AgCl/glass sphere system.

CHAPTER 5

Equilibrium Shape of Prismatic Dislocation Loops Under Uniform Stress

1. Introduction

Prismatic dislocation loops are closed dislocations which, in an unstressed crystal, lie in the plane normal to their Burgers vector $\vec{b}$ and are entirely edge in character. As shown in the previous chapter, significant numbers of these dislocations are formed around hard inclusions during cooling from the recrystallization temperature as a result of thermal misfit between matrix and inclusion.

In this chapter, we assume the temperature is low enough that climb is inoperative. Under these conditions, prismatic loops are stable in an unstressed crystal. In this respect they differ from shear loops, which collapse in the absence of an applied stress. The difference arises because the slip plane—the plane which contains both $\vec{b}$ and the dislocation line sense $\hat{\xi}$—of a prismatic loop is parallel to $\vec{b}$. READ 1953 proved that a gliding prismatic dislocation loop cannot change its projected area normal to $\vec{b}$; slip can occur only within the glide cylinder defined by the loop or in planes containing $\vec{b}$.

In an unstressed crystal, the equilibrium configuration of the loop is that which minimizes its total energy, that is, the configuration of minimum dislocation length. This is obtained when the loop lies entirely in one plane. When a shear stress is applied to the crystal, the loop elongates in its glide cylinder. When the loop elongates to the point at which $\hat{\xi}$ is parallel to $\vec{b}$, the dislocation can cross slip and leave the glide cylinder. This process is illustrated in Figure 1, taken from READ 1953.

The plastic work done by the loop is insignificant before cross slip occurs. After this point, the cross-slipped segments act as normal shear loops which can propagate across the crystal. For this reason, it is of interest to predict the critical stress τ^* at which prismatic loops cross slip. This question was addressed by GRILHÉ 1963, who derived the equilibrium shape of circular loops and infinite helices under the assumption of isotropic dislocation line tension.

Grilhé calculated that loops can leave the glide cylinder at a critical resolved shear stress of

$$\tau = \frac{W_\perp}{br},$$

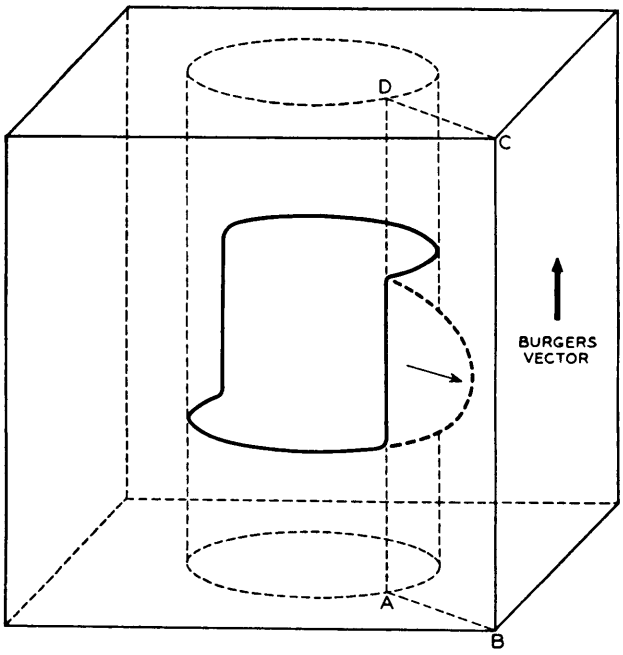

FIGURE 1. Prismatic dislocation loop elongated under stress. Below the critical stress, the loop is constrained to slip within the cylinder indicated. Above the critical stress, it can cross slip onto a plane such as $ABCD$, the plane of maximum shear stress. In all cases, the projected area of the loop is constant.

where r is the loop radius and $W_\perp$ is the (constant) energy per unit length of dislocation. Grilhé predicted that supercritical loops could form Frank-Read sources.

In this chapter we extend Grilhé's derivation to address the influence of an orientation dependent line tension (ODLT). In this model, the variation in a dislocation's line energy as it changes from edge to screw is incorporated into the calculation of its equilibrium shape. We also present a very simple approximate solution for the problem.

We then compare the predictions of the three models and present experimental results for prismatic loops in the AgCl-glass system. Finally, we discuss the possibility that supercritical loops will form Frank-Read sources.

2. Analysis

2.1. The Orientation Dependent Line Tension Solution.

2.1.1. *Assumptions:* We generally follow Grilhé's assumptions for calculating the equilibrium configuration of a dislocation loop. These assumptions are that the crystal is an isotropic continuum, that the "line tension" approximation can be used to approximate the self-stress of the dislocation

(restricting our analysis to loops greater than about 50 nm in diameter), that we can ignore all dynamic effects, and that the stress state in the crystal is uniform.

We choose a fixed orthonormal coordinate system, which leads to somewhat longer intermediate results than in Grilhé's derivation but which is advantageous when comparing predictions of the model to experimental data.

2.1.2. *Defining the loop:* A circular prismatic dislocation loop $\vec{s}$ with Burgers vector $\vec{b}$ is described parametrically as a function of θ in the xy plane. The loop is contained in a cylinder of radius r centered on the z-axis when there is no applied stress. The z position of the loop at each θ is given by the function $Z(\theta) = rA(\theta)$, so that

$$\vec{s}(\theta) = \begin{bmatrix} r\cos\theta \\ r\sin\theta \\ rA(\theta) \end{bmatrix}.$$

Our goal is to determine $A(\theta)$ as a function of the applied stress.

Since the unit line sense $\hat{\xi} = d\vec{s}(\theta)/d\theta$, we have

$$\hat{\xi} = \frac{1}{\sqrt{1 + A'(\theta)^2}} \begin{bmatrix} -\sin\theta \\ +\cos\theta \\ +A'(\theta) \end{bmatrix}.$$

Initially $\vec{b}$ is parallel to $\hat{z}$, so

$$\vec{b} = \begin{bmatrix} 0 \\ 0 \\ b \end{bmatrix}.$$

Under the **FS**/*RH* convention[1] as defined by HIRTH AND LOTHE 1968, b is negative for an interstitial loop and positive for a vacancy loop.

2.1.3. *Forces which extend the loop:* Beginning with a uniform applied stress tensor $\boldsymbol{\sigma}$, we apply the equation of PEACH AND KOEHLER 1950:

$$\vec{F}_s = (\vec{b} \cdot \boldsymbol{\sigma}) \times \hat{\xi}.$$

This gives the force $\vec{F}_s$ per unit length on each piece of dislocation line ds,

$$\vec{F}_s = \frac{b}{\sqrt{1 + A'(\theta)^2}} \begin{bmatrix} \sigma_{xy}A'(\theta) - \sigma_{zz}\cos\theta \\ -\sigma_{xz}A'(\theta) - \sigma_{zz}\sin\theta \\ \sigma_{xz}\cos\theta + \sigma_{yz}\sin\theta \end{bmatrix}.$$

We simplify this expression by defining a resolved shear stress term τ (which corresponds to Grilhé's σ):

$$\tau = \sigma_{xz}\sec\alpha \tag{5}$$

[1] Form a closed, right-handed Burgers circuit around the dislocation in the real crystal. Redraw the Burgers circuit in the reference crystal; this circuit will be open. The vector from finish **F** to start **S** in the reference crystal defines $\vec{b}$.

where

$$\tan\alpha = -\frac{\sigma_{yz}}{\sigma_{xz}}. \tag{6}$$

We rewrite $\vec{F}_s$ in the orthonormal basis

$$\hat{t} = \begin{bmatrix} -\sin\theta \\ \cos\theta \\ 0 \end{bmatrix}, \quad \hat{z} = \begin{bmatrix} 0 \\ 0 \\ 1 \end{bmatrix}, \quad \hat{r} = \begin{bmatrix} \cos\theta \\ \sin\theta \\ 0 \end{bmatrix}$$

to separate the glide ($\hat{t}$ and $\hat{z}$) and climb ($\hat{r}$) components of $\vec{F}_s$. This yields:

$$\vec{F}_s = -\frac{b}{\sqrt{1+A'(\theta)^2}} \begin{bmatrix} A'(\theta)\,\tau\cos(\alpha+\theta) \\ -\tau\cos(\alpha+\theta) \\ A'(\theta)\,\tau\sin(\alpha+\theta)+\sigma_{zz} \end{bmatrix}. \tag{7}$$

2.1.4. *Forces which restrain the loop:* Opposing the applied stress is the dislocation's "self-stress." For small dislocation loops, it is important to calculate the effect of the entire dislocation on the self-stress of a segment ds. (See HIRTH AND LOTHE 1968 and BROWN 1964). When $r \gg b$, as is the case with loops formed around inclusions, non-adjacent components of the loop have only a small effect on the self-stress and use of the line tension approximation is appropriate.

The energy of a screw dislocation is (FRIEDEL 1964)

$$W_\odot = \frac{Gb^2}{4\pi}\ln\frac{R}{r_o}, \tag{8}$$

where R and r_o are the effective outer and core radii of the dislocation. Since the magnitude of the log term changes only slowly as the loop is elongated, we may take $W_\odot$ to be a constant with $\ln R/r_o \approx \ln r/b$. Then, if ψ is the angle between $\vec{b}$ and $\hat{\xi}$, the energy $W_\perp(\psi)$ of a long, straight dislocation in an isotropic solid is

$$W_\perp(\psi) = W_\odot\frac{(2-\nu)-\nu\cos 2\psi}{2(1-\nu)}. \tag{9}$$

DEWIT AND KOEHLER 1959 show the line tension of a curved dislocation is proportional to $W_\perp(\psi) + d^2W_\perp(\psi)/d\psi^2$, so the restoring force F_r is

$$F_r = \kappa\left[W_\perp(\psi) + \frac{d^2W_\perp(\psi)}{d\psi^2}\right]\hat{N}, \tag{10}$$

where κ is the curvature and $\hat{N}$ is the principal unit normal vector.

Starting with Equation 14.4-13 of THOMAS AND FINNEY 1984, we see

$$\hat{N} = \frac{1}{\kappa}\frac{d\hat{\xi}}{ds} = \frac{1}{\kappa}\cdot\frac{d\hat{\xi}/d\theta}{\|ds/d\theta\|},$$

eliminating κ. Since $\tan\psi = A'(\theta)^{-1}$, we can express (10) in terms of $A'(\theta)$:

$$\vec{F}_r = \frac{W_\odot}{1+A'(\theta)^2}\cdot\frac{(1+\nu)A'(\theta)^2+1-2\nu}{(1-\nu)}\cdot\frac{d\hat{\xi}/d\theta}{\|ds/d\theta\|}.$$

Rewriting the force in the new coordinate system $(\hat{t}\,\hat{z}\,\hat{r})$, we obtain

$$\vec{F}_r = -\frac{W_\odot\left[(1+\nu)A'(\theta)^2+1-2\nu\right]}{r(1-\nu)(1+A'(\theta)^2)^3}\cdot\begin{bmatrix} A'(\theta)\,A''(\theta) \\ -A''(\theta) \\ 1+A'(\theta)^2 \end{bmatrix}. \tag{11}$$

2.1.5. *Combining the forces:* The equilibrium position of the loop can then be determined by finding $A(\theta)$ such that $F_s + F_r = 0$ for all θ. Setting the sum of (7) and (11) to zero, we obtain for both the $\hat{t}$ and $\hat{z}$ directions the differential equation

$$-\Omega\cos(\alpha+\theta) = \frac{A''(\theta)[(1+\nu)A'(\theta)^2+1-2\nu]}{(1-\nu)[1+A'(\theta)^2]^{5/2}}, \tag{12}$$

where we have introduced the dimensionless parameter Ω,

$$\Omega = \frac{rb\tau}{W_\odot}. \tag{13}$$

Integrating both sides of (12), we obtain

$$-\Omega\sin(\alpha+\theta)+C_1 = A'(\theta)\frac{1-2\nu+(1-\nu)A'(\theta)^2}{(1-\nu)(1+A'(\theta)^2)^{3/2}}. \tag{14}$$

For a single prismatic loop[2], $A'(\theta)$ must be periodic on the interval 0 to 2π. Thus, $C_1 = 0$.

Instead of solving Equation 14 for $A'(\theta)$, we solve its square, a sextic equation in $A'(\theta)$, using the symbolic computation program *Mathematica* (Wolfram Research, Champaign, IL). These solutions are lengthy polynomials in $\Omega\sin(\alpha+\theta)$ and ν. Retaining the real root $\sqrt{F(\theta)}$, we use the requirements that $A'(\theta)$ be continuous, positive for $\pi-\alpha<\theta\le 2\pi-\alpha$, and antisymmetric about $\theta=-\alpha$ and $\theta=\pi-\alpha$ to determine the sign of the function $A'(\theta)$. The solution to (14) is then

$$A'(\theta) = \begin{cases} -\sqrt{F(\theta)} & \text{when} \quad -\alpha\le\theta\le\pi-\alpha, \\ \sqrt{F(\theta)} & \text{when} \quad \pi-\alpha<\theta\le 2\pi-\alpha. \end{cases}$$

We can then numerically integrate $A'(\theta)$ to obtain $A(\theta)$ for particular values of ν and Ω.

2.1.6. *Critical values of* Ω*:* When $A'(\theta)\to\pm\infty$, the dislocation has screw dislocation character over a portion of its length and can cross slip. $A'(\theta)$ reaches its extrema at $\theta+\alpha=\pm\pi/2$. The expression $A'(\pi/2-\alpha)$ has denominator 0 when $\Omega=1$ and, for $0\le\nu\le 1/2$, negative and non-zero numerator. Thus $A'(\pm\pi/2-\alpha)\to\mp\infty$ when $\Omega\to\pm1$ so

$$\Omega^* = \pm 1.$$

where Ω^* is the critical value of Ω.

[2]In his paper, Grilhé considers the more general case of an infinite helix, in which case $C_1\neq 0$.

2.2. Grilhé's Solution.

2.2.1. *Assumptions and derivation:* We recover Grilhé's solution by setting $W_\perp(\psi)$ in (10) equal to the self-energy of a pure screw dislocation, $W_\odot$. The choice of the constant used in place of $W_\perp(\psi)$ is arbitrary; the use of $W_\odot$ is appropriate because it most closely approximates the restoring force of the dislocation line in a near-critical loop.

Integrating and taking $C_1 = 0$, we obtain

$$A'(\theta) = -\frac{\Omega \sin(\alpha+\theta)}{\sqrt{1-\Omega^2\sin^2(\alpha+\theta)}}, \tag{15}$$

which, after integration and application of the boundary condition $A(\theta) = 0$ at $\alpha + \theta = \pm\pi/2$, yields

$$A(\theta) = \ln\left[\Omega\cos(\alpha+\theta) + \sqrt{1-\Omega^2\sin^2(\alpha+\theta)}\,\right] - \frac{1}{2}\ln\left[1-\Omega^2\right]. \tag{16}$$

2.2.2. *Critical values of* Ω*:* From (15) we see that $A'(\pm\pi/2-\alpha) \to \mp\infty$ as $\Omega \to \pm 1$. Thus

$$\Omega^* = \pm 1,$$

which is the same result as determined using the ODLT analysis.

2.3. Approximate Solution.

2.3.1. *Assumptions and derivation:* An approximate solution can be determined by equating the net z-axis force on a half-loop with the z component of the dislocation line tension at $\theta = \pm\pi/2 - \alpha$ and then assuming that the loop takes the shape of an ellipse. We again take the self-energy of the dislocation to be constant and equal to $W_\odot$.

The net force in the z direction on a half-circle can be computed from z component of (7),

$$F_s = \int_{-\frac{\pi}{2}-\alpha}^{\frac{\pi}{2}-\alpha} b\sigma\cos(\alpha+\theta) r d\theta = 2rb\sigma.$$

The restoring force F_r is the sum of the line tensions at $\theta = \pm\pi/2 - \alpha$,

$$F_r = 2W_\odot \sin\Psi,$$

where Ψ is the angle between $\hat{\xi}$ and $\hat{t}$ at $\theta = \pm\pi/2 - \alpha$. Setting $F_r + F_s = 0$, we obtain

$$\Psi = \sin^{-1}\Omega.$$

If we assume the loop takes the form of an ellipse at angle Ψ to the xy plane, $A(\theta)$ is given by:

$$\begin{aligned} A(\theta) &= \tan\Psi\cos(\alpha+\theta) \\ &= \frac{\Omega}{\sqrt{1-\Omega^2}}\cos(\alpha+\theta). \end{aligned} \tag{17}$$

2.3.2. *Critical values of* Ω*:* The critical value of Ω is obtained by solving for $\Psi = \mp\pi/2$, which yields

$$\Omega^* = \pm 1,$$

which is the same result obtained with the other two methods.

3. Discussion

3.1. Comparison of Models. The three models predict identical critical values of Ω; however, they predict quite different loop shapes, especially at smaller values of Ω. These shapes are plotted in their "unrolled" shape (plots of $A(\theta)$ vs. θ) in Figure 2. Also shown are the maximum values of $A(\theta)$ as a function of Ω (Figure 3). While there is no analytical expression for $\max[A(\theta)]$ in the ODLT model, the following power series can be used when $\Omega < 0.8$:

$$\max[A(\theta)] \approx 2.649\,\Omega - 2.294\,\Omega^3 + 3.112\,\Omega^5.$$

At small values of Ω, the predictions of the Grilhé model and elliptical model are almost identical. The ODLT model predicts a more canted loop. This can be understood in light of the fact that the ODLT loop becomes more screw-like as it elongates, so the average energy per unit length of dislocation decreases as the ODLT loop expands.

Note that the center of mass of a prismatic loop will not change as the stress is increased. This is a consequence of the uniform stress state of the crystal. If the stress field were to be inhomogeneous (such as would be found in the vicinity of an inclusion), the whole loop should move down the gradient of the hydrostatic component of the stress.

3.2. Dislocation Multiplication. For values of Ω above the critical value, prismatic dislocation loops become unstable; the loop elongates in the direction of $\vec{b}$, generating pure screw segments at $\theta + \alpha = \pm\pi/2$ which can leave the glide cylinder via cross slip. We calculate the force on the screw segments by taking the limit of (7) as $A'(\theta) \to \pm\infty$ at $\theta + \alpha = \pm\pi/2$, obtaining

$$F_s = \begin{bmatrix} 0 \\ 0 \\ b\sigma \end{bmatrix},$$

as expected. The force is radially outwards.

Grilhé argues that loops and helices can, at this point, become Frank-Read sources and produce large numbers of dislocations on the cross-slip plane. It is hard to see how this could occur in the case of a loop; a Frank-Read source requires a dislocation segment to be pinned at its endpoints, whereas in the present case the endpoints of the cross-slipped system are two

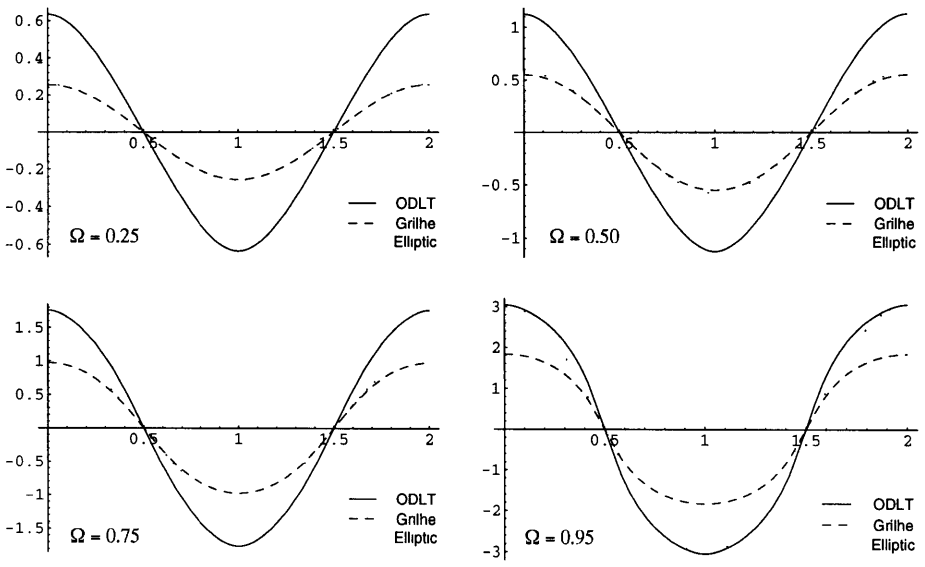

FIGURE 2. Plots of $A(\theta)$ vs. θ (in units of π) for ODLT, Grilhé and elliptical loops at four values of Ω. As Ω increases, the difference between the ODLT solution and the other two solutions decreases.

mobile half-loops which also expand along with the cross-slipping segments.[3] We expect that a supercritical prismatic loop will take the form of a shear loop with two "ears"—the two half-loops of the original prismatic loop—which will then expand across the crystal much like a shear loop. As work of JOHNSTON AND GILMAN 1959 conclusively demonstrated that ordinary shear loops can multiply under a high applied stress, we are not stating that the present loops cannot become dislocation sources, only that the Grilhé mechanism cannot operate until both of the half-loops become pinned by an obstacle.

3.3. Incorporating a Non-Zero Flow Stress. The above analysis incorporates only the effects of a dislocation's line tension. This yields a lower bound on the stress required to obtain a particular configuration. In a real crystal, factors such as the Peierls stress, any solute atmosphere or second phase precipitates, and the presence of other dislocations will increase the critical stress required for the loop to cross slip.

The extent to which the analysis is relevant to a real material depends on the relative strengths of the loop and the matrix. The first three effects can

[3]During the initial formation of the cross-slipping loop, half-loops can provide stable anchors for small bowing angles. This is a consequence of the line tension of the dislocation increasing (as a result of increasing edge character) more rapidly than the decrease in the z-component of the force, which goes as the cosine of the angle. The effect is not significant.

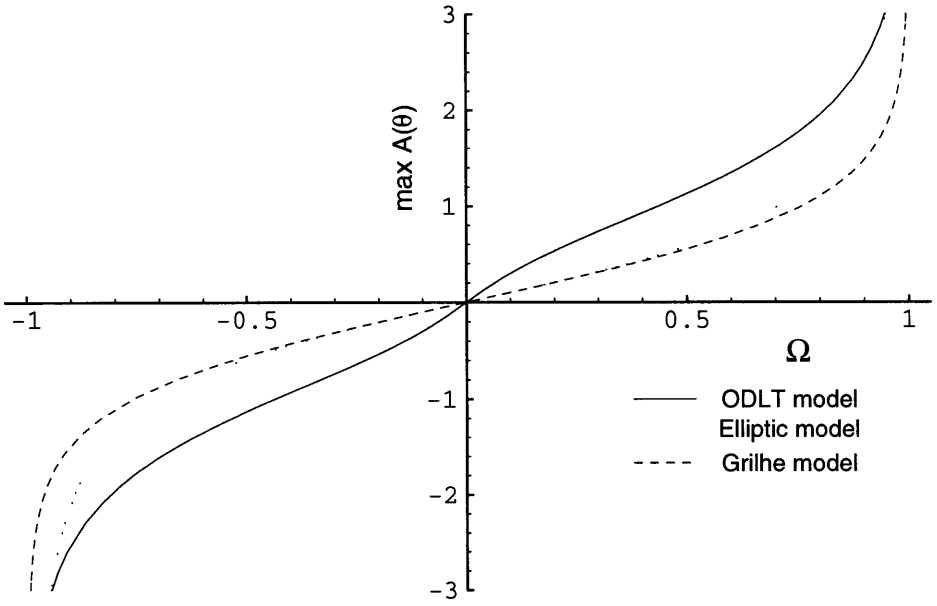

FIGURE 3. Plot of $\max[A(\theta)]$ vs. Ω for ODLT, Grilhé and elliptical loops. At small values of Ω, the ODLT analysis predicts a more canted loop. This is because the average energy per unit length of dislocation decreases as the loop increases its screw character. The models predict similar values of $\max[A(\theta)]$ at higher values of Ω.

be approximated with a friction stress term, τ_f. The dimensionless friction stress v was given in Chapter 4 as

$$v = \frac{2\pi d(1-\nu)\tau_f}{Gb}.$$

The parameter v is a ratio of the friction stress to the "intrinsic strength" of an edge dislocation. This is a useful parameter for determining the relevance of the analysis.[4] When v is less than about 5, the ODLT analysis should provide reasonably accurate predictions. When v is much greater than 5, the intrinsic strength of a loop is insignificant in comparison with the flow characteristics of the matrix. In this case, the behavior of prismatic loops will be similar to that of straight dislocation segments in the same matrix; the analysis presented above is unimportant to the mechanical properties of the material.

[4]While the self-energy of a screw dislocation would be more appropriate than of an edge dislocation as is used in the definition of v, this definition is adequate given the nature of the computation which follows.

We correct for a non-zero friction stress by substituting $\tau - \tau_f$ for τ in the definition of Ω. With this substitution,

$$\Omega = \begin{cases} \dfrac{\tau}{|\tau|} \cdot \dfrac{rb(|\tau| - \tau_f)}{W_\odot} & \text{when} \quad |\tau| - \tau_f \geq 0, \\ 0 & \text{when} \quad |\tau| - \tau_f < 0. \end{cases} \tag{18}$$

We use this definition of Ω in the experimental study. Subtracting the mean value of τ_f from τ will compensate, on average, for the effects of the real matrix on the shape of the loop. Locally, however, the effective value of the friction stress will vary from location to location because it is determined by random interactions with precipitates and solute atoms.

4. Experimental Results

4.1. Model System. In this section we compare predictions of the above analysis with experiment. To make this comparison, we measured the shape of prismatic interstitial loops in AgCl under an applied tensile stress. The loops were generated prior to the application of the external stress by thermal mismatch between the AgCl and 1-5 μm glass spheres.

The AgCl-glass system is useful for testing the theory because the loops so generated are fairly large and known to be glissile. Using the value of $\tau_f = 0.36$ MPa determined in Chapter 4, v is in the range 0.4 to 2 in this system. This suggests the ODLT analysis is appropriate for modeling loop behavior.

4.2. Effects of Crystal Anisotropy. A limitation of the ODLT analysis is that it assumes crystal isotropy. Like all cubic crystals except tungsten, AgCl is anisotropic. The magnitude of the anisotropy in such crystals is often characterized by the anisotropy factor A, where

$$A = \frac{2c_{44}}{c_{11} - c_{12}}.$$

The value of A for AgCl calculated from the elastic constants c_{11}, c_{12} and c_{44} of LOJE AND SCHUELE 1970 is given in Table 1. Also shown are values of A for a few other crystals, from HIRTH AND LOTHE 1968. Values for G

TABLE 1. Values of the anisotropy coefficient A

Crystal	Cu	Al	W	NaCl	AgCl	Nb
A	3.01	1.21	1.00	0.694	0.522	0.51

and ν were also calculated from the data of LOJE AND SCHUELE 1970, using the Voigt averaging procedure. These averaged elastic constants are:

$$\begin{aligned} G &= 8.55 \text{ GPa} \\ \nu &= 0.409. \end{aligned}$$

Starting with the work of ESHELBY ET AL. 1953, FOREMAN 1955 developed a technique for computing the energy of straight dislocations in

TABLE 2. Expressions for the energy factor K for a $\frac{1}{2}\langle 110\rangle$ screw dislocation and a $\frac{1}{2}\langle 110\rangle$, $\hat{\xi} = \langle 100\rangle$ edge dislocation.

	Isotropic	Cubic
pure screw	G	$\sqrt{\frac{(c_{11}-c_{12})c_{44}}{2}}$
pure edge	$\frac{G}{1-\nu}$	$(c_{11}+c_{12})\sqrt{\frac{c_{44}(c_{11}-c_{12})}{c_{11}(c_{11}+c_{12}+2c_{44})}}$

TABLE 3. Numerical values of the energy factor K in AgCl.

	AgCl (Isotropic)	AgCl (Cubic)
pure screw	8.55 GPa	8.66 GPa
pure edge	14.46 GPa	14.55 GPa

anisotropic solids. We did not apply this technique to the ODLT analysis because it greatly increases the complexity of the calculation. However, application of Foreman's method to a few simple dislocation configurations in AgCl suggests that a full anisotropic analysis would generate results similar to those predicted by the ODLT analysis. These calculations follow.

Foreman defined an energy factor K which replaces the elastic constants in (8) and (9). In this formulation,

$$W_{\perp} = \frac{Kb^2}{4\pi} \ln \frac{R}{r_o},$$

where K includes all dislocation orientation effects. In presenting Foreman's method, HIRTH AND LOTHE 1968 calculated K in the NaCl crystal structure for a pure screw dislocation with $\vec{b} = \frac{1}{2}\langle 110\rangle$ and a pure edge dislocation with $\vec{b} = \frac{1}{2}\langle 110\rangle$ which lies in a $\langle 100\rangle$ direction. Since AgCl is isomorphic to NaCl and has the same Burgers vector, we can apply these results directly and compare the actual values of K with those obtained from isotropic elasticity. These comparisons are presented in Tables 2 and 3.

The results from the isotropic approximation are very nearly the same as the exact results for these two cases. This suggests that the errors associated with the use of isotropic elasticity are minor for AgCl.

4.3. Micrographs. Examples of loops in their unstressed configuration are shown in Figures 4 and 5, from Sample G11. Loops which are in the plane of focus look like straight line segments in these micrographs. Examples of the effect of stress on these loops can be seen in Figures 6 and 7, from Sample G18.

4.4. Calculating σ and α. The shear stress on a loop depends on the loop's orientation with respect to the applied tensile stress. Let the reference frame of sample be described by the coordinate system e_i. In this frame,

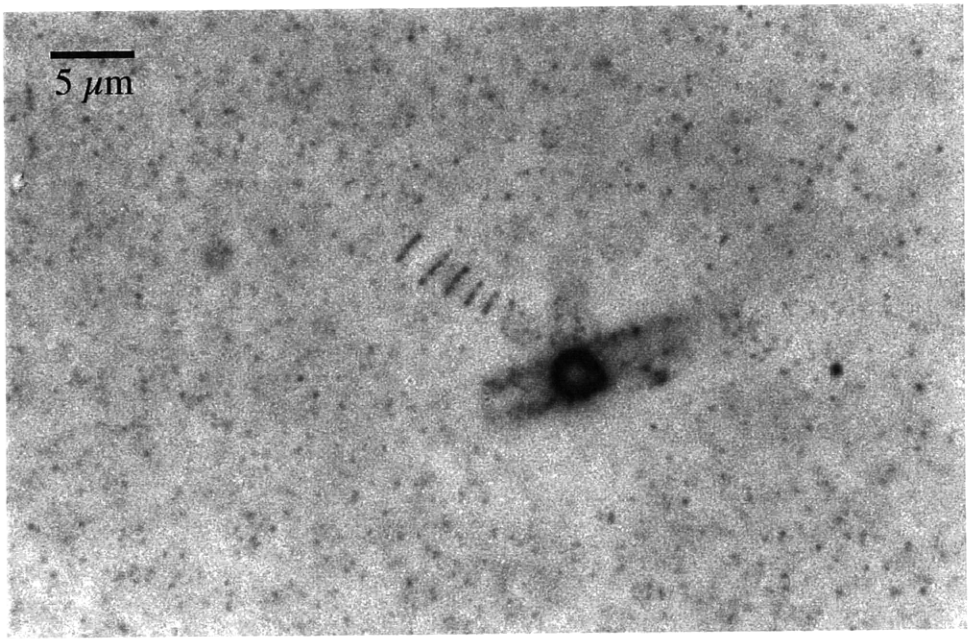

FIGURE 4. Sphere from Sample G11, applied strain = 0 MPa. Depth of sphere ≈ 22 μm.

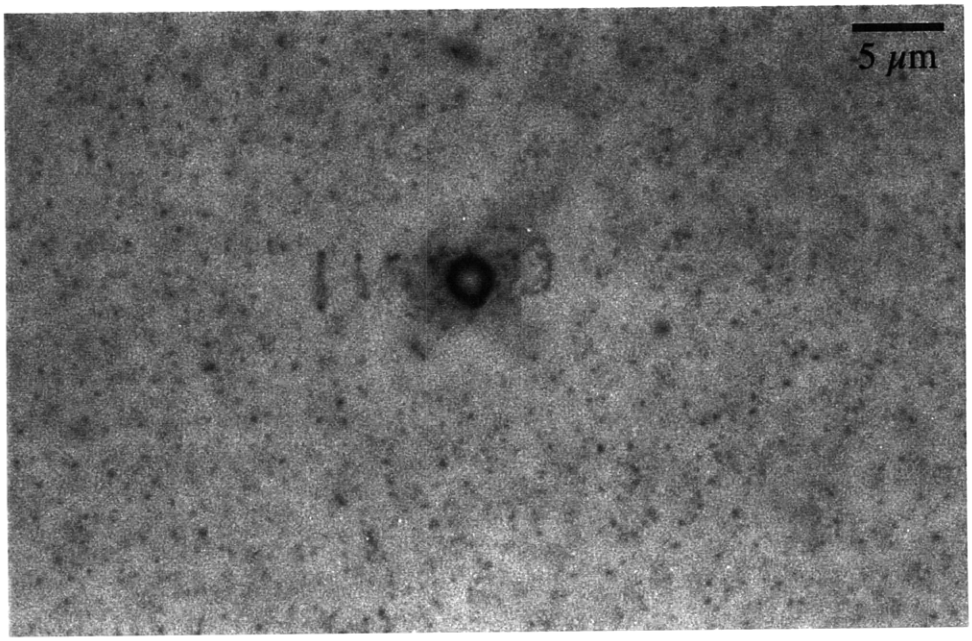

FIGURE 5. Sphere from Sample G11, applied strain = 0 MPa. Depth of sphere ≈ 9 μm.

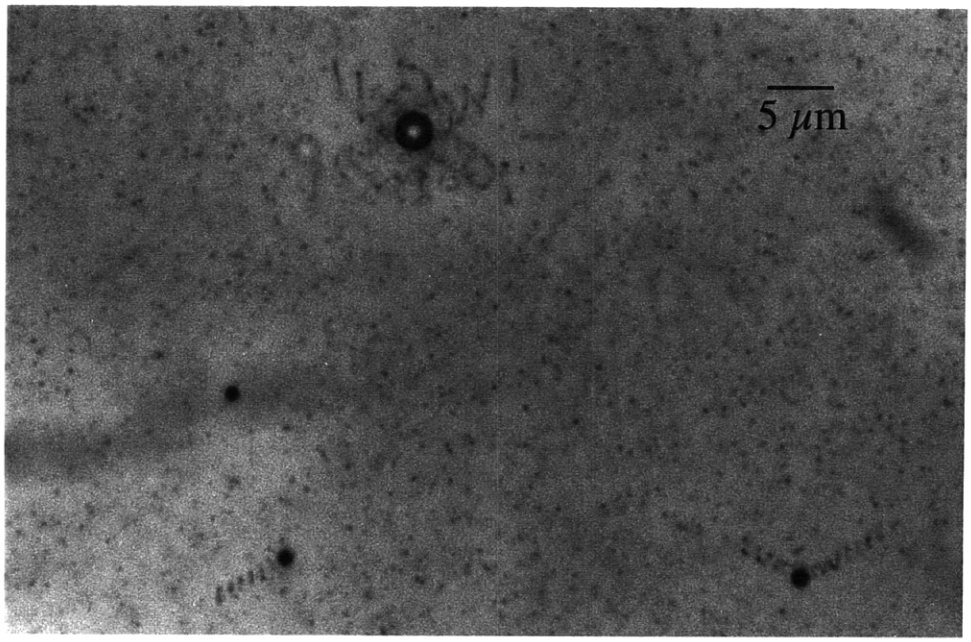

FIGURE 6. Dislocation loops canting under an applied stress. Loading direction is left-right. Far-field stress is approximately 2.08 MPa. The shear stress varies as $\sin 2\omega$, where ω is the angle which $\vec{b}$ makes with the loading direction.

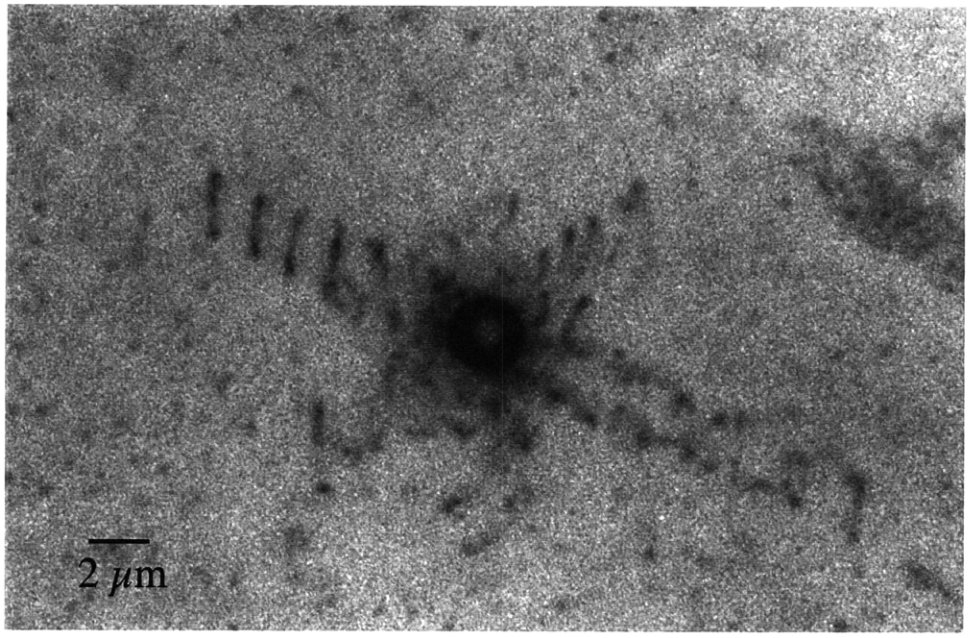

FIGURE 7. Dislocation loops canting under an applied stress of approximately 2.08 MPa. Loading direction is left-right.

the tensile load is applied along e_3 and the microscope axis is parallel to e_2. The stress tensor $\boldsymbol{\sigma}$ is

$$\boldsymbol{\sigma} = \begin{bmatrix} 0 & 0 & 0 \\ 0 & 0 & 0 \\ 0 & 0 & \sigma_{33} \end{bmatrix}.$$

Next, define an angle ω to be the angle between $\hat{z}$ in the loop frame and the loading direction $\hat{e}_3$. Define a second angle ϕ to be the angle between $\hat{e}_2$ and the projection of $\hat{z}$ against the plane defined by $\hat{e}_3$. These angles are similar to the definitions of latitude (ω) and longitude (ϕ) on a globe with the load applied along the polar axis. Using these angles, we can write the original xyz coordinate system of the ODLT analysis in terms of the reference frame by defining basis vectors $\hat{e}'_i$. The $\hat{e}'_i$ are defined as

$$\hat{e}'_1 = \begin{bmatrix} \cos\phi \sin\omega \\ \sin\phi \sin\omega \\ -\cos\omega \end{bmatrix}, \quad \hat{e}'_2 = \begin{bmatrix} -\sin\phi \\ \cos\phi \\ 0 \end{bmatrix}, \quad \hat{e}'_3 = \begin{bmatrix} \cos\phi \cos\omega \\ \sin\phi \cos\omega \\ \sin\omega \end{bmatrix},$$

for $\hat{e}_3 \geq 0$. Basis vectors for $\hat{e}_3 < 0$ are $\{-\hat{e}'_1, -\hat{e}'_2, \hat{e}'_3\}$.

If we define the direction cosines $L_{ij} = \hat{e}'_i \cdot \hat{e}_j$, then $\boldsymbol{\sigma}' = L \cdot \boldsymbol{\sigma} \cdot L^{-1}$, so

$$\boldsymbol{\sigma}' = \frac{\sigma_{33}}{2} \begin{bmatrix} 2\cos^2\omega & 0 & -\sin 2\omega \\ 0 & 0 & 0 \\ -\sin 2\omega & 0 & 2\sin^2\omega \end{bmatrix}.$$

Then, from (5) and (6),

$$\begin{aligned} \tau &= -\frac{\sigma_{33}}{2} \sin 2\omega \\ \alpha &= 0. \end{aligned}$$

The southern hemisphere is obtained by reflection. Since b is negative for interstitial loops, Ω is positive.

4.5. Data Selection. To minimize the complicating influence of the glass sphere and neighboring loops, we collected data only from the outermost solitary loops in a loop train. Figure-eight loops, helical structures, and incompletely formed loops were excluded, as were loops which were close to a grain boundary or intersected by slip bands.

The applied stress was determined from the applied strain and the stress-strain curve given in Chapter 1.

4.6. Measurements. Under the stress state given, the loop reaches its maximum extent at $A(0)$. All three models predict a loop shape that is not too different from an ellipse; hence, the easiest way to measure $\max[A(\theta)]$ is to measure the angle that the loop makes with the plane defined by $\hat{e}'_3$. When the microscope axis is parallel to $\hat{e}'_2$, this angle can be measured directly since the semimajor axis of the real loop lies in the focal plane of the microscope. In general, however, the loop's semimajor axis does not

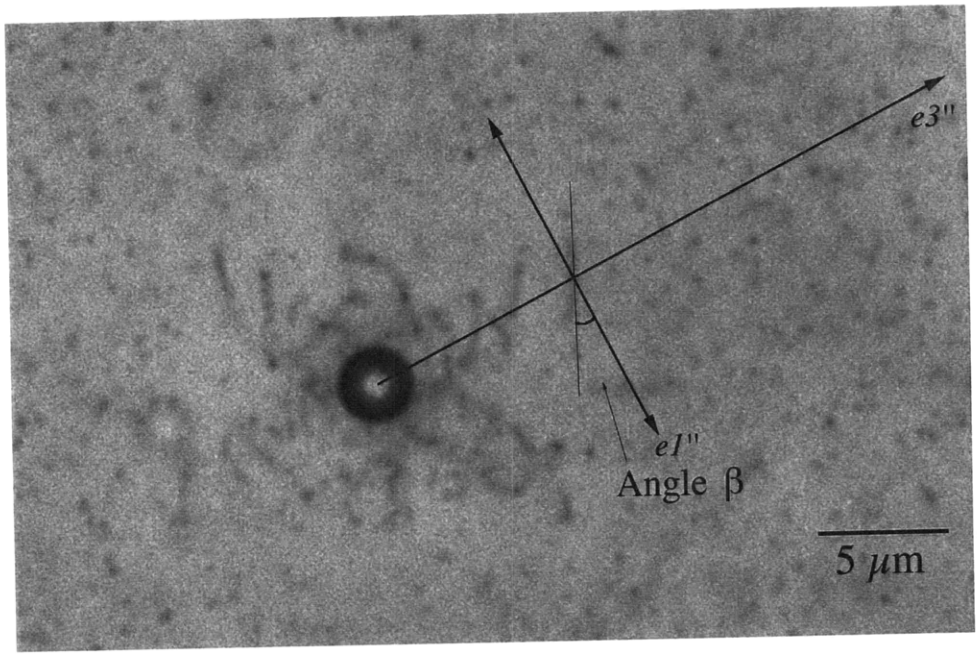

FIGURE 8. Coordinate system used for making measurements. The basis vector $\hat{e}_3''$ is drawn from the center of the sphere outwards through the center of the glide cylinder. Taking e_2'' to be into the plane of the paper, $\hat{e}_1'' = \hat{e}_2'' \times \hat{e}_3''$. The angle β is defined to be that between $\hat{e}_1''$ and the semimajor axis of the projected ellipse.

lie in the focal plane and the measurement needs to be corrected for the position of the observer.

This process is as follows. First, rewrite the equation of the loop in a coordinate system defined by the projection of the $\hat{e}_i'$ onto the plane defined by $\hat{e}_2$. We obtain

$$s''(\theta) = M \cdot s(\theta),$$

where $M_{ij} = \hat{e}_i'' \cdot \hat{e}_j'$ and, with $k = 1/\sqrt{\cos^2\phi\cos^2\omega + \sin^2\omega}$, the basis vectors $\hat{e}_i''$ are

$$\hat{e}_1'' = k \begin{bmatrix} \sin\omega \\ 0 \\ -\cos\phi\cos\omega \end{bmatrix}, \quad \hat{e}_2'' = \begin{bmatrix} 0 \\ 1 \\ 0 \end{bmatrix}, \quad \hat{e}_3'' = k \begin{bmatrix} \cos\phi\cos\omega \\ 0 \\ \sin\omega \end{bmatrix}.$$

This coordinate system represents what is actually seen in the microscope. The maximum extent of the loop in the $\hat{e}_i''$ frame, $\max[A(\theta)_{\text{apparent}}]$, occurs at $s_1''(\theta) = 1$. Since $\max[A(\theta)_{\text{apparent}}] = \tan\beta$, in practice we measure the angle β that the loop makes with $\hat{e}_1''$. (See Figure 8.)

In the $\hat{e}_i'$ frame, the maximum value of the ellipse occurs at $\theta = 0$. For the projected loop, the maximum occurs at $\theta = \gamma$, where γ is an angle.

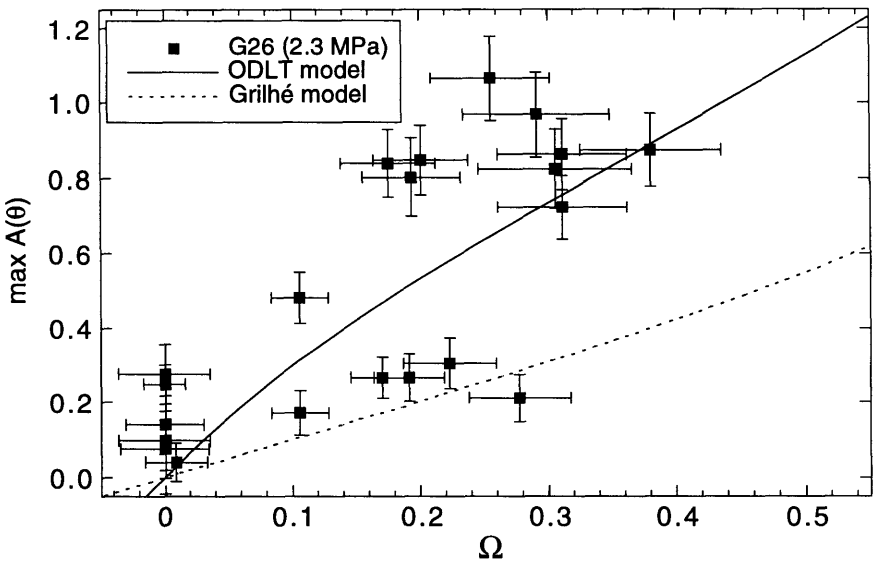

FIGURE 9. Real values of $\max[A(\theta)]$ determined from sample G26, loaded to an applied strain of 2.3 MPa. (Error bars indicate the estimated errors of the measurements.)

We first solve numerically for γ, a function of ω and ϕ only. Once γ is determined, since

$$\max[A(\theta)_{\text{apparent}}] = s_3''(\gamma),$$

we can solve numerically for the true value of $\max[A(\theta)]$.

4.7. Results. We calculate values of Ω using the definition of Ω given in (18), computing the applied stress from the bulk stress-strain curve and taking the flow stress $\tau_f = 0.36$ MPa. The results are given in Figure 9.

There is considerable scatter in the data. Similar measurements made on an unstrained sample (where Ω is assumed to be zero) are given in Figure 10 and show similar variability. This variability is likely due to pinning of the loops by obstacles in the matrix as they glide away from the sphere under the influence of the thermal misfit stress. Such interactions are "random" and no more likely to result in positive canting than negative canting. (The average value of $\max[A(\theta)]$ for the seven points in Figure 10 is in fact close to zero.) Hence, it is reasonable to average the results so as to look for a net influence of the applied stress.

We averaged the data in Figure 9 by dividing the data into five equally spaced groups ($\Delta\Omega = 0.1$) and calculating the mean of the points in each group. The averaged data is presented in Figure 11. There is only one data point in the 0.35 to 0.45 range, and only two in the 0.05 to .15 range, which limits our confidence in the result. Nevertheless, the data are consistent

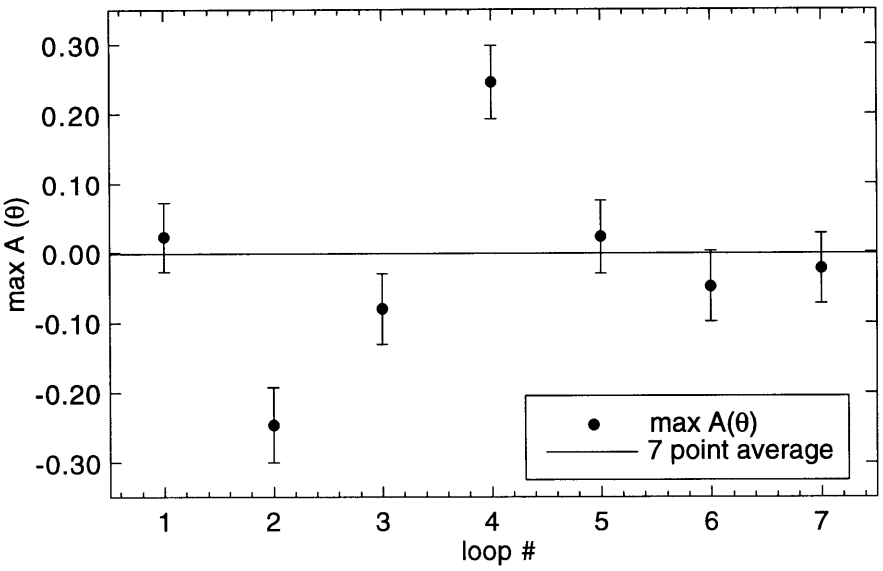

FIGURE 10. Variation in values of max$[A(\theta)]$ in seven loops from an unstrained sample, G11. The straight line in the figure represents the seven-loop average. (Error bars indicate the estimated errors of the measurements.)

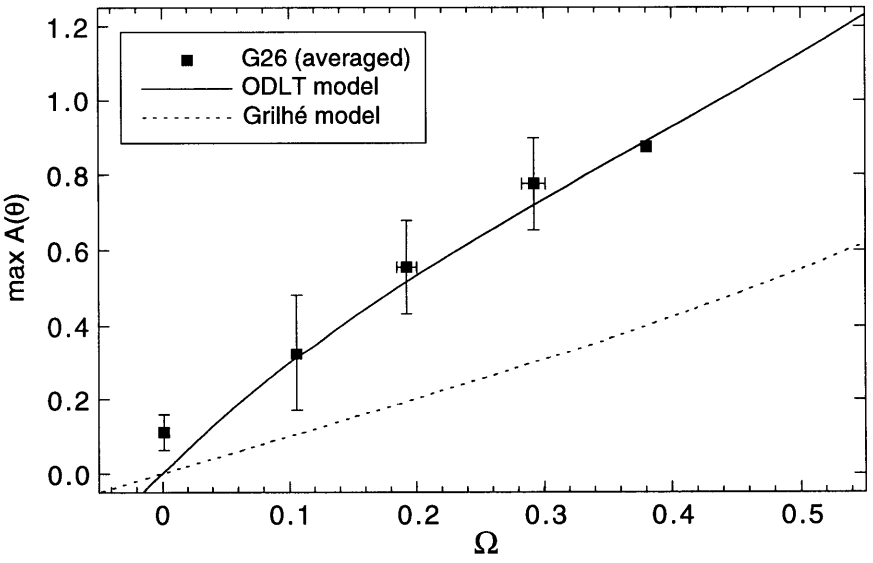

FIGURE 11. Data from Figure 9 averaged as described in the text. (Error bars represent the standard error of the mean.)

with the ODLT model, which predicts higher values of $\max[A(\theta)]$ at given values of Ω than Grilhé's model.

5. Conclusion

In this chapter, we presented an analysis of the shape of a prismatic loop under stress and compared the predictions to measurements made on interstitial loops in AgCl. The experimental results fit the current model, in which the orientation dependence of a dislocation's line energy is considered, better than Grilhé's model, in which the line energy is taken to be constant. Both models predict that prismatic loops can cross slip and leave their glide cylinder when the value of the dimensionless stress parameter $\Omega = 1$. In terms of resolved shear stresses, the critical stress for cross-slip is approximately $\tau^* = Gb/r$.

In the following chapter, we consider the possibility that these cross-slipped loops nucleate slip bands in polycrystals.

CHAPTER 6

Origins of Slip in Inclusion-Containing Polycrystals Under Small Tensile Strains

1. Introduction

As discussed in Chapter 1, the origin of slip in metals has been of interest for more than 60 years. Some of the most informative experimental work has been conducted on silicon iron,[1] which has a high yield stress and in which dislocations can be studied using the etch-pit technique. CARRINGTON AND MCLEAN 1965 studied the nucleation of slip bands in silicon iron below its bulk yield stress. While the earlier silicon iron work of STEIN AND LOW 1960 and SUITS AND CHALMERS 1961 led those researchers to suggest that slip initiates on inclusions in grain interiors, CARRINGTON AND MCLEAN 1965 suggested that the distribution of slip bands in their samples indicated that slip begins at grain boundaries.

Today, there is general agreement that grain boundaries are an important source of dislocations in unreinforced polycrystals (see MEYERS AND ASHWORTH 1982). Nevertheless, the relative importance of grain boundaries and inclusions in the nucleation of slip needs further study. In particular, we expect that as the volume fraction V_f of the inclusion phase increases, the importance of inclusions in the slip nucleation process should also increase. At present, there are few quantitative studies of the nucleation process at any value of V_f, so little can be said about the inclusion concentrations required to bring about a significant change in the mechanical behavior of a polycrystal.

For these reasons, we re-address the role of hard inclusions in the nucleation of slip. The experimental system used is polycrystalline silver chloride which contains glass spheres and particles. In contrast to the experimental work of previous researchers, these inclusions were added intentionally. As a result, they are of known composition and, in the case of the spheres, known size and shape. The transparency of silver chloride allows interactions between inclusion and slip band to be observed below the surface of the sample, an important advantage over etch-pitch studies. In what follows, we present both qualitative and quantitative observations on the role of inclusions in the earliest stages of polycrystalline plastic deformation. Specifically, we try

[1]This alloy, 3 to 4% silicon in iron, has a BCC crystal structure and is used in transformer cores and other magnetic applications (CHEN 1986).

to determine what factors determine where the first slip bands form as a load is applied to the polycrystal.

2. Experimental

2.1. Experiments Performed. All samples used for the experimental work were taken from the same homogenized ingot of doped silver chloride,"Ingot G," and all were tested in the fully recrystallized state.[2] Tensile strains were applied using the beam-bending rig described in Chapter 3. Samples were decorated while under load, ensuring that the dislocations were pinned in their "stressed" configuration. The strain rates applied during the bending tests were on the order of 50–100 $\mu\epsilon$/sec, within a factor of 4 of the strain rate used in the bulk tensile tests presented in Chapter 3.

Five samples were tested to strains between 100 $\mu\epsilon$ and 200 $\mu\epsilon$ as shown in Table 2.1. Values of the applied stress and plastic strain are estimates calculated from the stress-strain curve.

TABLE 1. List of experiments performed.

Sample I.D.	Applied Strain ϵ_t	Plastic Strain ϵ_p	Calculated Stress σ
G18	97 $\mu\epsilon$	10 $\mu\epsilon$	2.08 MPa
G41	137 $\mu\epsilon$	45 $\mu\epsilon$	2.22 MPa
G4	190 $\mu\epsilon$	94 $\mu\epsilon$	2.31 MPa
G26	191 $\mu\epsilon$	95 $\mu\epsilon$	2.31 MPa
G2	206 $\mu\epsilon$	109 $\mu\epsilon$	2.33 MPa

2.2. Data Collection Methods. Quantitative data were collected on one sample, Sample G41. Data were collected from Regions 1 and 2 as shown in Figure 1. The data collection procedure was as follows: select a region of the sample, then for each grain that is at least partially contained in the selected region, measure the following in the top 41.1 μm of the sample.[3]

- For each grain, we noted:
  - The grain's perimeter, area, and centroid.
  - The number of triple junctions.
  - The presence of slip bands.
- For each inclusion, we noted:
  - The type of inclusion (sphere/particle).
  - The diameter (spheres) or major and minor projected axes (particles).
  - Whether the inclusion was intersected by a grain boundary or was fully contained in one grain.
  - Whether the inclusion touched the surface or not.

[2]All samples were annealed at temperatures above 570 K.

[3]At 546 nm, the refractive index of AgCl is 2.079 and that of immersion oil 1.518. The correction factor is the former divided by the latter, so 30 ± 0.5 μm of stage motion corresponds to an examined depth of 41.1 ± 0.7 μm.

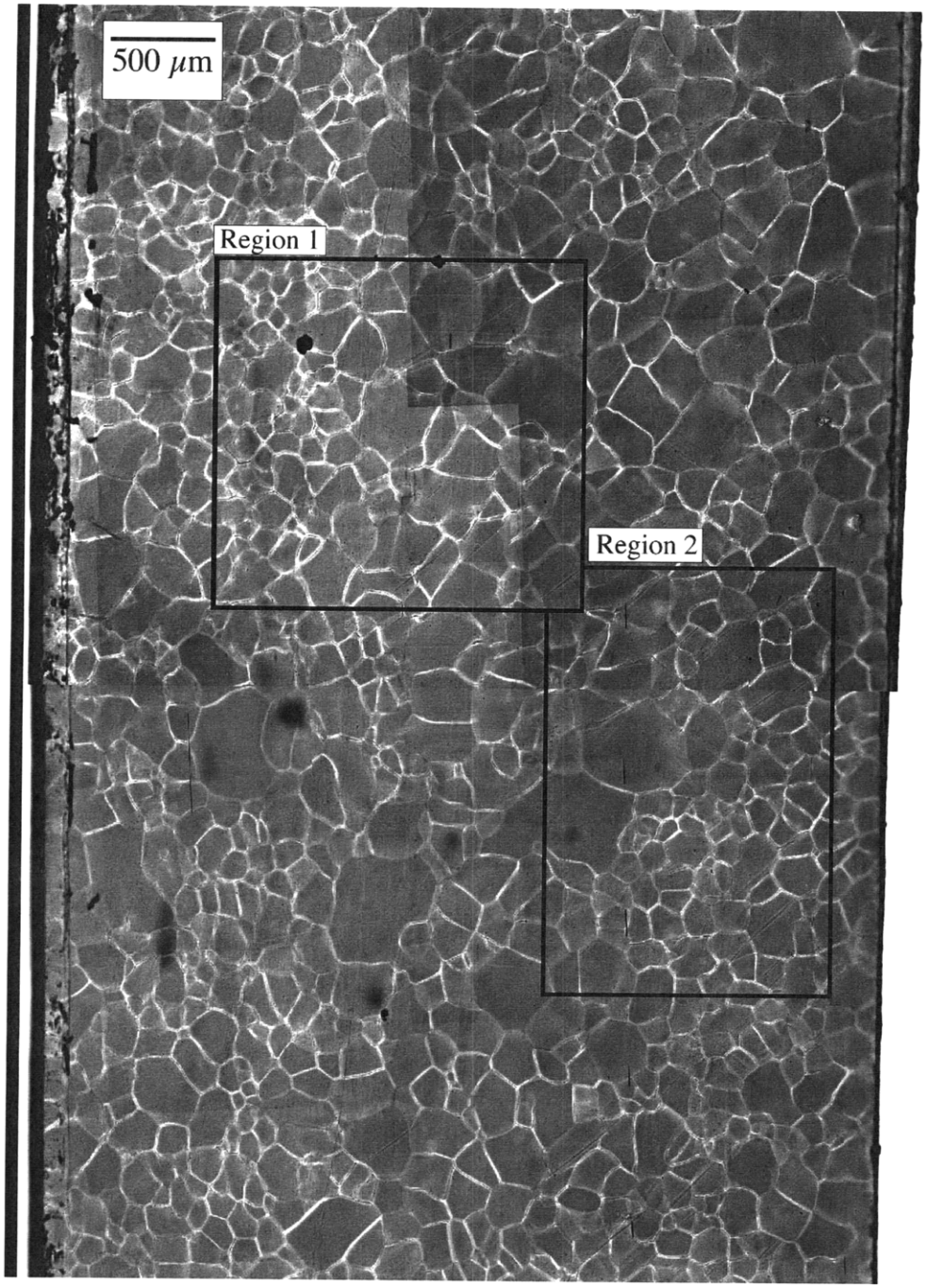

FIGURE 1. Section of Sample G41 showing Regions 1 and 2 from which quantitative data were measured. This photo shows the full width of the sample but only about 30% of the gauge length. Direction of the applied stress in this photo is up-down.

  - Whether the inclusion was isolated or part of a cluster.
  - Whether thermal misfit dislocations were present or not present.
  - Whether the inclusion was in a slip band. If so, the slip band identifier was noted.
- For each slip band, we noted:
  - The width and length of the band. If the width was not constant, we measured the area of the band. Since slip bands appeared to retain their shape through the depth of the measured region, the volume of a slip band was taken to be its area times the thickness of the sampled volume.
  - The number of triple junctions intersected by the slip band.
  - The angles which the slip band made with the grain boundaries at its endpoints.

All length measurements were calibrated against micrographs of a 1000 line per inch nickel mesh obtained from Ladd Research. Quantitative measurements of grain shape were made from a mosaic of video frames grabbed at 100× magnification using the image processing software *IPLab*. The grain perimeter was approximated by the perimeter of a polygon chosen to follow the grain boundary closely.[4]

Measurements of particle size were made on the video screen (magnification approximately 2400×) using an overlay of calibrated circles sized to measure diameters from 1 to 6.5 μm in 0.5 μm increments. Measurements of larger particles and slip band widths were made with a ruler against the video screen. Slip band lengths were measured made using *IPLab*.

The particle counting statistics can be assumed accurate in all size ranges except the 0.5 μm category. The submicron particles were numerous and easy to miss; it is likely that a significant number of particles of this size went uncounted.

Error estimates for these measurements are given in Table 2.2.

TABLE 2. Measurement Error Estimates

Measurement	Error Type	Error
sampled thickness	absolute	$\pm 0.7\mu$m
sphere diameter	absolute	± 0.5 μm
slip band width	relative	$\pm 18\%$
slip band length	relative	$\pm 0.6\%$
grain areas	relative	$\pm 2.8\%$

3. Qualitative Observations

[4]The goal of this process was to estimate the perimeter using the standard Euclidean metric. The blob analysis perimeter measurement of *IPLab* uses a Manhattan metric (CARTER ET AL. 1997) which follows the pixelated border of the selected blob.

3.1. General. At these small levels of plastic strain, slip was highly inhomogeneous. Large portions of some grains were slipped while other grains remained entirely elastic.

The propagation of many dislocations on a single slip plane results in a *slip band.* The propagation of a single shear loop across a crystal or grain results in a *slip line* on the surface or crystal boundary. Slip bands can be seen on the surface of metals with an optical microscope; slip lines generally cannot because the displacement is too small. In decorated AgCl, slip bands were readily distinguished because of the large number of dislocations decorated through the volume of the band. Slip lines could be seen if trapped within the decorated volume of the crystal. These were rare; nearly all dislocations in the slipped regions were in the form of slip bands. The high contrast between slip bands and the surrounding crystal allowed grains to be relatively unambiguously divided into "slipped" and "unslipped" regions and the volumes of each measured.

Nearly all slip bands made contact with a grain boundary at least at one end. Most slip bands propagated entirely across a grain, contacting a grain boundary at both ends. Often, a slip band in one grain was continued by a slip band in a neighboring grain. In some grains, several slip bands were observed; in many cases these other slip bands were not on the same slip system. In some cases slip bands on different slip systems intersected grain boundaries at the same location. Slip bands in samples tested to higher levels of plastic strain were wider than those in samples tested to lower levels of plastic strain. Larger grains appeared to be more likely to deform plastically than smaller grains at a given applied stress. As the stress was increased, the fraction of grains slipped and the fraction of each grain covered by slip bands increased.

These observations agree with the etch-pit study of CARRINGTON AND MCLEAN 1965. Below, we discuss five potential sources of slip in greater detail:

- propagation of plastic deformation from neighboring grains.
- expansion of "free" dislocation loops around inclusions.
- Frank-Read sources in grain interiors.
- grain boundaries, especially grain boundaries formed by the intersection of three grains (triple junctions).
- free surfaces.

3.2. Propagation of Slip from Neighboring Grains. An example of slip nucleation due to plastic compatibility considerations is shown schematically in Figure 2 and in a photograph in Figure 3. A higher magnification photo of slip band propagation from one grain to the next is given in Figure 4. Slip bands are easy to identify in the microscope at this magnification because one can adjust the plane of focus up and down and follow

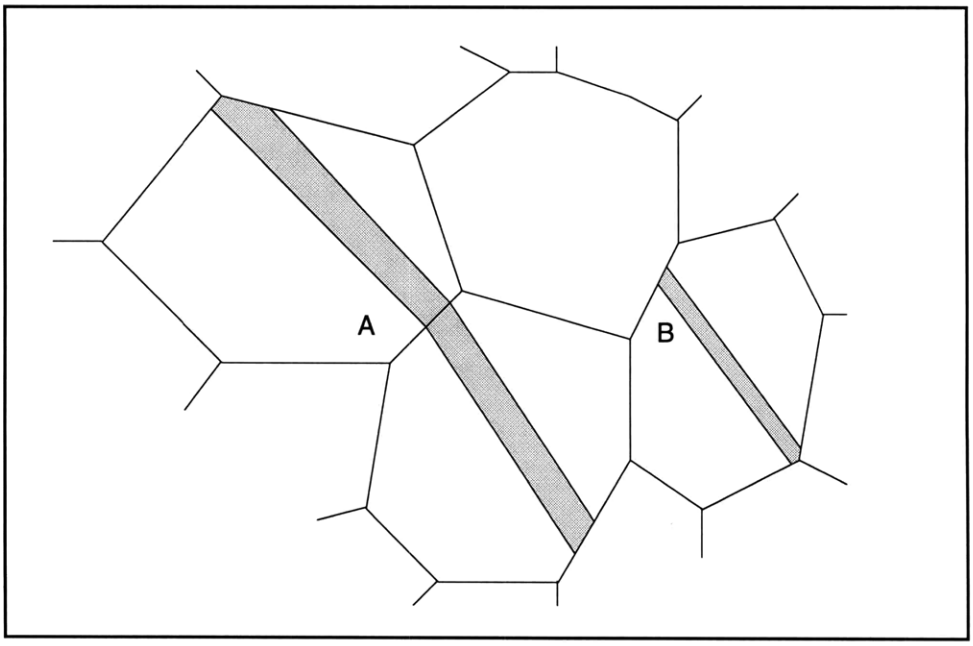

FIGURE 2. Schematic of slip bands in polycrystal. Slip propagates from one grain to another at "A." It is not possible to tell which of the two bands slipped first. At "B" a single slip band does not propagate into neighboring grains.

the dislocation lines. In any one still image, only short segments of dislocations are visible; this makes images such as Figure 4 much more difficult to interpret.

Nucleation of a slip band in one grain by a slip band in a neighboring grain is clearly an important mechanism. Even when the overall level of deformation is low, a significant fraction of slip bands are nucleated by propagation of slip from neighboring grains. There is not any obvious way to determine which grain initiated a slip band that passes through two or more grains. For this reason, even though we are primarily interested in factors leading to the nucleation of the initial slip bands, no attempt was made to filter out those slip bands which were likely nucleated by slip in a neighboring grain. The disadvantage of this approach is that it weakens any potential correlation between microstructural features and the initial occurrence of slip. The advantage is that no bias is introduced by the observer.

3.3. Free Dislocation Loops as Slip Sources. In Chapter 4, we presented data on the number, size, and distribution of free prismatic dislocation loops around hard spherical inclusions due to thermal misfit. In Chapter 5, we presented a model for the shape of prismatic loops under an applied stress, with the result that these loops should cross slip at a critical value of the dimensionless stress parameter $\Omega = 1$. Possible examples

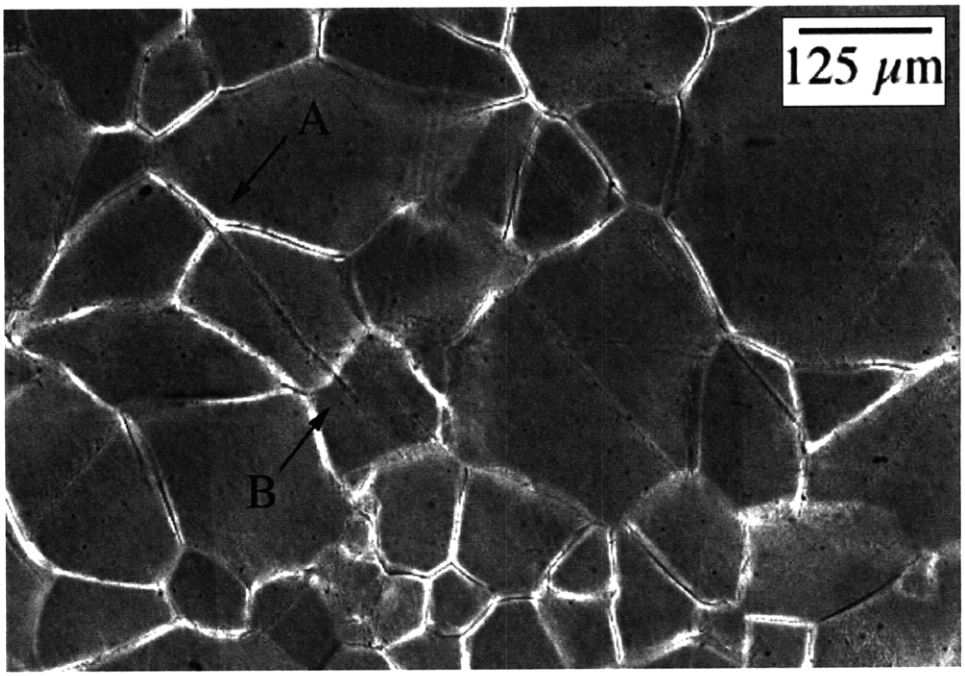

FIGURE 3. Photo from Sample G41 ($\sigma = 2.22$ MPa) showing slip band contacting triple junction at "A" and propagation of slip from grain to grain at "B."

of just-critical loops are shown in Figure 5. In the model, the probability of finding a just-critical loop is very small because as soon as $\Omega = 1$, the loop can expand across the grain. In a real material, where the stress is not necessarily uniform, such events might be easier to find. For example, the stress state around an inclusion will be higher than that in the bulk of the material; this could create an $\Omega > 1$ condition near the inclusion that does not extend beyond a few inclusion radii.

Once a free dislocation loop cross slips, it will expand across the crystal leaving a slip line on the boundary of the crystal or grain. If this loop were to multiply under the action of the applied stress (via multiple cross-slip or otherwise) it should form a slip band. A possible example of a slip band created by this process is shown in Figure 6.

Examples such as shown above do not prove that inclusions initiate slip; the intersection of slip band and inclusion shown could have been the result of chance interaction. We seek a way to study systematically the relationship between inclusions and the first slip bands which form.

Consider the earliest stages of plastic deformation, when the fractional volume slipped is much less than one. If we were to assume that free loops around inclusions are the *only* sources of dislocations, then the crystal should remain fully elastic until these inclusion sources activate. The first slip bands would form at the largest inclusions and spread outwards to the boundaries

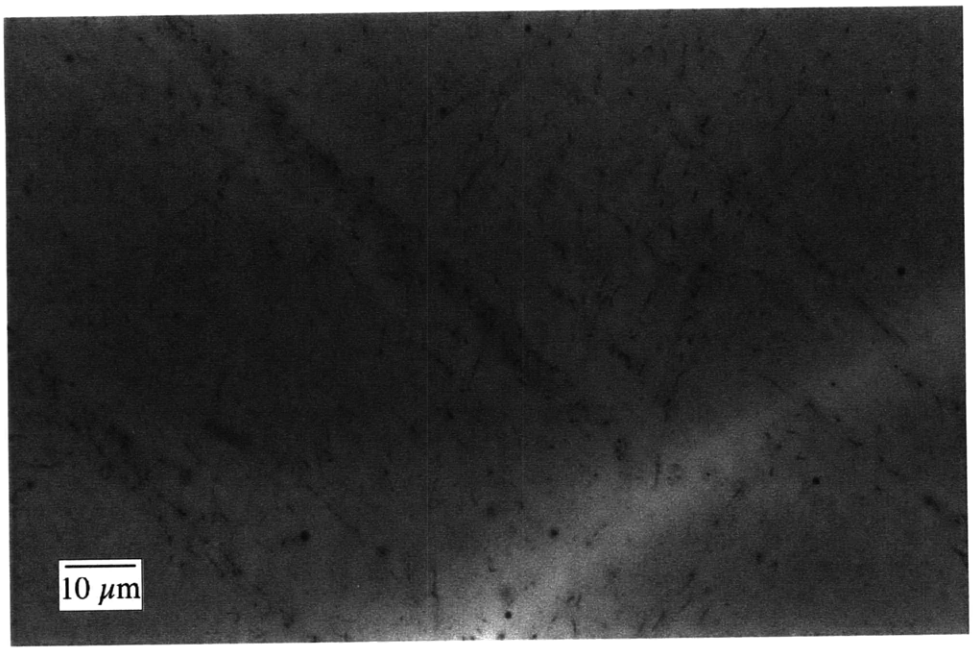

FIGURE 4. Photo of slip bands propagating across a grain boundary. The grain boundary is the lighter line in the lower right corner of the photograph.

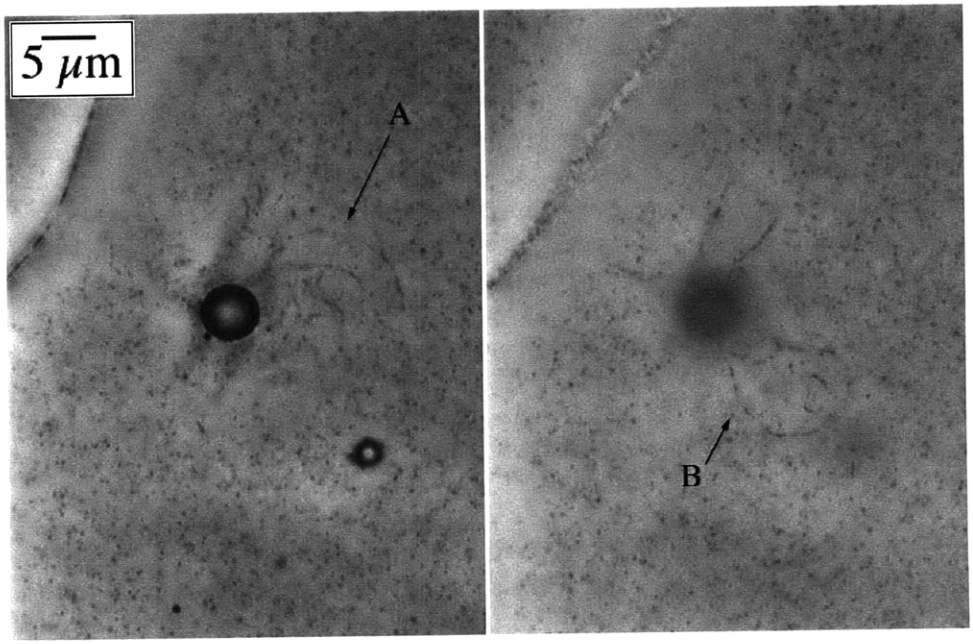

FIGURE 5. Possible just-critical loops at "A" and "B." The calculated value of Ω is approximately 0.97. Loading direction is left-right, $\sigma = 2.2$ MPa.

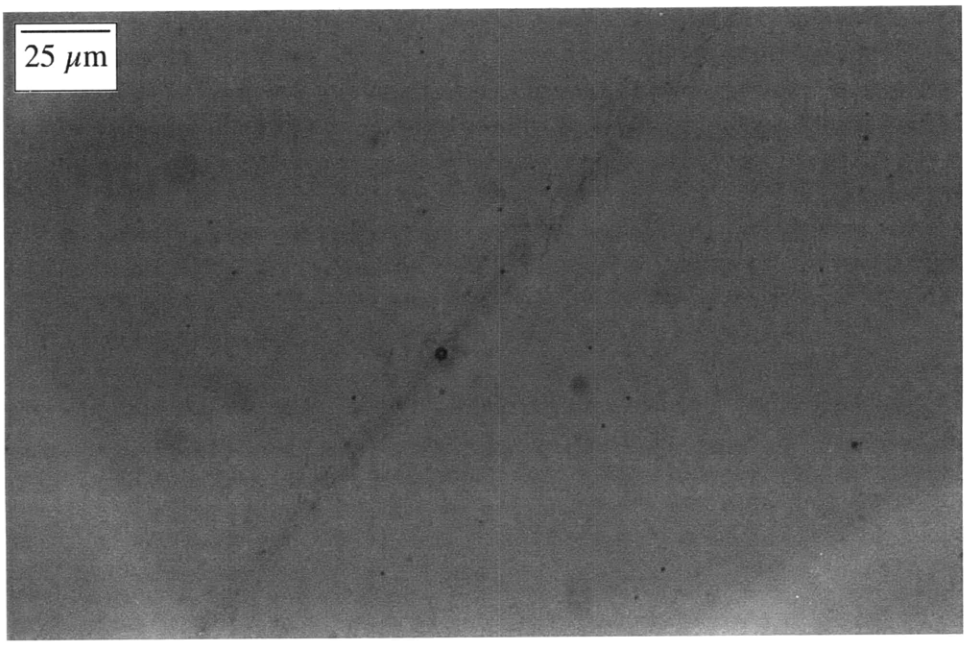

FIGURE 6. Slip band intersecting a sphere of approximately 2.5 μm in diameter. Load of 2.3 MPa applied in the left-right direction.

of the grain, resulting in a higher concentration of large inclusions in the slipped regions than in the crystal as a whole. Statistically, we would find the occurrence of slip to be positively correlated with the presence of inclusions. On the other hand if *other* sources of slip were to activate at stresses below those required to activate inclusion sources, or if expanding slip lines cannot multiply into slip bands, the concentration of inclusions in the slipped region should be about the same as the overall concentration. In this case, we would find the occurrence of slip to be independent of the presence of inclusions.

Such a test of independence is useful even in absence of a perfect model; while the exact mechanism described above may be inaccurate since the effects of both thermal residual and elastic incompatibility stresses around the inclusion have been ignored, a slip band which nucleates at an inclusion can be reasonably assumed to contain that inclusion. Hence, a test of independence between slip bands and inclusions which can show positive correlation (inclusions encourage nucleation of slip), negative correlation (inclusions suppress nucleation of slip), or no correlation (inclusions play no role in the nucleation of slip) is helpful given the lack of experimental data in the literature at even this level of generality. This is our primary method of analyzing the experimental data.

3.4. Frank-Read Sources. The $\Omega = 1$ criterion developed in Chapter 5 corresponds to a critical resolved shear stress of approximately Gb/r for a dislocation loop of radius r. This is approximately the same stress required

to activate a Frank-Read source formed by the pinning of a dislocation between two particles at spacing r. Thus, larger Frank-Read sources will activate at lower stresses than smaller ones. At the low applied strains used in this study, active Frank-Read sources would have to be larger than about 3–5 μm. Features of this size are readily seen with the dislocation decoration technique.

No such Frank-Read sources were observed. Their contribution to the nucleation of slip cannot be completely ruled out because, while a source of this size would be easily recognized when in the plane of the microscope, most of the slip bands studied were of an orientation that would require a source to be roughly perpendicular to the plane of observation.

Inactive pinned dislocation segments, on the other hand, should exist and should be visible at many orientations. No such segments were seen; hence, we have no evidence for the existence of Frank-Read sources in grain interiors. Consequently, these sources are not considered further.

3.5. Grain Boundaries. As shown in Chapter 1, there is considerable evidence that plastic deformation initiates at grain boundaries in polycrystals. The slip direction and, to a lesser extent, slip plane, are defined by the grains' crystallographic orientation. According to the work of Margolin and co-workers, (e.g., HASHIMOTO AND MARGOLIN 1983a) the slip plane on which the resolved shear stress is highest (not necessarily that with the highest Schmid factor) is the plane on which plastic deformation begins. This model predicts that slip bands form at locations where the resolved shear stress is greatest. These bands would incorporate inclusions only through chance interactions, so slip bands and inclusions would be independent.

Plastic deformation might initiate at locations on grain boundaries which are under high stress due to elastic incompatibility considerations. Triple junctions, linear features created by the intersection of three grains, have been shown to have stress concentrations of this type. (See Chapter 1.)

Triple junctions are likely to be important because, unlike the stress concentration caused by an inclusion embedded in a grain boundary, the stress concentration can take the form of a linear stress singularity like that at a crack tip. This is a favorable boundary condition for loop nucleation (See Figure 7). A larger amount of strain energy is relieved by an expanding dislocation in this case than in the case when the stress concentration is a point source. The boundary condition is also favorable for loop nucleation; the loop can expand as a shear loop without any cross slip.

These factors suggest that triple junctions could be important early sources of slip. In this model slip would begin at triple junctions in the boundary and cross the grain in manner determined by the far-field stress and the crystallographic orientation of grain. Hence, we would expect to find a correlation between slip bands and triple junctions, but no correlation between slip bands and inclusions.

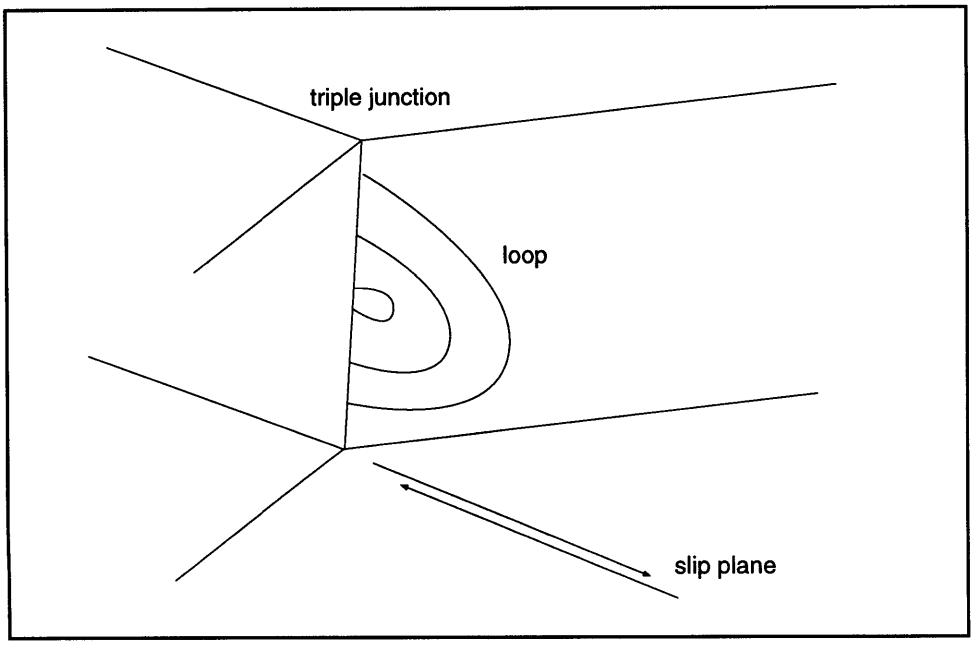

FIGURE 7. Schematic of a loop nucleated at a triple junction. Triple junctions have the stress concentrations, potential nucleation sites, and boundary conditions suitable for loop nucleation.

A photo illustrating a potential triple junction source is given in Figure 8. Here, the slip band intersects a triple junction and not a nearby sphere. Another possible example of triple junction activity is given in Figure 9. In this photo, a triple junction appears to have nucleated dislocations in two grains while having no effect on a third. Two rows of prismatic loops are also visible emerging from the triple junction.

It is possible that the prismatic loops in Figure 9 are artifacts of the decoration technique. Since grain boundaries are good sinks for photolytic silver, silver particles grow rapidly in these locations. Misfit is generated by the precipitation process; this misfit might cause prismatic dislocation punching. Similar features were occasionally observed in unstrained samples, especially when small glass inclusions were present in the boundary. Regular (shear) dislocations, however, were never seen emanating from the boundary in unstrained samples which suggests that these dislocations are not artifacts.

Figure 10 shows a triple junction just beginning to operate as a dislocation source. This photograph suggests that active triple junction sources might be able to generate very large numbers of dislocations.

3.6. Other Sources of Slip. Other features which could be sources of slip include free surfaces and surface damage. Surface damage should cause

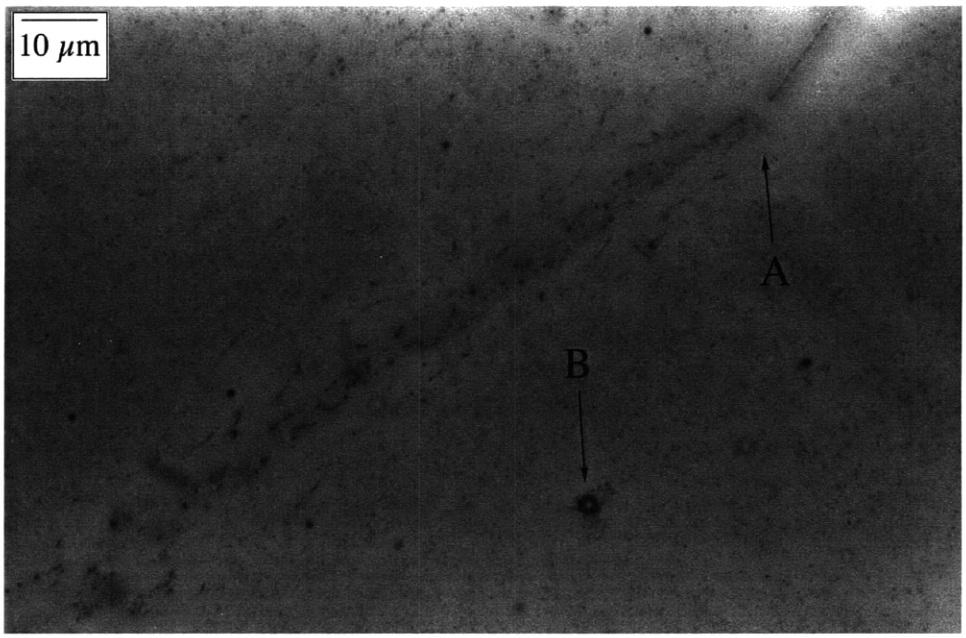

FIGURE 8. Slip band in AgCl loaded to 2.2 MPa. Stress direction is left-right. Triple junction at "A" potentially nucleated the slip band. Inclusion at "B" is not contained within the slip band.

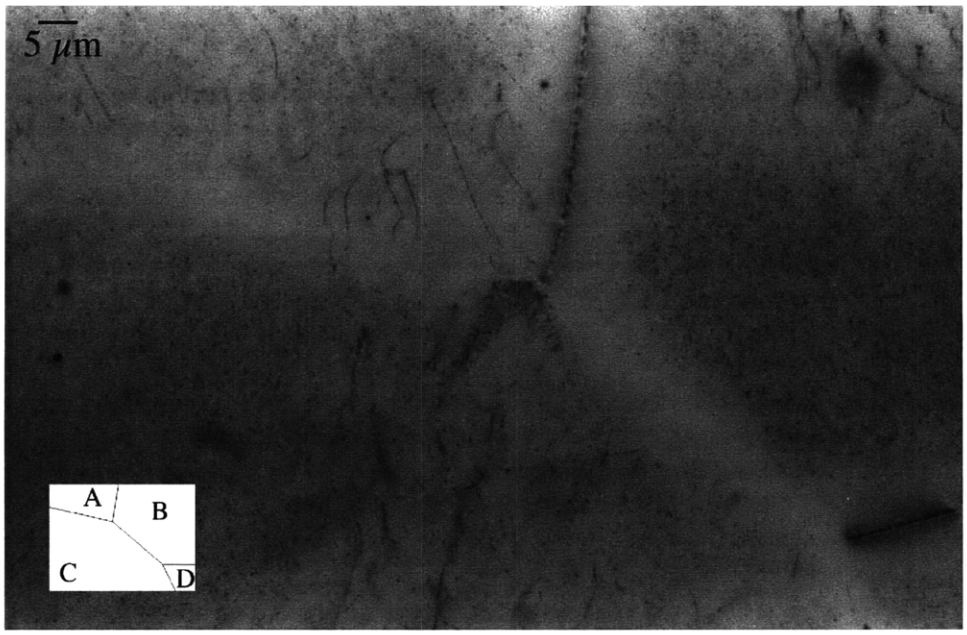

FIGURE 9. Active triple junction in Sample G26.

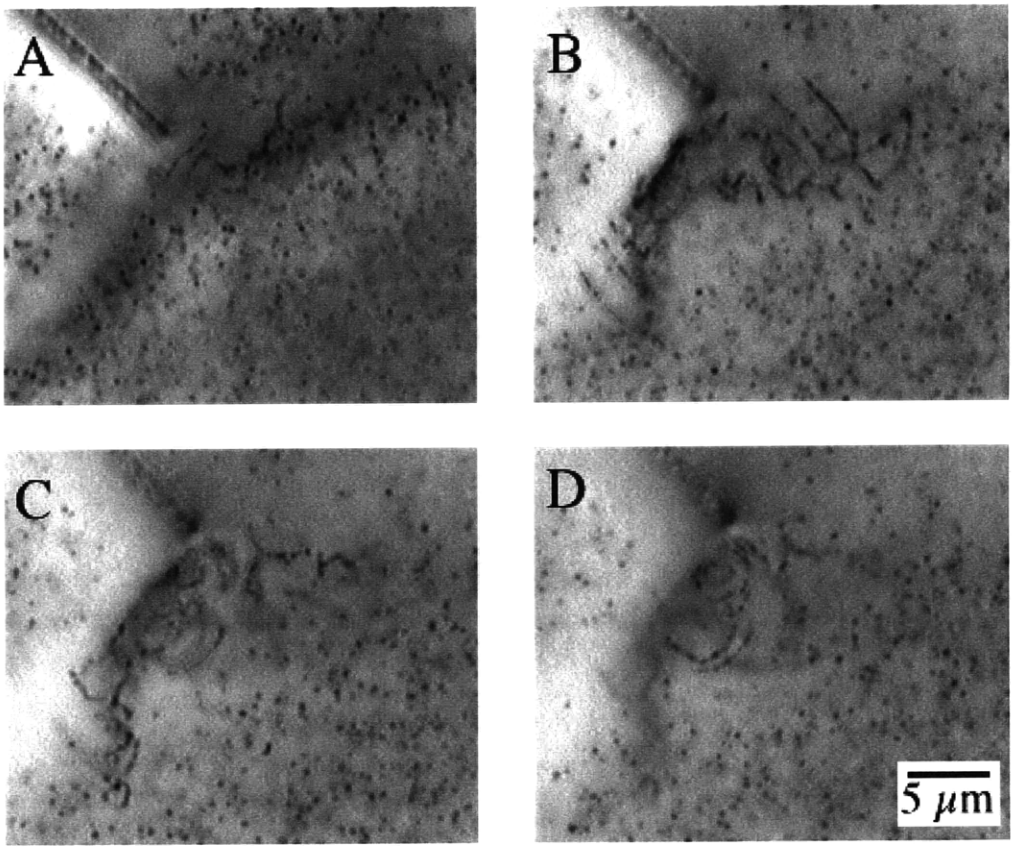

FIGURE 10. Triple junction just beginning to nucleate dislocation loops. Stress direction is left-right. Photo depths are: A, 11 μm; B, 14 μm; C, 16 μm; D, 19 μm. From Sample G26, $\sigma = 2.3$ MPa.

slip bands to form which contain the surface damage; while a few examples of surface damage-induced plasticity were observed, more commonly slip bands bypassed the largest surface defects. The slip bands which were formed by surface damage appeared to be the result of an object resting on the surface of the material during annealing although no object was seen by the time the samples were observed microscopically. Such bands did not expand under an applied stress.

We surmise that the stress concentrations at surfaces are not as strong as those at triple junctions or grain boundaries. A possible reason is that sharp features produced during rolling become rounded during annealing. This would significantly reduce the magnitude of such stress concentration. Since there are no elastic compatibility effects between the crystal and air, without a geometric stress concentration dislocations cannot be nucleated.

Even if dislocations did not nucleate at free surfaces, it seems likely that these interfaces had some effects on dislocation nucleation and growth

because the samples were thin in comparison with the grain size. Results from this study may therefore not be applicable to samples in which surface effects are minimal.

4. Quantitative Observations

We found slip bands that appeared to have been initiated by inclusions, by triple junctions, by surface damage and by slip in other grains as well as slip bands for which there was no obvious cause. It was not possible to determine which factors were responsible for dislocation nucleation from such qualitative observations alone. For this reason, the systematic study described in Section 2.2 was undertaken. A total of 268 grains containing 2132 inclusions and 102 slip bands were analyzed in order to determine the correlation between the presence of inclusions and slip in a sample loaded to 2.2 MPa. In the two regions sampled, the overall and slipped volumes were:

$$\begin{aligned} V_{\text{slipped}} &= (2.745 \pm 0.046) \times 10^7 \ \mu\text{m}^3 \\ V_{\text{total}} &= (2.456 \pm 0.008) \times 10^8 \ \mu\text{m}^3. \end{aligned}$$

The slipped fraction of the sample X_s was therefore

$$X_s = 0.112 \pm 0.002.$$

Errors in the final result were computed using the error propagation equation from BEVINGTON AND ROBINSON 1992,

$$\sigma_x^2 \simeq \sigma_u^2 \left(\frac{\partial x}{\partial u}\right)^2 + \sigma_v^2 \left(\frac{\partial x}{\partial v}\right)^2 + \ldots + 2\sigma_{uv}^2 \left(\frac{\partial x}{\partial u}\right)\left(\frac{\partial x}{\partial v}\right) + \ldots$$

under the assumption that the covariance σ_{uv}^2 was 0. Only measurement error terms were included in calculating the error in X_s.

As shown in Figures 11 and Figures 12, the amount of plastic deformation varied considerably from one region of the sample to the next and did not appear to be uniformly distributed.

4.1. Grain Statistics. In this study, a grain size parameter d is defined to be the square root of the grain's area at the surface,

$$d = \sqrt{A_{\text{surf}}}.$$

The grain size using this definition was 134 ± 73 μm. A plot of the grain size distribution is given in Figure 13. Since the mean grain size was about the same as the sample thickness h, the sample does not meet the standards for true polycrystalline deformation. (See KOCKS 1970.) Therefore, the results of this study may not be applicable to polycrystalline deformation generally.

Grain size was observed to have a strong influence on the appearance of slip bands; see Figure 14. The small number of large grains reduces our confidence in the results for $d > 250$ μm.

The number of triple junctions shared by each grain increased with the grain size, but with large scatter (Figure 15). The mean number of triple

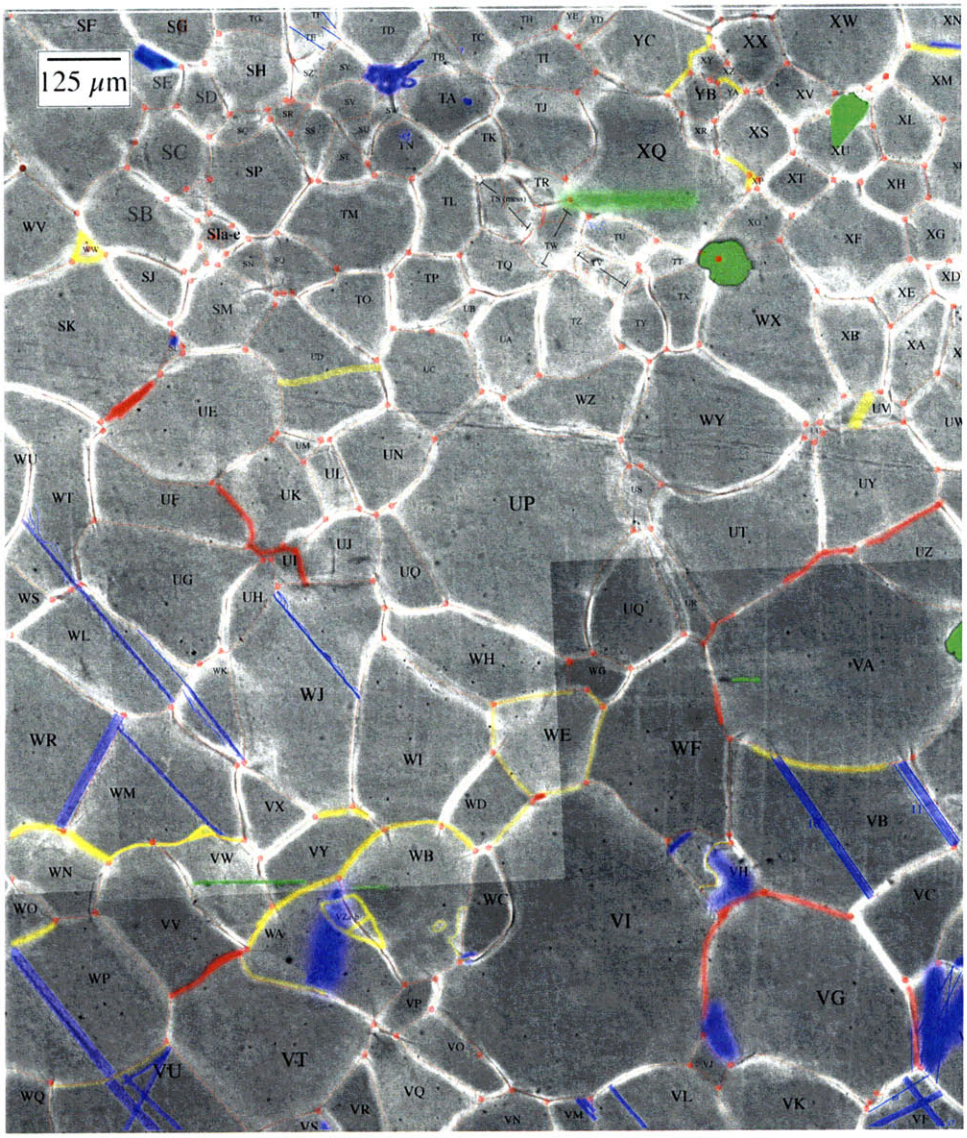

FIGURE 11. Region 1 from Sample G41. Slip bands are in blue. Surface damage is indicated in green; grain boundaries with gas-induced porosity are in red.

junctions for all grains was 6.08 ± 1.93 and the median was 6. The increase in grain size with the number of triple junctions is consistent with the usual two-dimensional model of capillarity-driven grain growth as described in, for example, PORTER AND EASTERLING 1981.

4.2. Inclusions Statistics. We analyzed the inclusions found in the sampled regions. The overall volume fraction of the inclusions V_f was

$$V_f = 7 \pm 1 \times 10^{-5}.$$

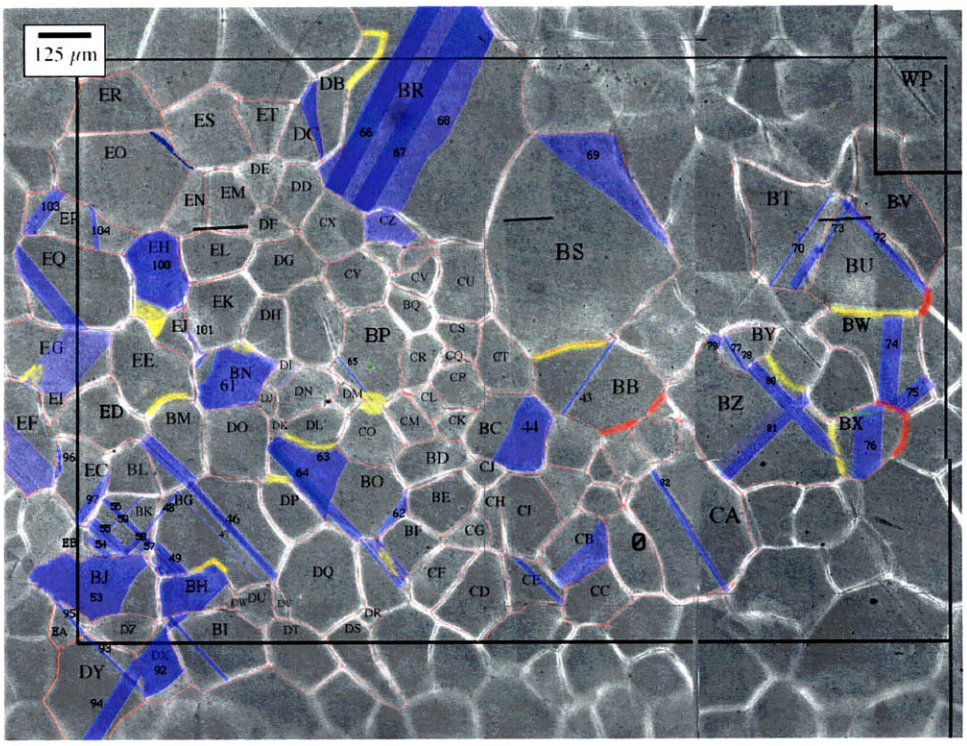

FIGURE 12. Region 2 from Sample G41. Slip bands are in blue. Surface damage is indicated in green; grain boundaries with gas-induced porosity are in red.

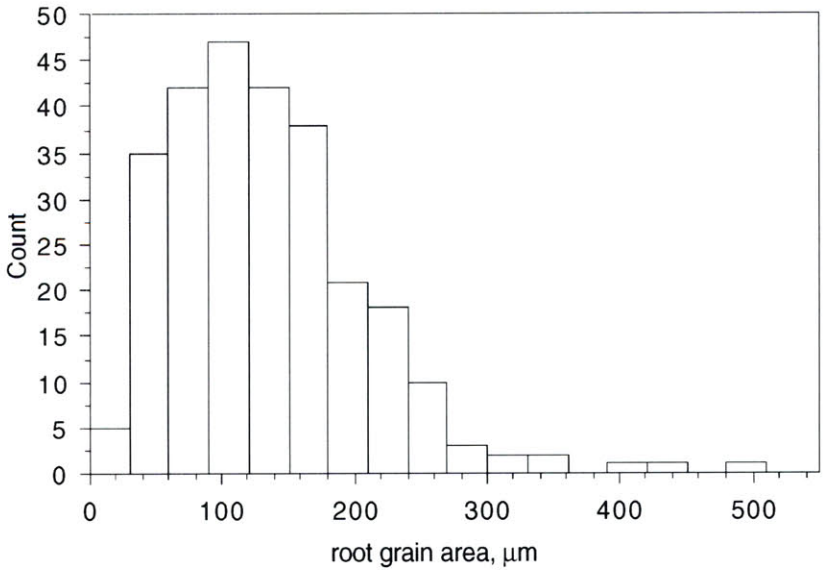

FIGURE 13. Distribution of grain sizes.

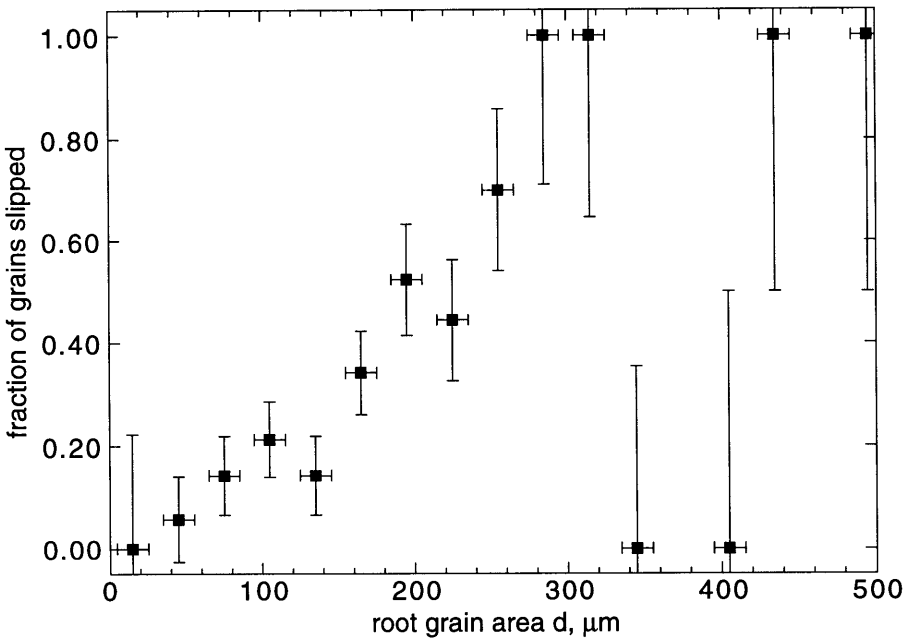

FIGURE 14. Fraction of grains slipped vs. grain size. Grain diameter d is from the center of each bin used in Figure 13. Error bars are based on an assumed binomial distribution with $p = 1/2$. Results for $d > 250$ μm should be discounted.

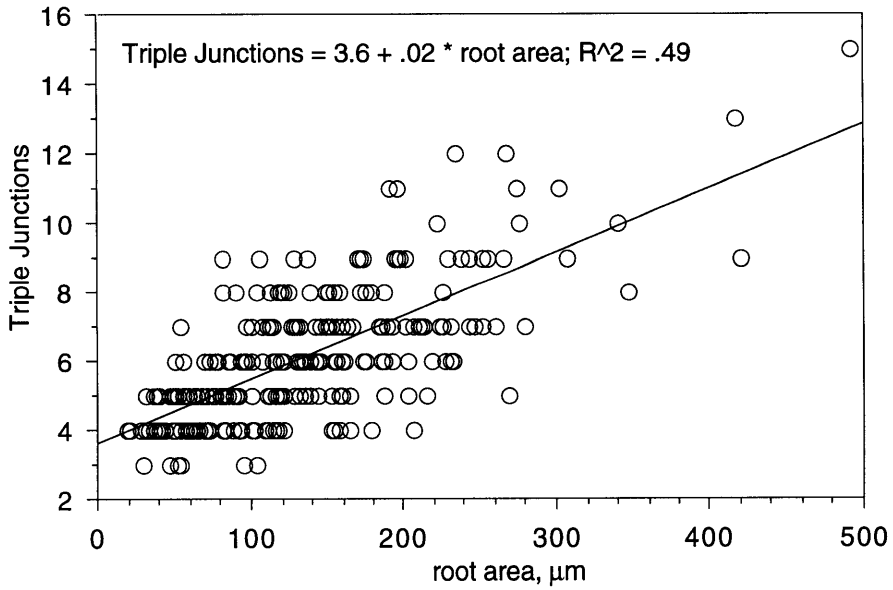

FIGURE 15. Number of triple points as a function of grain size.

TABLE 3. Effects of a free surface.

diameter, μm	total number of inclusions	slipped in bulk	slipped at surface	unslipped in bulk	unslipped at surface
0.5	666	78	17	425	146
1.0	228	24	3	188	13
1.5	333	37	4	243	49
2.0	349	40	9	268	32
2.5	259	38	3	190	28
3.0	137	13	2	99	23
3.5	91	15	2	57	17
4.0	27	2	0	21	4
4.5	14	2	0	12	0
5.0	5	1	0	4	0
5.5	5	2	1	2	0
6+	18	5	0	9	4

Spheres made up 82.5% of the inclusions; the rest were particles of varying shape. Some of these particles were borosilicate frit intentionally added; others were pieces of quartz from the crucible. The latter comprised the largest inclusions. The effective diameter for non-spherical particles $\overline{d_p}$ was defined to be

$$\overline{d_p} = \sqrt{\frac{(l_1^2 + l_2^2)}{2}},$$

where l_1 and l_2 are the major and minor projected axes. Particles larger than or equal to 6 μm were bundled into the "6+" μm bin. There were no spheres greater than 6 μm.

In addition to the 2132 measured inclusions, there was one very large quartz fragment which did not generate any slip bands and which was excluded from further analysis. 16.7% of inclusions touched the sample surface; 3.9% were found in a grain boundary; 6.9% were part of a cluster. Clusters could be either in the form of spheres welded together or as non-contacting but closely spaced inclusions.

Each inclusion was assigned either to a particular slip band or to unslipped status. The location of an inclusion at a free surface did not appear to have an effect; this is demonstrated in Table 3. The number of inclusions found in grain boundaries was too small to determine the influence of grain boundary inclusions with certainty, but they did not appear to have a strong effect. (7 out of 77, or 9.1%, of inclusions embedded in grain boundaries were also found in slip bands.)

The distribution of inclusions in unslipped and slipped regions of the sample is given in Figure 16. The distributions were quite similar; there was a slightly greater number of 6+ μm inclusions in the slipped region.

No inclusions appeared to be debonded from the matrix.

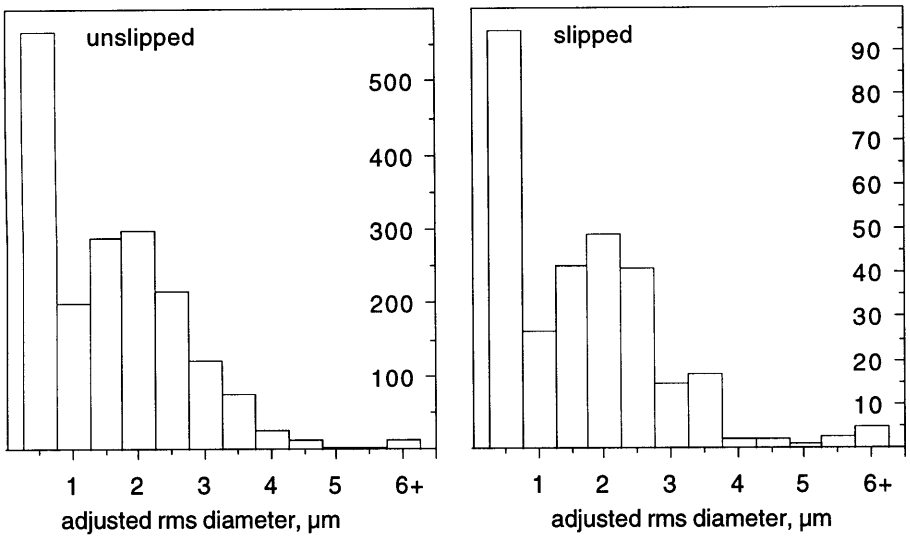

FIGURE 16. Distribution of inclusions in unslipped (left) and slipped (right) portions of the composite. Distributions appear quite similar.

4.3. Slip Band Statistics. We define "Type I" slip bands to be sharp, well-defined slip bands in which the normal to the slip plane lies in the plane of the sample. (See Figure 17.) They usually ran close to high shear stress directions (±45 degrees to the loading direction, in plane) and had relatively well-defined terminal points. An approximate width w and length l could be assigned to these slip bands. Usually, both ends of these bands terminated in a grain boundary. In a few cases a Type I band intersected a grain boundary on one side but faded out in the middle of a grain on the other, as the individual dislocations which made up the band exited the sample at the top (free) surface.

All other bands were defined to be "Type II." Many Type II bands were likely the result of deformation on high shear planes which ran in or out of the plane of the sample. (See Figure 18.) No measurement of the width w was possible; instead, the slipped area and intercept perimeter were measured directly using image analysis. Of the 102 bands measured, 89% were of Type I and 11% were of Type II.

5. Significance Testing

5.1. Statistical Methods. To test the correlation between various microstructural features and the occurrence of slip, we compare the actual number of features (such as 3.5 μm inclusions) found in the slipped region with the value predicted by a simple stochastic model.

The number of features actually found will generally differ from the predicted value even when the model used is valid. A standard way (see MCPHERSON 1990 or ROTA 1995) to test the possibility that the measured

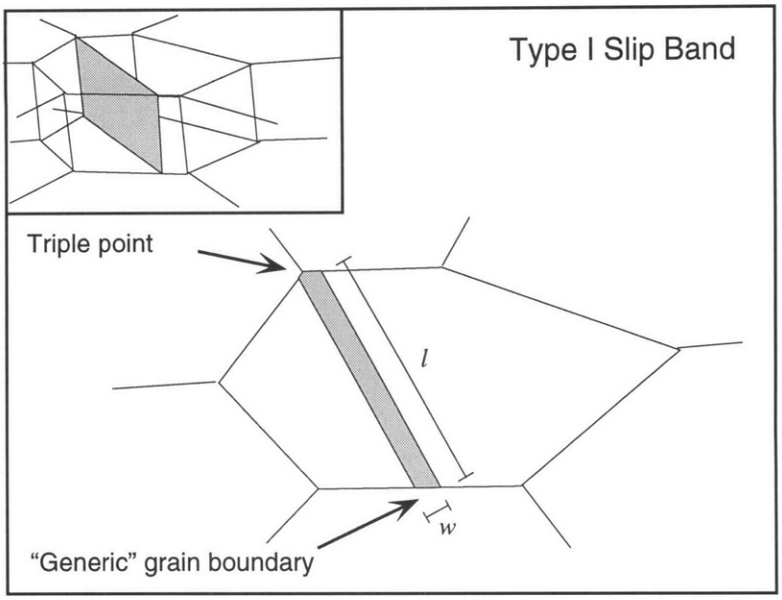

FIGURE 17. Type I Slip Band.

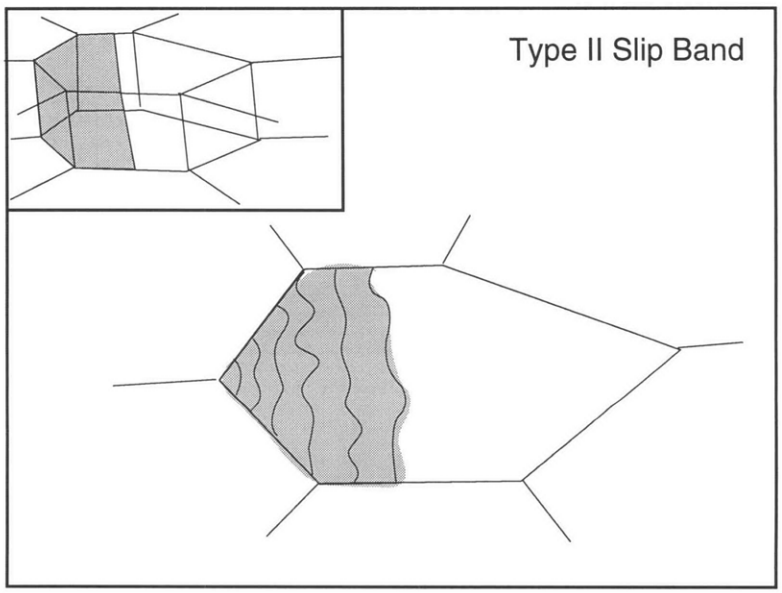

FIGURE 18. Type II Slip Band.

value is only the result of statistical fluctuations is to compute a *significance level* for the result. Typically, the significance level is phrased as a *p-value.* The p-value is defined to be the probability that normal statistical fluctuations could result in data at least as extreme as the experimental data. Thus

a p-value is a number between 0 and 1, with a smaller number indicating a more significant result. In many fields, a p-value of 0.05 (also called the 95% confidence interval) is used as a benchmark of significance. At this level, there is only one chance in twenty that the data are the result of normal statistical variations. ROTA 1995 defines an experiment with a p-value of 0.05 to be "significant" and p-value of 0.01 to be "very significant."

The calculation of significance levels requires a model for the underlying stochastic process. In experiments like coin tossing, the underlying model (the Bernoulli process) has solid theoretical and empirical bases. There is no such simple and compelling statistical model for probability that a slip band will pass through a certain region. In the current analysis, however, we assume that the number of features found within a slipped region *can* be modeled as a simple Bernoulli process in which the probability that a feature is found within a slipped region is equal to the fraction of the region slipped.

Statistical computations of this type require that each event be independent. Often this is problematic; for example, the propagation of slip from one grain to another suggests that the occurrence of plasticity in adjacent grains is not independent.[5] We minimize these effects by studying a sample with a very small amount of plastic strain, 45 $\mu\epsilon$. Even so, only 43 (42%) of slip bands were in grains isolated from other slipped grains. As a result, the assumptions implicit in the statistical models below may not be fully justifiable.

5.2. Triple Junction Interactions. Qualitative observations suggest that slip bands often start at triple junctions. If this were to be the case, triple junctions should be found in slip bands more often than expected from chance interaction. To test this hypothesis, we compare the actual number of triple junctions contained in slip bands with the number predicted by a stochastic model. The simplest model is to assume triple junctions are distributed randomly and independently around the perimeter[6] of the grain.

Let the grain containing the i-th slip band have a total of n_i triple junctions, m_i of which are intersected by slip band i. We assume that the probability p_i that a given triple junction will be found in a portion of the grain's perimeter containing the i-th slip band is

$$p_i = \frac{x_{i,\mathrm{sb}}}{x_{i,\mathrm{total}}},$$

where $x_{i,\mathrm{total}}$ is the perimeter of the grain containing the i-th slip band and $x_{i,\mathrm{sb}}$ is the grain perimeter intercepted by the slip band. For each slip band, n_i, m_i and p_i were determined experimentally. For Type I bands, $x_{i,\mathrm{sb}}$ was

[5]That grains cannot deform independently in fact forms the basis of many work hardening theories, e.g. TAYLOR 1934 or ASHBY 1970.

[6]Since we assume that grains are invariant in shape through the sample thickness, it is appropriate to perform these calculations as if the grains were two-dimensional polygons and the slip bands lines of various widths.

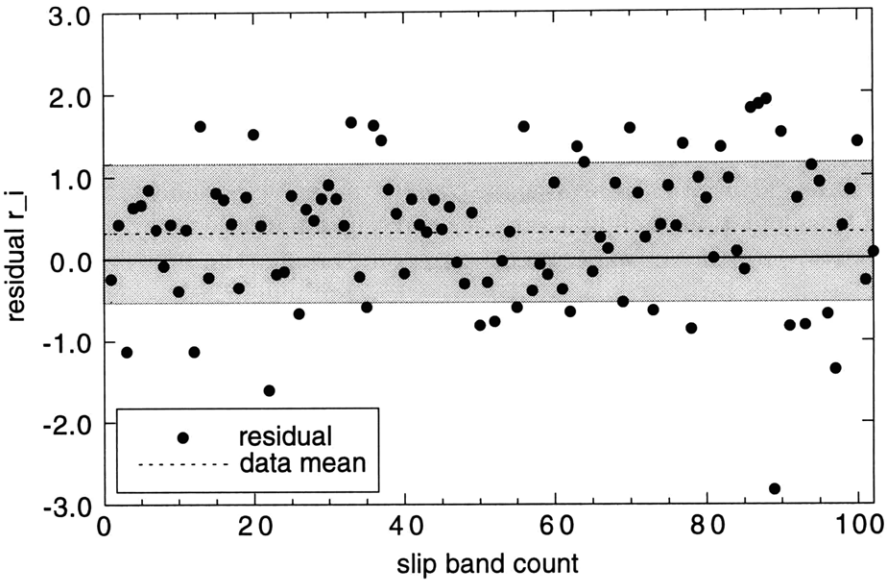

FIGURE 19. Plot of triple junction residuals, $r_i = m_i - p_i n_i$. The dotted line indicates the data mean; the gray area indicates $\pm$ one standard deviation from the data mean. The mean of the residuals is 0.323, too large to be explained by uncorrelated interactions between slip bands and triple junctions.

calculated from the measured width w and grain boundary intercept angles. For Type II slip bands, $x_{i,\mathrm{sb}}$ was measured directly using image analysis.

Our model predicts that, on average, $p_i n_i$ triple junctions should be found in the i-th slip band. Considering the residual $r_i = m_i - p_i n_i$, the actual number number minus the predicted number, allows us to evaluate the model. A univariate plot of the r_i is given in Figure 19.

We also compare a summary statistic with its predicted value. Let

$$S = \sum_{i=1}^{N} m_i$$

where N is the number of slip bands, 102 in the present case. Comparing the value of S computed from data[7] with the distribution predicted by our model yields a p-value of 4.13×10^{-5}. This indicates that the data are very significant; the probability that our experimental value of S could have been

[7]We compute the p-value by summing the last $1 + \sum_i (n_i - m_i)$ coefficients of the polynomial $f(z)$ where

$$f(z) = \prod_{i=1}^{N} ((1 - p_i) + p_i z)^{n_i}.$$

obtained by a random process is about 1 in 500,000. We conclude that slip must be positively correlated with triple junctions.

A few further observations follow. The mean of the residuals r_i is 0.323. (This is used in the model presented in Section 7.2 below.) If we consider only isolated slip bands of Type I, 27 out of 36 (75%) intersected at least one triple junction. A subjective count of the number of slip bands initiated, in the eye of this observer, by triple junctions was 57/102 or 56%.

Triple junctions appear to be an important site of slip band nucleation. Other grain boundary sites of stress concentration are also likely to be important. A possible mechanism is: a slip band nucleates at triple junction favorably located at a high resolved shear stress plane. The slip band propagates across the grain, possibly incorporating inclusions. As the strain is increased, slip accumulates at the ends of the slip band, via a pile-up mechanism or simple displacement of the boundary. This nucleates a new slip band in a neighboring grain.

This mechanism can explain many, but not all, slip bands. As only 21% of triple junctions intersected slip bands, there must be additional factors that influence which triple junctions activate. Possible factors include grain size, the crystallographic orientation of the three grains which define the triple junction and inclusions in the grain. In the next section, we consider the latter possibility.

5.3. Inclusion Interactions. In this section, we use methods similar to those used above to quantify the correlation between inclusions and slip bands. We consider each size of inclusion independently.

5.3.1. *Test 1: Comparison with overall background:* Overall, a fraction X_s (11.2%) of the region studied was slipped. If n_j inclusions of size j were to be independently and uniformly distributed at random in a sample with slipped fraction X_s, on average $n_j X_s$ inclusions should end up in the slipped volume. We compare the predictions of this model with experiment.

Divide the inclusions by diameter into 12 bins as previously described. Let X_j be the fraction of inclusions of size range j found in slipped regions. Then

$$X_j = \frac{m_j}{n_j}$$

where n_j is the number of inclusions that were found in the sample overall and m_j is the number found in slipped regions. A plot of X_j from Sample G41 is given in Figure 20.

Next, we determine a p-value for each size range by computing the probability under our model that values of m_j at least as extreme as the experimental values could occur. Since n_j is as small as 5, we compute the p-values

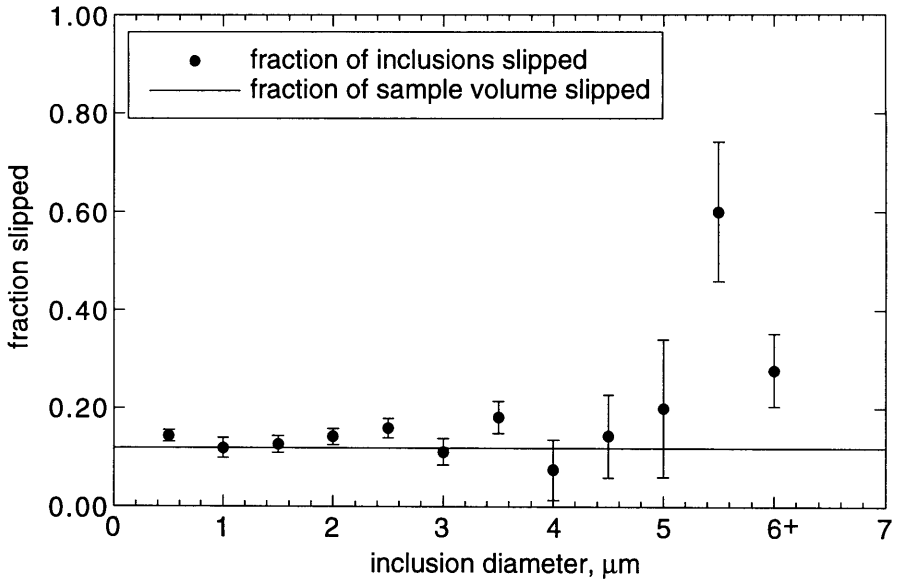

FIGURE 20. Fraction of inclusions of size d_p which were found in slipped regions. For comparison, the line shown indicates the fraction of the entire sample volume which was slipped. If the data points fall on the line, it is likely that slip was independent of the presence of inclusions.

directly from the discrete distributions assumed in the model.[8] The results are given in Table 4.

5.3.2. *Test 2: Grain-by-grain approach:* A problem with Test 1 is that it assumes the inclusions are randomly distributed over the entire region sampled. Empirically, the inclusion concentrations varied too much from grain to grain for this to be true. Often inclusions are inhomogeneously distributed in materials of this type; see, for example, BARLOW AND HANSEN 1989. Inhomogeneous distribution of reinforcement leads to inhomogeneous distribution of grain sizes during recrystallization due to pinning during grain growth (GHOSH 1993). As grain size was observed to have a strong influence on the likelihood of slip (Figure 14), these effects could bias the outcome of Test 1.

[8]The j-th p-value is given by

$$\sum_{k \geq m_j}^{n_j} \binom{n_j}{k} p^k (1-p)^{n_j - k}$$

where $p = X_s$. This is the sum of the last $1 + n_j - m_j$ coefficients of the polynomial

$$f(z) = ((1-p) + pz)^{n_j}.$$

TABLE 4. Test 1 Results

$d_{p,j}$ (μm)	n_j	m_j	X_j	p-value	significance
0.5	666	95	14.2%	0.00836	very significant
1.0	228	27	11.8%	0.406	not significant
1.5	333	41	12.6%	0.280	not significant
2.0	348	49	14.1%	0.0548	not significant
2.5	258	41	15.9%	0.0135	significant
3.0	136	15	11.0%	0.562	not significant
3.5	94	17	18.1%	0.0309	significant
4.0	27	2	7.4%	0.821	not significant
4.5	14	2	14.3%	0.477	not significant
5.0	5	1	20.0%	0.447	not significant
5.5	5	3	60.0%	0.012	significant
6+	18	5	27.8%	0.043	significant

TABLE 5. Test 2 Results

$d_{p,j}$ (μm)	$\sum n_{i,j}$	$\sum p_i n_{i,j}$	$\sum m_{i,j}$	p-value	significance
0.5	492	173.5	95	1.00	not significant
1.0	120	34.5	27	0.969	not significant
1.5	152	41.8	41	0.605	not significant
2.0	167	44.6	49	0.209	not significant
2.5	124	32.1	41	0.0281	significant
3.0	55	12.0	15	0.181	not significant
3.5	45	12.3	17	0.0425	significant
4.0	10	1.45	2	0.443	not significant
4.5	4	1.38	2	0.434	not significant
5.0	2	0.401	1	0.368	not significant
5.5	3	0.678	3	0.00603	very significant
6+	7	2.91	5	0.0616	not significant

One way to address this is to calculate a p-value using a statistic which considers each grain independently. Then we need to assume only that inclusions are randomly distributed within each grain. Essentially, this statistic yields the number of inclusions we expect to find in slipped regions if the path taken by slip bands across each grain is independent of the location of inclusions in that grain.

The calculation proceeds as follows. The local fraction slipped (comprising one or more slip bands) of the i-th grain is

$$X_{s,i} = \frac{V_{\text{slip band 1},i} + V_{\text{slip band 2},i} + \cdots}{V_{\text{grain},i}}$$

where V_x is the volume of region x. The i-th grain contains $n_{i,j}$ inclusions of size j, $m_{i,j}$ of which are in the slipped portion of the grain. For comparison, in the model we assume the $n_{i,j}$ inclusions are independently and uniformly

distributed at random in grain i. Thus, in the model, the probability p_i of finding an inclusion in a slipped part of the grain is $X_{s,i}$ and the expected number of inclusions found slipped regions is $p_i n_{i,j}$.

The summary statistic S_j is

$$S_j = \sum_{i=1}^{N} m_{i,j}$$

where N is the total number of grains with at least one slip band. Values of $\sum_i n_{i,j}$, $\sum_i p_i n_{i,j}$ and $\sum_i m_{i,j}$ are given in Table 5 along with the p-values computed[9] from the measured values of S_j.

5.4. Discussion. We compared the data to two stochastic models. The results are similar with the exception of the $j = 0.5$ μm bin. Data of this inclusion size should be discounted because of likely data collection errors. (Inclusions of this size range are easily missed in the microscope.)

Both tests suggest that the 2.5 μm and 3.5 μm data are "significant." Since both tests also suggest that the 2.0, 3.0 and 4.0 μm data are "not significant," it seems unlikely that these results are meaningful. Of the two largest size ranges, only the 5.5 μm was found to be "significant" or "very significant" using both tests. We note there were only 5 inclusions in the 5.5 μm range, which cast doubt on these results. Thus while large inclusions *might* be positively correlated with the occurrence of slip, more data are needed to confirm the significance of the result.

In order to obtain a clearer picture of the extent of slip around large inclusions, a second examination was made of the entire sample. In this data set, spheres (only) of size 3 μm and larger were counted and their status (in a slip band or not) recorded. In this case, the fraction of the sample slipped is not known; we use X_s as an estimate. Figure 21 shows the fraction of spheres found in slipped regions for seven size ranges. There are still very few data in the largest size ranges, so it is not possible to draw firm conclusions. Nevertheless, this experiment corroborates the results of Tests 1 and 2 in that it is clear that inclusions do not "cause" slip in a deterministic sense.

The results above support the conclusion that the appearance of slip bands in a polycrystal which contains a low volume fraction of inclusions is unrelated to the presence of the inclusions. The data are conclusive on the role of particles of size $1.0 \leq d_p \leq 4.5$ μm; for larger particles, there is inadequate data to completely rule out a causal relationship between the inclusions and the appearance of slip bands. These results are consistent

[9]The j-th p-value is computed by summing the last $1 + \sum_i (n_{i,j} - m_{i,j})$ coefficients of the polynomial

$$f(z) = \prod_{i=1}^{N} ((1 - p_i) + p_i z)^{n_{i,j}}.$$

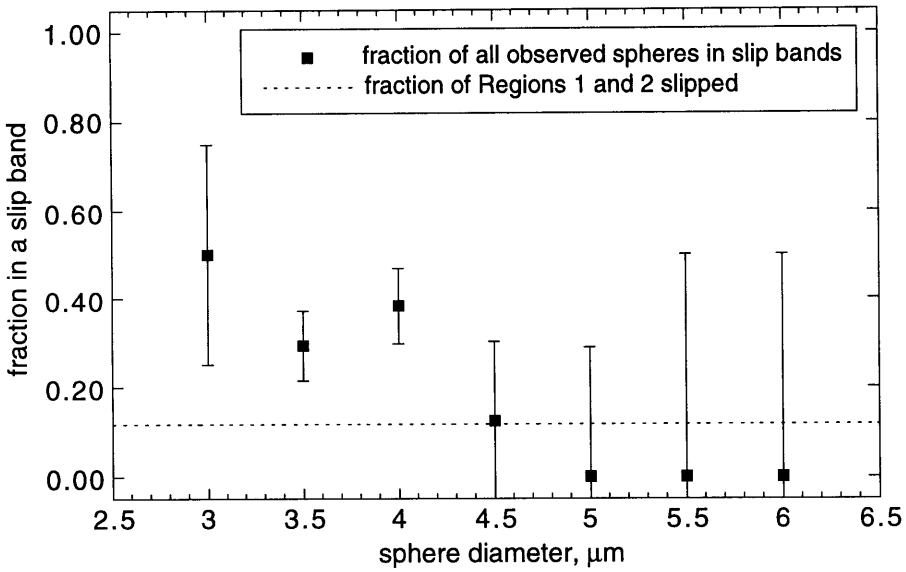

FIGURE 21. Fraction of large, isolated spheres found in a slip band. Data collected from a much larger sample volume than Regions 1 and 2. Fractional volume of sample slipped is estimated from the fractional volume slipped determined from Regions 1 and 2.

with the model developed in Chapter 5. In that model, prismatic loops could cross slip at $\Omega = 1$. At a far-field stress of 2.2 MPa, the critical particle diameter for which $\Omega = 1$ is 5.8 μm, the tail of the particle distributions shown in Figure 16.

If the matrix were stronger or the inclusions larger or more numerous, inclusions should play a more important role.

6. Effects of a Higher Inclusion Volume Fraction

That the mechanical behavior of the matrix in the present work resembles that of an unreinforced material is perhaps unsurprising since the volume fraction of inclusions in the material was very small. ($V_f \approx 7\times10^{-5}$.) As the volume fraction of inclusions increases, we expect they will play a more important role in the deformation of the material. In particular, as the matrix grows stronger, the importance of dislocation nucleation on the overall mechanical properties of the composite should decrease. This is because the stress required for dislocation motion will no longer be insignificant in comparison with that required for dislocation nucleation.

Using established models from the literature, we briefly speculate on the volume fraction V_f of spheres required to have a significant effect on the mechanical properties of the material. Arbitrarily, we chose a 5% increase

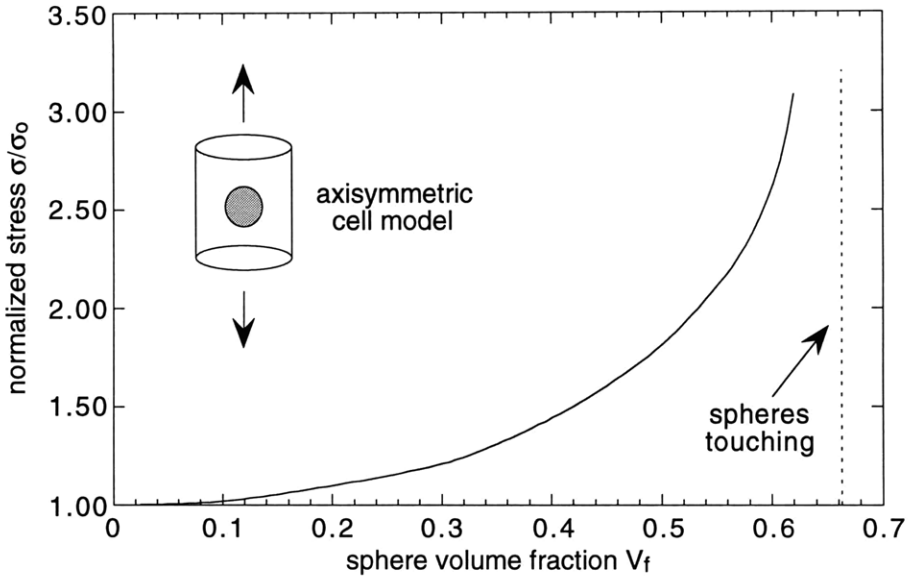

FIGURE 22. Predicted increase in normalized flow stress (average composite flow stress divided by matrix flow stress) for an elastic-perfectly plastic matrix containing non-deformable spheres. From HUTCHINSON AND MCMEEKING 1993.

in the flow stress to indicate a "significant" effect and denote the requisite volume fraction V_f^*.

A simple continuum mechanics model applicable to the present material is the axisymmetric cell model in which a non-deformable sphere is surrounded by an elastic/perfectly plastic matrix. Results from this FEM model are given in Figure 22, taken from HUTCHINSON AND MCMEEKING 1993. This model suggests that a volume fraction $V_f^* \approx 0.15$ would increase the flow stress by 5%. Since this is a continuum plasticity model, no inclusion size dependence is predicted.

Dislocation-based models do predict a dependence on inclusion size. There are two simple dislocation models of interest. The first, the Orowan mechanism, relates the strength of a solid to the average interparticle spacing l. (Pages 351–2 of HAASEN 1986.)

$$\tau_o \approx \frac{Gb}{l} \approx \frac{2Gb\sqrt{V_f}}{d_p}$$

The magnitude of Orowan strengthening is small for large particles like those used in the present study. With average particle diameter $d_p = 2.5$ μm, a value of $V_f^* \approx .10$ would be required to increase the flow stress by 5% from the 0.82 MPa value taken from the stress-strain curve.

The other simple model for composite strength is dislocation strengthening. Following LI AND CHOU 1970,

$$\tau \approx \tau_0 + \alpha G b \sqrt{\rho}$$

where ρ is the dislocation density and α is on the order of 0.5. Following the assumptions of ARSENAULT 1991 an upper bound on ρ from dislocations created by CTE mismatch is

$$\rho \leq \frac{12}{\sqrt{2}} \frac{\Delta\alpha\Delta T}{rb} \left(\frac{V_f}{1 - V_f} \right).$$

A more realistic (and lower) value of ρ in our samples is obtained from a best fit to the data from Figure 8 in Chapter 4. Even this lower value of ρ suggests substantial strengthening; a 5% improvement in strength is predicted for $V_f^* \approx 5 \times 10^{-5}$ and $d_p = 2.5$ μm.

Thermal misfit dislocations are not in fact uniformly spread across the sample and the effects of thermal residual stresses (which make the composite more compliant; see HUTCHINSON AND MCMEEKING 1993) have been ignored. Hence, this is probably a lower bound on V_f^*. Since the elastic-purely plastic matrix modeled in HUTCHINSON AND MCMEEKING 1993 represents an upper bound, reasonable bounds on the value of V_f^* are

$$10^{-5} \leq V_f^* \leq 0.15.$$

The present data are at the lower end of this range.

7. A Simple Grain Size Model

What factors, then, do influence where slip begins in polycrystals? Given the importance of average grain size on the macroscopic yielding behavior of polycrystals (e.g., HIRTH 1972), it is unsurprising that grain size also plays a strong role in the appearance of slip at the level of individual grains. This was shown in Figure 14.

In Chapter 4, good agreement between theory and experiment was obtained by building on the approach of ASHBY AND JOHNSON 1969. In the model of ASHBY AND JOHNSON 1969, a nucleation criterion was derived by calculating the critical misfit required for dislocation emission to become thermodynamically feasible. In our model, we further required the presence of some heterogeneous nucleation site. The number of nucleation sites was taken to be in proportion to a surface area term, with good results.

This approach might be useful in predicting the onset of plastic deformation in polycrystalline materials as well.

7.1. Model. A reasonable approach is to assume there are "perfect" sources of dislocations in polycrystals (such as triple junctions, or a pileup of dislocations from another grain) which emit dislocations when it is thermodynamically feasible to do so. This is the point at which the work done by the stress sweeping out some area A is just greater than the energetic cost of the dislocation line needed to bound A. Such a model was proposed in

LANGFORD AND COHEN 1969b and LANGFORD AND COHEN 1969a. They found this approach yields a Hall-Petch style relationship

$$\tau^* = \tau_o + k_1 G b d^{-1},$$

with an exponent of -1 instead of the usual $-1/2$. They found good agreement between this model and the flow stress of strain-hardened iron wire when the transverse cell size of the iron was used for d.

This calculation can be repeated for the present system. For a spherical grain, the total length of dislocation formed, l, is

$$l = \pi d$$

or for the columnar microstructure used in the present study,

$$l = 2d + 2h$$

where h is the sample thickness.

If τ_f is the friction stress, the work done by the stress is roughly

$$W = (\tau - \tau_f) b \pi (d/2)^2$$

for a spherical grain, or

$$W = (\tau - \tau_f) b d h$$

for the present system.

Using Gb^2 as the line tension of the dislocation and setting the change in the energy of the system to zero, the critical shear stress required for formation of a loop is

$$\tau = \tau_f + \frac{4Gb}{d}$$

for a spherical grain, or

$$\tau = \tau_f + \frac{2Gb(d+h)}{dh}$$

for the present system.

Substituting in $\tau = 1.11$ MPa, $\tau_f = 0.36$ MPa, $h = 120$ μm, $G = 8.55$ GPa, $b = 0.392$ nm, we obtain

$$d^* = 9.7 \ \mu\text{m}.$$

This is a lower bound on d^*; if the dislocation path is longer than the shortest path, d^* will increase. From Figure 14, the smallest size range for which one or more grains are slipped is the 30 to 60 μm bin; for the first grain which slipped, $d = 32$ μm; for the smallest grain $d = 19$ μm. This value of d^* seems reasonable as a lower bound.

In Chapter 4, a good fit to the data was obtained by assuming that a thermodynamic condition was necessary, but not sufficient, for nucleation to occur; in the model used, heterogeneous nucleation sites on the surface of the sphere generated dislocations. The number of these sites was assumed to be proportional to the surface area of the sphere.

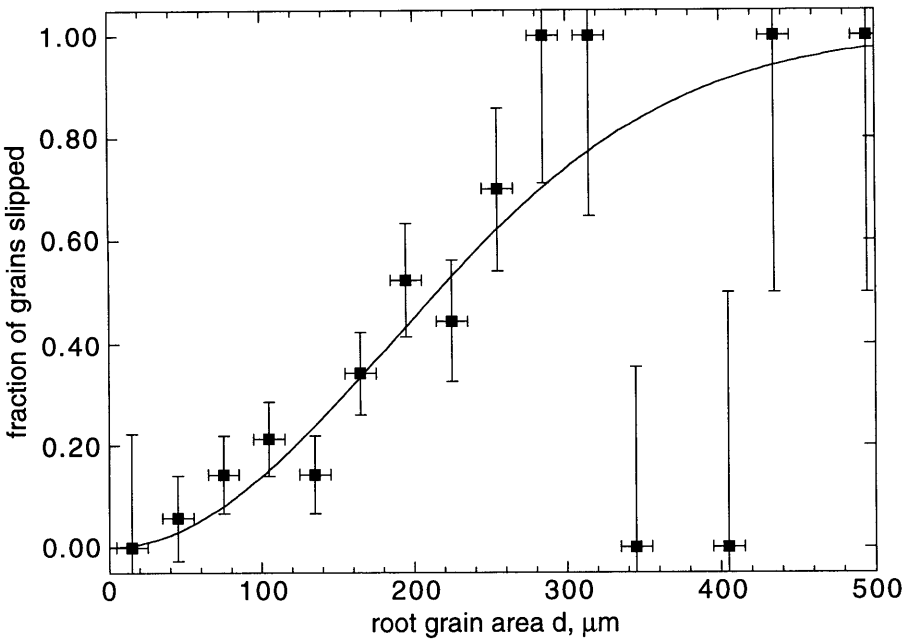

FIGURE 23. Fit of $1-\exp(-cd^2)$ to fraction of grains slipped vs. grain size parameter d. $R^2 = 0.812$, $c = 1.50 \times 10^{-5}$ μm^2.

A similar argument can be made in the case of a polycrystalline solid. The thermodynamic calculation above gives a necessary, but insufficient, condition for nucleation of slip. This condition is met by all grains in the sample.

A simple model for the yielding of individual grains in a polycrystal is again to assume that heterogeneous nucleation sites are needed, and that the number of these nucleation sites is proportional to an area term. From Figure 14, the grain size parameter d has a clear influence on grain yielding; hence, we choose d^2 as the area term. Following the probabilistic approach given in Chapter 4, under this assumption the probability that a grain has one or more nucleation sites k is

$$\Pr[k \geq 1] = 1 - e^{-cd^2}.$$

This yields a reasonable fit to the data from Figure 14; this fit is given in Figure 23. One justification for a fit of this kind is the grain boundary source concept of J.C.M. Li (see LI 1963, LI AND CHOU 1970 and LI 1980), who proposed that dislocation sources in the boundary can emit length l of dislocation line per unit area. This corresponds to a point source like that illustrated in Figure 7 emitting a given number of loops. These grain boundary sources could occur at triple points or at other regions of high compatibility stress between grains.

7.2. Discussion. The value of the constant c is 1.50×10^{-5} μm^2. Multiplying times the square of the mean grain size (134 μm) yields the mean number of active nucleation sites per grain, in this case 0.269. If each of these sites were triple junctions, we would expect the sum of the residuals defined in Section 5.2 to be (0.269)(268) or 72.1. The actual sum of the residuals was 32.9; this suggests that about 32.9/72.1 or 46% of slip bands were initiated by triple junctions. This is in reasonable agreement with our subjective count that 57/102 or 56% of slip bands were nucleated at triple junctions.

We note that other probabilistic models can generate a reasonable fit to the data. SUITS AND CHALMERS 1961 proposed a model in which the number of nucleation sites (perhaps, they proposed, nonmetallic inclusions) is proportional to the volume, i.e. $k = cd^3$. They propose that the fraction of grains with a nucleation site can, for small k, be approximated as k. Then

$$\Pr[k \geq 1] \approx cd^3 \text{ for small values of } k$$

If we correct this calculation for larger values of k, we obtain

$$\Pr[k \geq 1] = 1 - e^{-cd^3}.$$

A plot of this fit is given in Figure 24. The fit is not as good as the d^2 model but shows that a reasonable fit can be obtained even when the exponent is varied. Therefore, this analysis alone cannot prove that slip begins at grain boundaries, especially since it ignores the obviously important grain-to-grain slip band propagation mechanism. Nevertheless, the overall evidence for grain boundary nucleation is strong.

8. Conclusions

We investigated the earliest stages of plastic deformation in silver chloride composites containing approximately 10^{-4} volume fraction of hard, nondeformable inclusions. A dislocation decoration technique was used to render slip bands visible in grain interiors. Slip was found to initiate at sources in grain boundaries, especially triple junctions, rather than at inclusions distributed in the interior of grains.

The evidence can be summarized as follows:

- Slip bands ran from one side of the grain to the other. This is contrary to the predictions of simple continuum plasticity models, which predict that plastic zones should form around inclusions and gradually expand under increasing load.
- The number of triple junctions intersected by slip bands was much higher than could be explained by random interactions, suggesting that triple junctions are potent slip nucleation sites. A simple model suggests that 46% of slip bands were initiated by triple junctions, close to our subjective estimate of 56%.

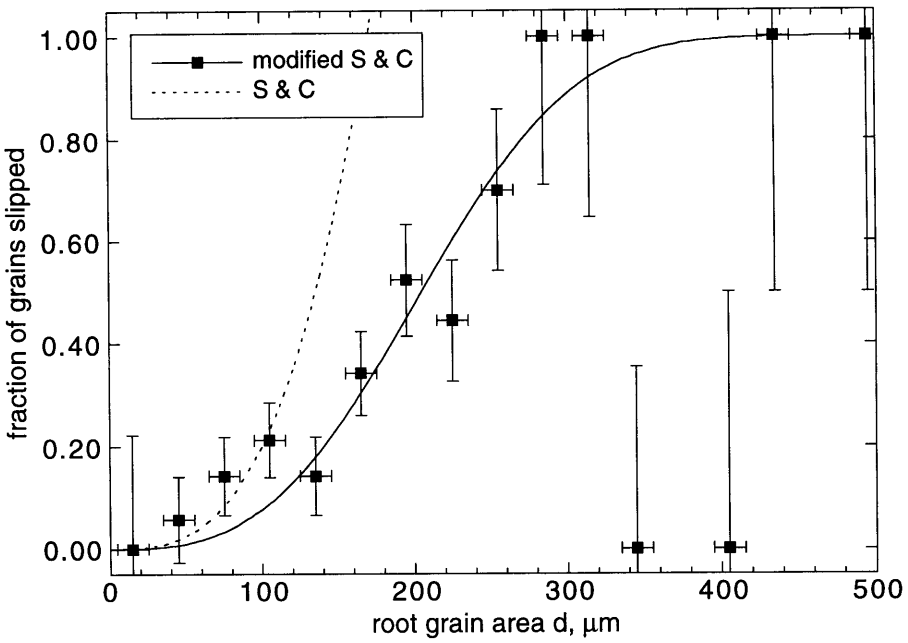

FIGURE 24. Fit of $1-\exp(-cd^3)$ to fraction of grains slipped vs. grain size parameter d, based on a model of SUITS AND CHALMERS 1961. Both original (cubic) and modified (sigmoidal) curves are given. For sigmoidal curve, $R^2 = 0.750$.

- The fraction of spheres found in slip bands was essentially equal to the fractional slipped volume of the sample for all size ranges but 5.5 μm, a size range for which there were only 5 data points.
- An analysis of the path taken by slip bands through slipped grains showed that the number and size of inclusions intersected was consistent with uncorrelated interactions except, again, in the suspect 5.5 μm size range.
- A further investigation of large spheres found no obvious trend in the likelihood that a sphere would be found in a slip band as the diameter of the sphere increased.
- The results are in agreement with a model presented in Chapter 5, which suggested that in the presence of other more easily activated sources of dislocations, only spheres larger than 5.8 μm could possibly nucleate slip bands.
- The appearance of slip in individual grains was a strong function of the grain size parameter d, and a reasonable fit to the data was obtained by assuming that the presence of slip in a grain was a function of the grain size only.

This study shows that the presence of a low volume fraction of 1–5 μm inclusions in a polycrystal does not have a significant effect on the small strain

mechanical properties. These results agree with work on unreinforced silicon iron (CARRINGTON AND MCLEAN 1965) and high purity copper (MALIS AND TANGRI 1978). Work on the fracture behavior of metals (e.g. ARGON ET AL. 1975) has demonstrated that inclusions are important in determining the fracture toughness of a material, but their effect on initial distribution of plasticity appears to be slight.

CHAPTER 7

Conclusions

Our goal was to improve the understanding of plastic deformation in polycrystalline materials that contain a small volume fraction of hard inclusions. We obtained novel and significant results on aspects of mechanical behavior for which there are few quantitative data in the literature. They are as follows:

- We developed a new method for producing decorable silver chloride composites. Samples made with this technique decorated reliably and reproducibly.
- We applied traditional techniques of mechanical metallurgy to decorable ingots of silver chloride and produced samples with few macroscopic defects and a very low level of lattice dislocations. This represents an improvement over the casting technique documented in the literature.
- We revisited the nucleation of dislocations at spherical inclusions due to thermal mismatch. We found the nucleation model of Ashby and Johnson generated accurate predictions for our material, in which the sphere diameters were roughly ten times larger than those used in previous studies.
- We developed a stochastic model for the distribution of nucleation sites on the surface of a misfitting spherical inclusion. The functional relationship predicted by the model generated a good fit to the data at two levels of misfit strain.
- We revisited a calculation of the equilibrium shape of a prismatic dislocation loop under stress, improving it by incorporating a more accurate expression for a dislocation's line energy and the effects of a matrix flow stress. The results of this calculation were in reasonable agreement with experimental measurements.
- We completed a quantitative study on the origins of slip bands in a sample with a low volume fraction of of inclusions. The results of this study were twofold: First, we found the path of slip bands to be independent of the location of inclusions. This suggests that slip bands did not nucleate at inclusions. Second, we found triple junctions were intersected by slip bands significantly more often than could be explained by chance interaction. We conclude that slip begins at grain boundaries, and that triple junctions are potent sites for dislocation nucleation.

CHAPTER 8

Future Work

The silver chloride dislocation decoration technique is a versatile tool for studying the mechanical behavior of ductile solids. Some promising areas of further research are detailed below.

1. Extension of Thesis Experiments

1.1. Nucleation Study. As discussed in Chapter 4, it would be very interesting to determine the functional relationship between the applied misfit strain ϵ^T and the value of the curve-fit parameter c by repeating the same low-temperature annealing experiments at a few other annealing temperatures.

In order to get the most out of further nucleation work, it would be useful to repeat the high-temperature decoration experiment described in Chapters 3 and 4 at temperatures in the range 450 to 500 K. This would allow for more precise estimation of T_{ep} and therefore of ϵ^T. Since the strobe bulb itself is quartz and capable of withstanding high temperatures, it should be possible to install and operate a strobe light directly inside of a moderate temperature oven by upgrading the wiring and connectors.

1.2. Strain Study. The quantitative study in Chapter 6 could be greatly extended by modifying some of the variables which characterize the composite. For example, the effects of grain size, inclusion volume fraction, inclusion size, and matrix flow stress (by alloying with AgBr) are all of interest. All use the same basic sample preparation technique; only the alloying requires further discussion.

We did cast an ingot of $AgCl_{70}/AgBr_{30}$ alloy with the usual level of CuCl. While dislocations could be decorated in the material, the quality of decoration was poor. The material was also too hard to roll without cracking. A few atomic percent of AgBr would probably be adequate to increase the friction stress τ_f significantly. AgCl can also be alloyed with NaCl; see STOKES AND LI 1962. It is not known whether AgCl/NaCl alloys can be decorated.

The major problem with extending the quantitative work of Chapter 6 is that data collection process is arduous. With hindsight, we can suggest a few changes which would make the process easier. First, it might be best to use only spherical inclusions. The addition of particles significantly complicates the analysis and makes comparisons with theory difficult. Second, a flatter

distribution of inclusion sizes should be used. The reinforcements used in the study were roughly normally distributed, which meant that thousands of inclusions had to be measured in order to find 3 or 4 large ones. While any purchased spheres are likely to be normally distributed, a flatter distribution of inclusion sizes could be obtained by mixing inclusions of more than one size range together.

2. Other Areas

2.1. Heterophase Interfaces. One of the most exciting area for future work is the nucleation of dislocations from heterophase interfaces. Sodium chloride has the same crystal structure as and a lattice parameter similar to silver chloride, but much different mechanical properties. In particular, the yield stress is much higher. An epitaxial layer of sodium chloride is easily grown on silver chloride by evaporation of a sodium chloride solution. (The solubility of silver chloride in water is negligible.)

Sodium chloride absorbs a negligible amount of UV light, so the decoration process works even when the epilayer is thick. Furthermore, the refractive index of NaCl is very similar to that of the immersion oil used in high resolution light microscopy, so flat regions of NaCl are almost invisible.

One sample with an epilayer was loaded to 2.2 MPa. Two photographs from the same location are shown in Figures 1 and 2. These photographs show a region of the solid where the coverage of the epilayer was incomplete. The lighter, triangular regions are NaCl crystals; the darker regions are decorated silver chloride. Dislocations correlated with the surface crystals visible in Figure 2. This sample was tested to the same strain as Sample G41 (Chapter 6), but showed a much higher dislocation density. The dislocation density was highest near the AgCl/NaCl interface and decreased deeper in the AgCl substrate. The large number of dislocations created by the heterophase interface under an applied stress supports a conclusion of the main body of the work, namely that elastic compatibility stresses at interfaces are efficient sources of dislocations.

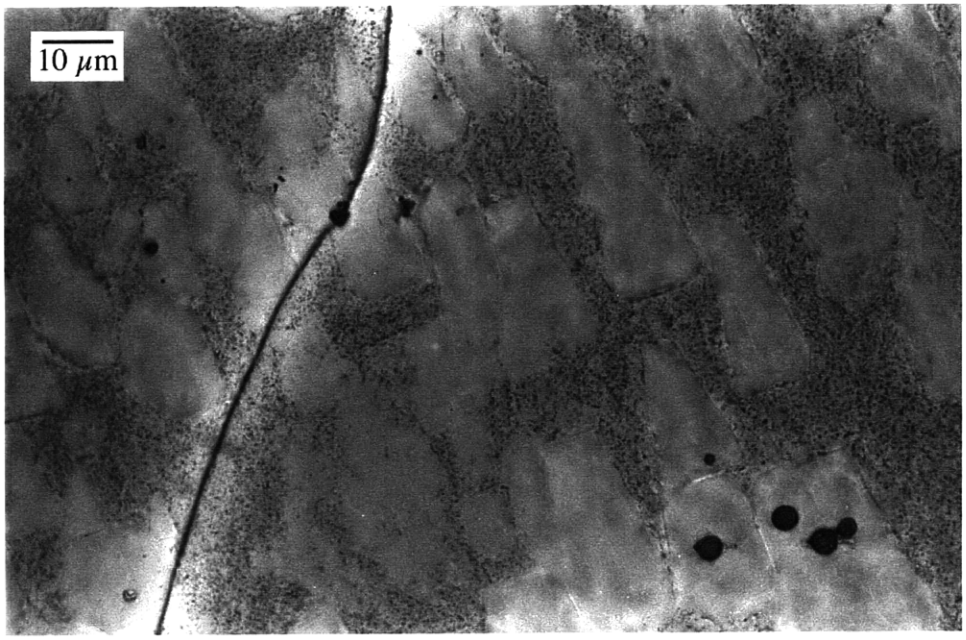

FIGURE 1. Surface of AgCl sample with imperfect NaCl epilayer. Lighter triangular regions are NaCl. An AgCl grain boundary and several inclusions are visible.

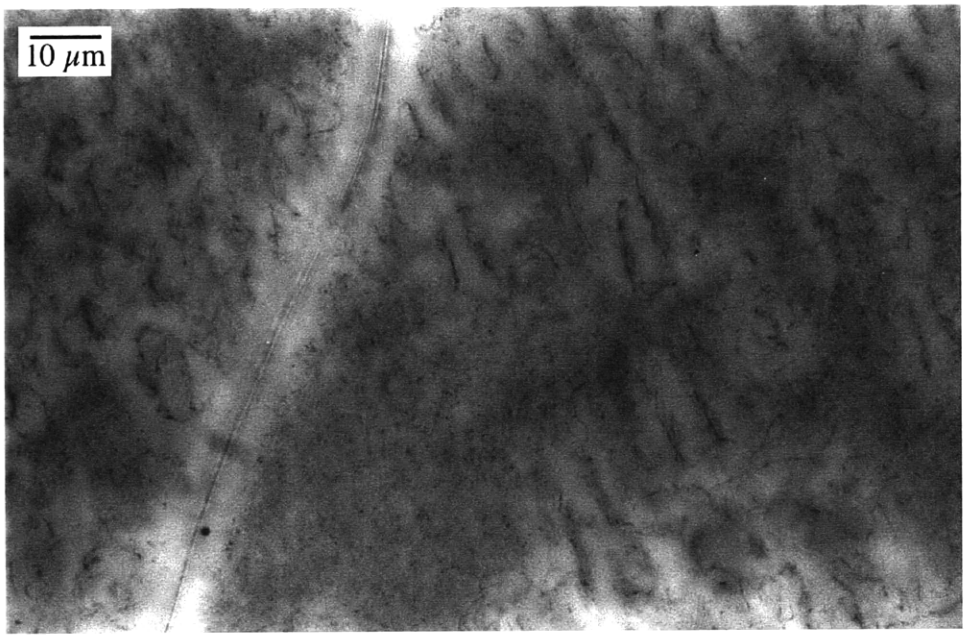

FIGURE 2. The same sample shown above, 7 μm below the heterophase interface. Dislocations visible in the AgCl phase follow the shape of the NaCl crystals above them.

APPENDIX A

Mathematica Code

1. Ashby-Johnson Calculator

This program does two things:

- Calculate the misfit strain in the AgCl-glass system
- Calculate the critical particle radius for nucleation given the misfit, or the misfit required for a given particle radius.

```
(* This is Mathematica 2.2.2 but it should work in any version *)

In[1]:= (*sets up the integrals from Ashby and Johnson 1969 *)
AJwork[r_] =  6 G z rp^3 b Integrate[x/(x^2 + y^2 + z^2)^(5/2),
            {x,c,c + (r Sqrt[Pi] / 2)},{y,-1*(r Sqrt[Pi] / 2),
            (r Sqrt[Pi] / 2)}];
AJenergy[r_]= G b^2 r (2 - nu) Log[(8 r / b) - 2] /(4 (1 - nu));
(* here, r is the loop radius and rp the sphere radius *)


In[4]:= (* nucleation can occur when this AJWtotal = 0 for r > 0*)
AJWtotal[r_] = AJenergy[r]- e11c AJwork[r] /. {z->rp/Sqrt[2],
               c->rp/Sqrt[2]};

In[6]:= (* so the critical value is when AJWtotal and its derivative
          are both equal to zero. *)
derivAJ[r_] = D[AJWtotal[r],r];

In[7]:=
(* below are lattice constants for AgCl as f(T), used to get CTE
   and Burgers vector *)
deltaa[T_]:= -0.0034874 - 2.5302 10^-5 T + 2.0573 10^-7 T^2 -
               3.3427 10^-10 T^3 + 2.1806 10^-13 T^4;
latticea[T_]:= 5.5496 10^-10 * (1 + deltaa[T]);
(* lattice constant of AgCl from delta [lattice constant a]
   data of Fouchaux and Simmons 1964 *)
bvec[T_] = latticea[T]/Sqrt[2];
totalpyrexstrain[T1_,T2_]:= 32 10^-7 * (T2-T1);

In[13]:=
eigenstrain[T1_,T2_]:= Log[latticea[T2]/latticea[(T1)]] -
                       totalpyrexstrain[T1,T2];
e11t = eigenstrain[273.15 + 21.5,447.9];
```

```
e11c:= e11t * 3 Kp / (3 Kp + 4 G);
taumax:= - 3 G e11c;
nu = 0.409;            (* Loje and Schuele 1970, Voigt average *)
G  = 8.55 10^9;       (* Loje and Schuele 1970, Voight average *)
b  = N[bvec[273.15 + 21]];   (* from Fouchaux's expansion data *)
Ep = 51 10^9;     (* from Corning tech support, for 7070 glass *)
nup= 0.22;             (*  Note we have no f(T) data for pyrex *)
Kp = Ep/(3 * (1 - 2 nup));               (*From Ugural eqn 2.21*)

In[35]:= (* For instance, here's the Burgers vector at room T *)
N[bvec[273.15 + 21.5]]

Out[35]=
          -10
3.9242 10

In[26]:=
(* Typical syntax for finding a critical particle radius rp* at
   a given value of misfit strain. What you enter is e11t, based
   on the estimated temperature change. So if we wanted to look
   at rp* for a change from 300 C to room temp, it would like this:
*)
e11t = eigenstrain[273.15 + 21.5,273.15 + 300];
FindRoot[{10^16 AJWtotal[r],10^10 derivAJ[r]},
         {r,.5 10^-6, .51 10^-6},{rp, .6 10^-6,.65 10^-6}
         ,MaxIterations->90]

Out[28]= (* with output like this *)
                -7                      -7
{r -> 1.5782 10   , rp -> 2.18293 10   }

(* It's a good idea to check the results graphically to make sure
   FindRoot didn't give you something nutty. *)
```

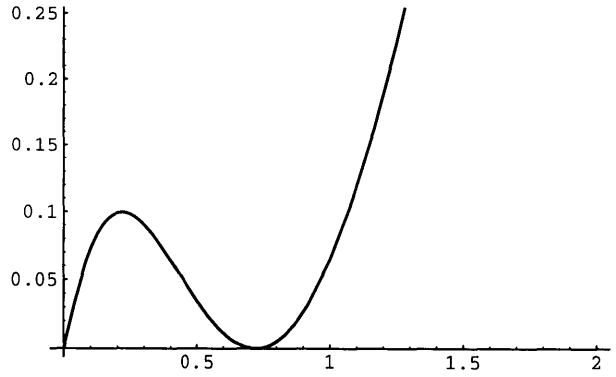


```
(* you may have to tweak starting values of r. You can use FindRoot
   to back calculate required misfit strains, etc. *)
```

2. Elastic Moduli Calculator

This code is adapted straight from the appropriate sections of HIRTH AND LOTHE 1968. It performs various tensor manipulations and calculates the elastic moduli of AgCl (Voigt and Reuss averages) as a function of temperature, based on LOJE AND SCHUELE 1970.

```
In[1]:=
transform2[A_,L_]:= Table[Sum[L[[i,m]] L[[j,n]] A[[m,n]],
    {m,1,3},{n,1,3}],{i,1,3},{j,1,3}];

transform2[A_,L_]:=
    Table[Sum[L[[i,p]] L[[j,q]] L[[k,r]] L[[l,s]] A[[m,n]],
    {p,3},{q,3},{r,3},{s,3}],{i,3},{j,3},{k,3},{l,3}];

returnindexpairs[n_]:= Module[{m},
If[n==1,m={1,1}];
If[n==2,m={2,2}];
If[n==3,m={3,3}];
If[n==4,m={2,3}];
If[n==5,m={3,1}];
If[n==6,m={1,2}];
If[n==7,m={3,2}];
If[n==8,m={1,3}];
If[n==9,m={2,1}];
m];

ReducedForm[A_]:= Module[{indx},
Table[indx = Flatten[{returnindexpairs[m],returnindexpairs[n]}];

A[[indx[[1]],indx[[2]],indx[[3]],indx[[4]]]],{m,6},{n,6}]];

c = Table[0,{i,3},{j,3},{k,3},{l,3}];
Do[
c[[i,i,j,j]] = c12; (* clean up ciiii later *)
c[[i,j,i,j]] = c44;  (* ditto *)
c[[i,i,i,i]] = c11; (* now set ciiii's *)
,{i,3},{j,3}];

reducedsprime = Inverse[ReducedForm[c]];
findconstant[i_,j_]:=Module[{rval},
If[((i<=3) && (j<=3)),rval = 1];
If[(((i>=4) && (j<=3)) || ((i<=3) && (j>=4))),rval = 1/2];
If[((i>=4) && (j>=4)),rval = 1/4];
rval];

reduceds = Table[reducedsprime[[i,j]] *
     findconstant[i,j],{i,1,6},{j,1,6}];

s  = Table[0,{i,3},{j,3},{k,3},{l,3}];
```

```
Do[
first2 = returnindexpairs[i];
last2 =  returnindexpairs[j];
index = Flatten[{first2,last2}];
s[[  index[[1]],index[[2]],index[[3]],index[[4]]  ]] =
     reduceds[[i,j]]
,{i,1,6},{j,1,6}];



In[13]:=
(* voigt shear modulus *)
mu := 1/30 *(3 * Sum[c[[i,j,i,j]], {i,1,3},{j,1,3}] -
    Sum[c[[i,i,j,j]],  {i,1,3},{j,1,3}] );
(* voigt lame constant *)
lambda:= 1/15 * (2 * Sum[c[[i,i,j,j]], {i,1,3},{j,1,3}] -
    Sum[c[[i,j,i,j]],  {i,1,3},{j,1,3}] );
(* voigt poisson ratio *)
nu := lambda / (2 * (mu + lambda));
(* anistropy ratio *)
a := 2 c44 / (c11 - c12);
(* voigt *)
youngs:= (mu * (3 lambda + 2 mu))/(mu + lambda);
J:= (reducedsprime[[1,1]] - reducedsprime[[1,2]] -
    (reducedsprime[[4,4]]/2));
(* reuss 1/E *)
oneOverEr:= reducedsprime[[1,1]] - (2/5)*J;
(*general: 1/15 * (2 Sum[s[[i,j,i,j]],{i,1,3},{j,1,3}] +
    Sum[s[[i,i,j,j]],{i,1,3},{j,1,3}] );*)
(* reuss nu/E *)
nuOverEr:= - reducedsprime[[1,2]] - (1/5) * J;
(* general: 1/15 * (Sum[s[[i,j,i,j]],{i,1,3},{j,1,3}] -
    2 Sum[s[[i,i,j,j]],{i,1,3},{j,1,3}]);*)
(* reuss 1/mu *)
oneOverMur:= reducedsprime[[4,4]] + (4/5)*J;
(* general 1/15 *(Sum[ 6 * s[[i,j,i,j]],{i,1,3},{j,1,3}] -
    Sum[2 * s[[i,i,j,j]],{i,1,3},{j,1,3}]);*)


In[33]:=
(*Using Loje's data we can determine cij at temperature T.
units from paper are 10^12 dynes /cm^2;
there are 10 dynes/cm^2 in 1 Pa, so multiply by 10^11 to get Pa*)
lojeC11[T_]:= .5985 * 10^11 Exp[ ((T-300) * -10.40 * 10^-4)];
lojeC12[T_]:= .3611 * 10^11 Exp[ ((T-300) * - 4.89 * 10^-4)];
lojeC44[T_]:= .0624 * 10^11 Exp[ ((T-300) * - 4.15 * 10^-4)];
In[37]:=
elasticConstants[temp_]:=Module[{},
```

```
values = {c11->lojeC11[temp],c12->lojeC12[temp],c44->lojeC44[temp]};
Print ["AgCl Values from Loje (1970), in Pa) at ",temp," K"];
Print["Voigt: G = ",mu /. values," E = ",youngs /. values,
  " nu = ",nu /. values," A = ",a /. values,
  " H = ",(2 c44 + c12 - c11) /. values];
Print["Reuss: 1/E = ",oneOverEr /. values," nu/E = ",
  nuOverEr /. values," 1/mu = ",oneOverMur /. values];
Print["Reuss: G = ",(1/oneOverMur) /. values," E = ",
  (1/oneOverEr) /. values," nu = ",(nuOverEr/oneOverEr) /. values];
Print[values]]
In[38]:=
elasticConstants[300]
AgCl Values from Loje (1970), in Pa) at 300 K
                    9              10
Voigt: G = 8.492 10   E = 2.3937 10    nu = 0.409
                              10
   A = 0.525 H = -1.126 10
                       -11                   -11                    -10
Reuss: 1/E = 4.5808 10     nu/E = 1.91181 10     1/mu = 1.29852 10
                     9                10
Reuss: G = 7.70106 10   E = 2.18302 10    nu = 0.417353
                  10                 10                 9
{c11 -> 5.985 10   , c12 -> 3.611 10   , c44 -> 6.24 10 }
```

References

ABRAMOV 1993. *Ultrasound in Liquid and Solid Metals.* CRC Press, Boca Raton.

ARGON, A. S. 1952. "Cross-slip in ionic crystals." *Acta Metallurgica* **10**, pp. 574–8.

ARGON, A. S., J. IM AND R. SAFOGLU 1975. "Cavity formation from inclusions in ductile fracture." *Metallurgical Transactions* **6A**, pp. 825–37.

ARSENAULT, R. J. 1991. "Strengthening of metal matrix composites due to dislocation generation through CTE mismatch." Appearing in *Metal Matrix Composites: Mechanisms and Properties*, vol. 2, R. K. Everett and R. J. Arsenault, eds., Academic Press, Boston, pp. 79–100.

ARSENAULT, R. J. AND R. M. FISHER 1983. "Microstructure of fiber and particulate metal matrix composites." *Scripta Metallurgica* **17**, pp. 67–71.

ARSENAULT, R. J., L. WANG AND C. R. FENG 1991. "Strengthening of composites due to microstructural changes in the matrix." *Acta Metallurgica et Materialia* **39**, pp. 47–57.

ASHBY, M. F. 1970. "The deformation of plastically non-homogenous metals." *Philosophical Magazine* **21**, pp. 399–424.

ASHBY, M. F., S. H. GELLES AND L. E. TANNER 1969. "The stress at which particles are generated at a particle-matrix interface." *Philosophical Magazine* **19**, pp. 757–71.

ASHBY, M. F. AND L. JOHNSON 1969. "On the generation of dislocations at misfitting particles in a ductile matrix." *Philosophical Magazine* **20**, pp. 1009–22.

AVERBACK, R. S. AND M. GHALY 1996. "Fundamental aspects of defect production in solids." *Nuclear Instruments and Methods in Physics Research, Section B* **127–128**, pp. 1–11.

BARIN, I. 1993. *Thermochemical Data of Pure Substances.* VCH Verlagshesellschaft mbH, Weinheim.

BARLOW, C. Y. 1991. "Microstructural evolution during straining of discontinuously reinforced metal matrix composites." Presented at *Metal Matrix Composites—Processing, Microstructure and Properties*, Risø National Laboratory, Risø National Laboratory.

BARLOW, C. Y. AND N. HANSEN 1989. "Deformation structures in aluminum containing small particles." *Acta Metallurgica* **37**, pp. 1313–20.

BARTLETT, J. T. AND J. W. MITCHELL 1958. "The decoration of dislocations with crystals of silver chloride with gold." *Philosophical Magazine* **3**, pp. 334–41.

BARTLETT, J. T. AND J. W. MITCHELL 1960. "The generation of dislocation loops at the surface of crystals of silver bromide." *Philosophical Magazine* **5**, pp. 445–50.

BATRA, A. P. AND L. M. SLIFKIN 1972. "Impurity ions and vacancies in silver halide crystals." Presented at *International Colloquium on the Physics and Chemistry of the Silver Halide Crystal*, Montreal, Society of Photographic Scientists and Engineers.

BAY, B., N. HANSEN, D. A. HUGHES AND D. KUHLMANN-WILSDORF 1992. "Evolution of F.C.C. deformation structures in polyslip." *Acta Metallurgica et Materialia* **40**, pp. 205–19.

BEVINGTON, P. R. AND D. K. ROBINSON 1992. *Data Reduction and Error Analysis for the Physical Sciences.* McGraw-Hill, New York.

BROOKS, H. 1952. *Metal Interfaces.* American Society for Metals, Cleveland.

BROWN, L. M. 1964. "The self-stress of dislocations and the shape of extended nodes." *Philosophical Magazine* **10**, pp. 441–66.

BROWN, L. M. AND G. R. WOOLHOUSE 1970. "The loss of coherency of precipitates and the generation of dislocations." *Philosophical Magazine* **21**, pp. 329–45.

BROWN, L. M., G. R. WOOLHOUSE AND VALDRÈ 1968. "Radiation-induced coherency loss in a Cu-Co alloy." *Philosophical Magazine* **17**, pp. 781.

BULLOUGH, R. AND R. C. NEWMAN 1960. "The spacing of prismatic dislocation loops." *Philosophical Magazine* **5**, pp. 921–6.

BYSTRICKY, P. 1997. "Plasticity of metal matrix composites reinforced with continuous alumina fibers.", Ph. D. Thesis, Massachusetts Institute of Technology, Cambridge.

CARRINGTON, W. P. AND D. MCLEAN 1965. "Slip nuclei in silicon iron." *Acta Metallurgica* **13**, pp. 493–9.

CARTER, W. C., J. E. TAYLOR AND J. W. CAHN 1997. "Variational methods for microstructural-evolution theories." *JOM* **49**, pp. 30–6.

CHAKRABARTY, J. 1987. *Theory of Plasticity.* McGraw-Hill, New York.

CHEN, C.-W. 1986. *Magnetism and Metallurgy of Soft Magnetic Materials.* Dover, New York.

CHEN, T.-K. AND H. MARGOLIN 1989. "Elastic interaction stresses: Part II. The influence of orientation on stresses generated in iso-axial bicrystals." *Metallurgical Transactions* **20A**, pp. 1461–73.

CHEREPANOV, G. P. 1997. *Methods of Fracture Mechanics: Solid State Physics.* Kluwer Academic, Dordrecht.

CHRISTIAN, J. W. 1975. *The Theory of Transformations in Metals and Alloys–Part I.* Pergamon Press, Oxford.

CHRISTMAN, T., A. NEEDLEMAN AND S. SURESH 1989. "An experimental and numerical study of deformation in metal-ceramic composites." *Acta Metallurgica* **37**, pp. 3029–50.

CLARK, P. V. M. AND J. W. MITCHELL 1956. "Experiments on photographic sensitivity." *The Journal of Photographic Science* **4**, pp. 1–20.

CLYNE, T. W. AND P. J. WITHERS 1993. *An Introduction to Metal Matrix Composites.* Cambridge University Press, Cambridge.

CORNING TECHNICAL STAFF 1997. Personal communication.

COTTRELL 1953. *Dislocations and Plastic Flow in Crystals.* Oxford University Press, London.

COTTRELL, A. H. AND B. A. BILBY 1949. "Dislocation theory of yielding and strain ageing of iron." *Proceedings of the Physical Society of London* **62A**, pp. 49–62.

DAO, M. AND R. J. ASARO 1996a. "Localized deformation modes and non-Schmid effects in crystalline solids. Part I. Critical conditions of localization." *Mechanics of Materials* **23**, pp. 71–102.

DAO, M. AND R. J. ASARO 1996b. "Localized deformation modes and non-Schmid effects in crystalline solids. Part II. Deformation patterns." *Mechanics of Materials* **23**, pp. 71–102.

DAS, G. AND S. V. RADCLIFFE 1969. "Pressure-induced development of dislocations at elastic discontinuities." *Philosophical Magazine* **20**, pp. 589–609.

DEWIT, G. AND J. S. KOEHLER 1959. "Interaction of dislocations with an applied stress in anisotropic crystals." *Physical Review* **116**, pp. 1113–20.

DUNAND, D. C. 1991. "Mechanics and structure of dislocations induced by thermal mismatch in composite materials.", Ph.D. Thesis, Massachusetts Institute of Technology, Cambridge, MA.

DUNAND, D. C. AND A. MORTENSEN 1991a. "On plastic relaxation of thermal stresses in reinforced metals." *Acta Metallurgica et Materialia* **39**, pp. 127–39.

DUNAND, D. C. AND A. MORTENSEN 1991b. "Reinforced silver chloride as a model material for the study of dislocations in metal matrix composites." *Materials Science and Engineering* **A144**, pp. 179–88.

EARHART, E. J. 1997. "Experimental investigation of stress and strain fields in a ductile matrix surrounding an elastic inclusion.", Ph.D. Thesis, Massachusetts Institute of Technology, Cambridge, MA.

ESHELBY, J. D. 1957. "The determination of the elastic field of an ellipsoidal inclusion, and related problems." *Proceedings of the Royal Society of London* **241A**, pp. 376–96.

ESHELBY, J. D. 1959. "The elastic field outside an ellipsoidal inclusion." *Proceedings of the Royal Society of London* **252A**, pp. 561–9.

ESHELBY, J. D. 1961. "Elastic inclusions and inhomogeneities." Appearing in *Progress in Solid Mechanics*, vol. 2, I. N. Sneddon and R. Hill, eds., North-Holland, Amsterdam, pp. 88–140.

ESHELBY, J. D., W. T. READ AND W. D. SHOCKLEY 1953. "Anisotropic elasticity with applications to dislocation theory." *Acta Metallurgica* **1**, pp. 251–9.

EVANS, A. G. 1978. "Microfracture from thermal expansion anisotropy—I. Single phase systems." *Acta Metallurgica* **26**, pp. 1845–53.

FISHER, J. C., E. W. HART AND R. H. PRY 1953. "The hardening of metal crystals by precipitate particles." *Acta Metallurgica* **1**, pp. 336–9.

FOREMAN, A. J. E. 1955. "Dislocation energies in anisotropic crystals." *Acta Metallurgica* **3**, pp. 322–30.

FOUCHAUX, R. D. AND R. O. SIMMONS 1964. "Measurement of thermal expansion and thermal equilibrium defects in silver chloride." *Physical Review* **136**, pp. A1664–A74.

FRANK, F. C. 1949. "The influence of dislocations on crystal growth." *Discussions of the Faraday Society* **5**, pp. 48,67.

FRANK, F. C. AND J. READ, W.T. 1950. "Multiplication process for slow moving dislocations." *Physical Review* **79**, pp. 722–3.

FRENKEL 1926. "Zur Theorie der Elastizitätsgrenze und der Festigkeit Kristallinischer Körper." *Zeitschrift für Physik* **37**, pp. 572–609.

FRIEDEL, J. 1964. *Dislocations.* Addison-Wesley, Reading, MA.

GHAHREMANI, F., J. W. HUTCHINSON AND V. TVERGAARD 1990. "Three-dimensional effects in microcrack nucleation in brittle polycrystals." *Journal of the American Ceramics Society* **73**, pp. 1548–54.

GHOSH, A. J. 1993. "Solid-state processing." Appearing in *Fundamentals of Metal-Matrix Composites.* S. Suresh, A. Mortensen and A. Needleman, eds., Butterworth-Heinemann, Boston, pp. 23–41.

GILMAN, J. J. 1994. "Micromechanics of shear banding." *Mechanics of Materials* **17**, pp. 83–96.

GOLDENBERG, S. S., C. T. KAO, L. G. ROWAN AND L. SLIFKIN 1992. "Tunneling migration of self-trapped holes in AgCl." *Physical Review B* **46**, pp. 2809–13.

GRIFFITH, A. A. 1921. "The phenomena of rupture and flow in solids." *Philosophical Transactions of the Royal Society of London* **A221**, pp. 163–97.

GRILHÉ, J. 1963. "Action d'une contrainte sur une dislocation helicoidale ou une boucle prismatique." *Acta Metallurgica* **11**, pp. 57–9.

GULDEN, M. E. AND W. D. NIX 1968. "Observations of dislocation sources in an aluminum-copper-silicon alloy." *Philosophical Magazine* **18**, pp. 217–28.

GURSON, A. L. 1977. "Continuum theory of ductile rupture by void nucleation and growth: Part I. Yield criteria and flow rules for porous ductile metals." *Journal of Engineering Materials Technology* **99**, pp. 2.

HAASEN, P. 1986. *Physical Metallurgy.* Cambridge University Press, Cambridge.

HALL, E. O. 1951. "The deformation and ageing of mild steel: III. Discussion of results." *Physical Society of London* **B64**, pp. 747–52.

HANSEN, N. 1985. "Polycrystalline strengthening." *Metallurgical Transactions* **16A**, pp. 2167–90.

HASHIMOTO, K. AND H. MARGOLIN 1983a. "The role of elastic interactions stresses on the onset of slip in polycrystalline brass: I. Experimental determination of operating slip systems and qualitative analysis." *Acta Metallurgica* **31**, pp. 773–86.

HASHIMOTO, K. AND H. MARGOLIN 1983b. "The role of elastic interactions stresses on the onset of slip in polycrystalline brass: II. Rationalization of the slip behavior." *Acta Metallurgica* **31**, pp. 787–800.

HAUSER, J. J. AND B. CHALMERS 1961. "The plastic deformation of bicrystals of F.C.C. metals." *Acta Metallurgica* **9**, pp. 802–18.

HAYNES, J. R. AND W. SHOCKLEY 1951. "The mobility of electrons in silver chloride." *Physical Review* **82**, pp. 935–43.

HEDGES, J. M. AND J. W. MITCHELL 1953a. "The observation of polyhedral sub-structures in crystals of silver bromide." *Philosophical Magazine* **44**, pp. 223–4.

HEDGES, J. M. AND J. W. MITCHELL 1953b. "Some experiments on photographic sensitivity." *Philosophical Magazine* **44**, pp. 357–88.

HILDENBRAND, D. L. AND K. H. LAU 1996. "Thermochemistry of gaseous AgCl, Ag3Cl3, and CuCl." *High Temperature and Materials Science* **35**, pp. 11–20.

HILL, R. 1950. *The Mathematical Theory of Plasticity.* Oxford University Press, Oxford.

HIRSCH, P. B. AND F. J. HUMPHREYS 1970. "The deformation of single crystals of copper and copper zinc alloys containing alumina Particles—I. Macroscopic properties and workhardening theories." *Proceedings of the Royal Society of London* **A318**, pp. 45–72.

HIRSCH, P. B., J. SILCOX AND R. E. SMALLMAN 1958. "Dislocation loops in quenched aluminum." *Philosophical Magazine* **3**, pp. 897–908.

HIRTH, J. P. 1972. "The influence of grain boundaries on mechanical properties." *Metallurgical Transactions* **3**, pp. 3047–67.

HIRTH, J. P. AND J. LOTHE 1968. *Theory of Dislocations.* McGraw–Hill, New York.

HIRTH, J. P. AND J. LOTHE 1982. *Theory of Dislocations.* John Wiley and Sons, New York.

HOOK, R. E. AND J. P. HIRTH 1967. "The deformation behavior of isoaxial bicrystals of Fe-3% Si." *Acta Metallurgica* **15**, pp. 535–51.

HOSFORD, W. F. 1993. *The Mechanics of Crystals and Textured Polycrystals.* Oxford University Press, New York.

HU, X. AND H. MARGOLIN 1990. "Stress gradients and extent of slip in alpha brass." *Metallurgical Transactions* **21A**, pp. 3075–84.

HULL, R. AND J. C. BEAN 1992. "Misfit dislocations in lattice-mismatched epitaxial films." *Critical Reviews In Solid State And Materials Sciences* **17**, pp. 507–46.

HUTCHINSON, J. W. AND R. M. MCMEEKING 1993. "Continuum models for deformation: discontinuous reinforcements." Appearing in *Fundamentals of Metal-Matrix Composites.* S. Suresh, A. Mortensen and A. Needleman, eds., Butterworth-Heinemann, Boston, pp. 158–73.

ISUPOV, L. P. 1996. "A variant of the theory of plasticity of two-phase composite media." *Acta Mechanica* **119**, pp. 65–78.

JACOB, K. T. AND K. H. E. JEFFES 1972. "An improved method for calculating activities from distribution equilibria." *High Temperatures - High Pressures* **4**, pp. 177–82.

JAIN, S. C., A. H. HARKER AND R. A. COWLEY 1997. "Misfit strain and misfit dislocations in lattice mismatched epitaxial layers and other systems." *Philosophical Magazine A* **75**, pp. 1461–515.

JOHNSON, W. C. AND J. K. LEE 1983. "A dislocation model for the plastic relaxation of the transformation strain energy of a misfitting particle." *Acta Metallurgica* **31**, pp. 1033–145.

JOHNSTON, W. G. AND J. J. GILMAN 1959. "Dislocation velocities, dislocation densities, and plastic flow in lithium fluoride crystals." *Journal of Applied Physics* **30**, pp. 129.

JONES, D. A. AND J. W. MITCHELL 1958. "Observations of helical dislocations in crystals of silver chloride." *Philosophical Magazine* **3**, pp. 1–7.

JUNQUA, N. AND GRILHÉ 1997. "Surface step-dislocation transition and dislocation nucleation at a solid free surface." *Philosophical Magazine Letters* **75**, pp. 125–30.

KIM, C. T., J. K. LEE AND M. R. PLICHTA 1990. "Plastic relaxation of thermoelastic stress in aluminum/ceramic composites." *Metallurgical Transactions* **21A**, pp. 673–82.

KOCKS, U. F. 1970. "The relation between polycrystal deformation and single crystal deformation." *Metallurgical Transactions* **1**, pp. 1121.

KOEHLER, J. S. 1952. "The nature of work hardening." *Physical Review* **86**, pp. 52–9.

KUHLMANN-WILSDORF, D. 1992. "Fundamentals of cell and subgrain structures in historical perspective." *Scripta Metallurgica et Materialia* **27**, pp. 951–6.

LANGFORD, G. AND M. COHEN 1969a. "Calculation of cell-size strengthening of wire-drawn iron." *Metallurgical Transactions* **1**, pp. 1478–80.

LANGFORD, G. AND M. COHEN 1969b. "Strain hardening of iron by severe plastic deformation." *ASM Transactions Quarterly* **62**, pp. 623.

LEE, J. K., Y. Y. EARMME, H. I. AARONSON AND K. C. RUSSELL 1980. "Plastic relaxation of the transformation strain energy of a misfitting spherical precipitate: ideal plastic behavior." *Metallurgical Transactions* **11A**, pp. 1837–47.

LI, J. C. M. 1961. "Cross slip and cross climb of dislocations induced by a locked dislocation." *Journal Of Applied Physics* **32**, pp. 593–9.

LI, J. C. M. 1963. "Petch relation and grain boundary sources." *Transactions of the Metallurgical Society of the AIME* **227**, pp. 239–47.

LI, J. C. M. 1980. "Dislocation sources." Presented at *Dislocation Modelling of Physical Systems*, Gainesville, FL, Pergamon Press.

LI, J. C. M. AND Y. T. CHOU 1970. "The role of dislocations in the flow stress grain size relationships." *Metallurgical Transactions* **1**, pp. 1145–59.

LIVINGSTON, J. D. 1959. "Critical size for precipitation hardening." *Trans. AIME* **215**, pp. 566–71.

LIVINGSTON, J. D. AND B. CHALMERS 1957. "Multiple slip in bicrystal deformation." *Acta Metallurgica* **5**, pp. 322–7.

LOJE, K. F. AND D. E. SCHUELE 1970. "The pressure and temperature derivatives of the elastic constants of AgBr and AgCl." *Journal of the Physical Chemistry of Solids* **31**, pp. 2051–67.

LOVE, A. E. H. 1927. *A Treatise on the Mathematical Theory of Elasticity.* Dover, New York.

LYNCH, C. T., ED. 1989. *Practical Handbook of Materials Science.* CRC Press, Boca Raton.

MAKENAS, B. J. AND H. K. BIRNBAUM 1980. "Phase changes in the niobium-hydrogen system I. Accomodation effects during hydride precipitation." *Acta Metallurgica* **28**, pp. 979–88.

MALINOWSKI, J. 1972. "Participation of addenda in the photographic process." Presented at *International Colloquium on the Physics and Chemistry of the Silver Halide Crystal*, Montreal, Society of Photographic Scientists and Engineers.

MALIS, T. AND K. TANGRI 1978. "Grain boundaries as dislocation sources in the premacroyield region." *Acta Metallurgica* **27**, pp. 25–32.

MARGOLIN, H. AND M. S. STANESCU 1975. "Polycrystalline strengthening." *Acta Metallurgica* **23**, pp. 1411–29.

MARGOLIN, H., Z. WANG AND T.-K. CHEN 1984. "Slip in a stress gradient: multiple slip and cross slip in an alpha brass single crystal oriented for easy glide." *Acta Metallurgica* **32**, pp. 977–85.

MASSARDIER, V., R. FOUGÈRES AND P. MERLE 1995. "Comparison between the experimental and theoretical tensile behavior of aluminum based metal matrix composites reinforced with preforms of α alumina platelets." *Materials Science and Engineering* **A203**, pp. 93–104.

MATSUURA, K., M. TSUKAMOTO AND K. WATANABE 1975. "The work hardening of Cu-Fe alloy single crystals containing iron precipitates." *Acta Metallurgica* **23**, pp. 1033–44.

MATTHEWS, J. W. 1971. "A mechanism for the formation of helices and loops at precipitate particles." *Scripta Metallurgica* **5**, pp. 1053–6.

MATTHEWS, J. W. 1977. "Misfit dislocations." Appearing in *Dislocations in Solids*, vol. 2, F. R. N. Nabarrow, ed., North-Holland, Amsterdam, pp. 461–545.

MCHUGH, P. E., R. J. ASARO AND C. F. SHIH 1993. "Crystal plasticity models." Appearing in *Fundamentals of Metal-Matrix Composites.* S. Suresh, A. Mortensen and A. Needleman, eds., Butterworth-Heinemann, Boston, pp. 139–57.

MCPHERSON, G. 1990. *Statistics in Scientific Investigation: Its Basis, Application, and Interpretation.* Springer-Verlag, New York.

MEES, C. E. K. AND T. H. JAMES 1966. *The Theory of the Photographic Process.* Macmillan, New York.

MEYERS, A. M. AND K. K. CHAWLA 1984. *Mechanical Metallurgy: Principles and Applications.* Prentice-Hall, Englewood Cliffs,NJ.

MEYERS, M. A. AND E. ASHWORTH 1982. "A model for the effect of grain size on the yield stress of metals." *Philosophical Magazine* **46**, pp. 737–59.

MITCHELL, J. W. 1957. "Photographic sensitivity." *Reports on the Progress of Physics* **20**, pp. 433–515.

MITCHELL, J. W. 1980. "Dislocations in crystals of silver halides." *Proceedings of the Royal Society of London* **A371**, pp. 149–59.

MORI, T. AND K. TANAKA 1973. "Average stress in matrix and average elastic energy of materials with misfitting inclusions." *Acta Metallurgica* **21**, pp. 571.

MOTT, N. F. 1952. "A theory of work hardening of metal crystals." *Philosophical Magazine* **43**, pp. 1151–78.

MOTT, N. F. AND F. R. N. NABARRO 1940. "An attempt to estimate the degree of precipitation hardening with a simple model." *Proceedings of the Physical Society* **52**, pp. 86.

MURA, T. 1968. "The continuum theory of dislocations." *Advances in Materials Research* **3**, pp. 1.

MURA, T. 1982. *Micromechanics of Defects in Solids.* Martinus Mijhoff, The Hague.

NABARRO, F. R. N. 1940. "The strains produced by precipitation in alloys." *Proceedings of the Royal Society of London* **A175**, pp. 519.

NABARRO, F. R. N. 1967. *Theory of Crystal Dislocations.* Clarendon Press, Oxford.

NABARRO, F. R. N., ED. 1979. *Dislocations in Solids*, vol. 1–10. North-Holland, Amsterdam.

NYE, J. F. 1964. *Physical Properties of Crystals: Their Representatives by Tensors And Matrices.* Clarendon Press, Oxford.

OROWAN, E. 1934. "Zur kristallplastizität. III." *Zeitschrift für Physik* **89**, pp. 634–659.

PARASNIS, A. S., F. C. FRANK AND J. W. MITCHELL 1963. "Linear compounds of dislocations in silver chloride with cupric ions." *Philosophical Magazine* **8**, pp. 1503–12.

PARASNIS, A. S. AND J. W. MITCHELL 1959. "Some properties of crystals of silver chloride containing traces of copper chlorides." *Philosophical Magazine* **4**, pp. 171–9.

PEACH, M. AND J. S. KOEHLER 1950. "The forces exerted on dislocations and the stress fields produced by them." *Physical Review* **80**, pp. 436–9.

PETCH, N. J. 1953. "The cleavage strength of polycrystals." *Journal of the Iron and Steel Institute* **174**, pp. 25–8.

PICU, C. R. 1997. "Three-dimensional stress concentration at grain triple junctions in columnar ice." *Philosophical Magazine Letters* **76**, pp. 159–66.

PICU, C. R. AND V. GUPTA 1997. "Three-dimensional stress singularities at the tip of a grain triple junction line intersecting the free surface." *Journal of the Mechanical Physics of Solids* **45**, pp. 1495–520.

POLANYI 1934. "Über eine Art Gitterstörung, die einen Kristall pastisch machén Könnte." *Zeitschrift für Physik* **89**, pp. 660.

PORTER, D. A. AND K. E. EASTERLING 1981. *Phase Transformations in Metals and Alloys.* Van Nostrand Reinhold, Wokingham.

PRANGNELL, P. B., T. DOWNES, W. M. STOBBS AND P. J. WITHERS 1994. "The deformation of discontinuously reinforced MMCs—I. The initial yielding behavior." *Acta Metallurgica et Materialia* **42**, pp. 3425–36.

READ, W. T. 1953. *Dislocations in Crystals.* McGraw-Hill book Company, New York.

RICE, J. R. AND R. M. THOMSON 1974. "Ductile vs. brittle behaviour of crystals." *Philosophical Magazine* **29**, pp. 73–97.

ROTA, G.-C. 1995. *Introduction to Probability Theory*, 3rd preliminary edition. Birkhäuser.

SAHIN, O. AND H. MARGOLIN 1991. "Elastic stresses and slip intersections with F.C.C. twins." *Acta Metallurgica et Materialia* **39**, pp. 2445–59.

SATO, A., Y. SUGISAKI AND T. MORI 1983. "Effect of external stress on formation of vacancy loops in quenched aluminum." *Acta Metallurgica* **31**, pp. 805–11.

SCHUSTER, E., A. F. SCHWIND, R. VÖTSCH AND K. G. WEIL 1979. "Solubilities of silver and copper in their molten halide mixtures $AgCl(x)$–$Br(1-x)$ and $CuCl(x)Br(1-x)$." *Zeitschrift Für Naturforschung* **34a**, pp. 1203–6.

SEITZ, F. 1950. "Prismatic dislocations and prismatic punching in crystals." *Physical Review* **79**, pp. 723.

SHEN, Y.-L., M. FINOT, A. NEEDLEMAN AND S. SURESH 1995. "Effective plastic response of two-phase composites." *Acta Metallurgica et Materialia* **43**, pp. 1701–22.

SHI, N., B. WILNER AND R. J. ARSENAULT 1992. "An FEM study of the plastic deformation process of whisker reinforced SiC/Al composites." *Acta Metallurgica et Materialia* **40**, pp. 2481–854.

SITTNER, P. AND V. PAIDAR 1989. "Observation and interpretation of grain-boundary compatibility effects in Fe 3.3 wt percent Si bicrystals." *Acta Metallurgica* **37**, pp. 1717–26.

STEIN, D. F. AND J. LOW, J.R. 1960. "Mobility of edge dislocations in silicon iron." *Journal of Applied Physics* **31**, pp. 362–9.

STEINSALTZ, D. 1997. Personal communication.

STOKES, R. J. AND C. H. LI 1962. "The sodium chloride-silver chloride alloy system." *Acta Metallurgica* **10**, pp. 535–42.

SUITS, J. C. AND B. CHALMERS 1961. "Plastic microstrain in silicon-iron." *Acta Metallurgica* **9**, pp. 854–60.

SURESH, S. AND K. K. CHAWLA 1993. "Aging characteristics of reinforced metals." Appearing in *Fundamentals of Metal-Matrix Composites.* S. Suresh, A. Mortensen and A. Needleman, eds., Butterworth-Heinemann, Boston, pp. 139–57.

SUTTON, A. P. AND R. W. BALLUFFI 1995. *Interfaces in Crystalline Materials.* Oxford University Press, Oxford.

TAYLOR, G. I. 1934. "The mechanism of plastic deformation of crystals, Part I. Theoretical." *Proceedings of the Royal Society of London* **A145**, pp. 362–87.

THOMAS, G. B. AND R. FINNEY 1984. *Calculus and Analytic Geometry.* Addison-Wesley, Reading, Massachusetts.

THOMPSON, A. W., M. I. BASKES AND W. F. FLANAGAN 1973. "The dependence of polycrystalline work hardening on grain size." *Acta Metallurgica* **21**, pp. 1017–28.

TVERGAARD, V. AND J. W. HUTCHINSON 1988. "Microcracking in ceramics induced by thermal expansion or elastic anisotropy." *Journal of the American Ceramics Society* **71**, pp. 157–66.

VAN HOUTTE, P. 1995. "Heterogeneity of plastic strain around an ellipsoidal inclusion in an ideal plastic matrix." *Acta Metallurgica et Materialia* **43**, pp. 2859–79.

VOGELSANG, M., R. J. ARSENAULT AND R. M. FISHER 1986. "An in situ HVEM study of dislocation generation at Al/SiC interfaces in metal matrix composites." *Metallurgical Transactions* **17A**, pp. 379–89.

WANG, Z. R. AND H. MARGOLIN 1984. "Slip in a stress gradient: multiple slip and cross slip in an alpha brass single crystal oriented for easy glide." *Acta Metallurgica* **32**, pp. 977–85.

WEATHERLY, G. C. 1968a. "A determination of the punching stress at the interface of particles during quenching." *Metals Science Journal* **2**, pp. 237–40.

WEATHERLY, G. C. 1968b. "Loss of coherency of growing particles by the prismatic punching of dislocation loops." *Philosophical Magazine* **17**, pp. 791–9.

WEERTMAN, J. 1957. "Helical dislocations." *Physical Review* **107**, pp. 1259.

WEERTMAN, J. AND J. R. WEERTMAN 1964. *Elementary Dislocation Theory.* Macmillan, New York.

WENG, G. J. 1978. "The stress fields of continuous distribution of dislocations and of their movement in a polycrystalline aggregate." *International Journal of Solids and Structures* **14**, pp. 535–44.

WENG, G. J., M. TAYA AND H. ABÉ 1990. *Micromechanics and Inhomogeneity.* Springer-Verlag, New York.

WITHERS, P. J., A. N. SMITH, T. W. CLYNE AND W. M. STOBBS 1989. "A photoelastic examination of the validity of the Eshelby approach to the modelling of MMCs." Presented at *Fundamental Relationships Between Microstructures and Mechanical Properties of Metal Matrix Composites*, Indianapolis, IN, TMS.

WOOLHOUSE, G. R. AND M. IPOHORSKI 1971. "On the interaction between radiation damage and coherent precipitates." *Proceedings of the Royal Society of London* **A324**, pp. 415.

WU, M. S. 1997. "Crack nucleation due to dislocation pile-ups at I-, U- and amorphized triple lines." *Mechanics of Materials* **25**, pp. 215–34.

YAO, Z. AND R. H. WAGONER 1993. "Active slip in aluminum multicrystals." *Acta Metallurgica et Materialia* **41**, pp. 451–68.

ZHU, H. T. AND H. M. ZBIB 1993a. "A continuum model for flow strength of metal matrix composites." *Scripta Metallurgica et Materialia* **28**, pp. 1323–8.

ZHU, H. T. AND H. M. ZBIB 1993b. "A macroscopic model for plastic flow in metal matrix composites." *International Journal of Plasticity* **11**, pp. 471–99.

Biographical Note

Rob Calhoun was born in Washington D. C. in 1968. He grew up in Alexandria, Virginia and attended George Washington and T. C. Williams High Schools. In 1986 he entered MIT as an undergraduate, receiving an S. B. and a "Best Undergraduate Thesis" award from the Department of Materials Science and Engineering in 1990. As an undergraduate, he lived at Tau Epsilon Phi, where he held a number of house offices and was renown for his late-night repairs of Kirby the vacuum cleaner.

After working at Los Alamos National Laboratory over the summer, Rob returned to MIT in the fall of 1990 with a National Defense Science and Engineering Grant Fellowship and qualified for the Ph.D. program a year later. In 1992 he gave a talk on MMCs at the University of Yaoundé in Cameroun and co-authored a paper with Andreas Mortensen, "Infiltration of fibrous preforms by a pure metal. Part IV. Morphological stability of the remelting front," *Metallurgical Transactions* **23A**, 2291.

In 1993 he changed thesis topics from photoplasticity to dislocation decoration and, in a unique visit to a dance club, met Elizabeth Wilmer, a graduate student in Mathematics at Harvard. They were married in June of 1994. While awaiting renewal of the NSF grant supporting the AgCl work, Rob worked for Quantum Corporation in 1995–6, where he developed a new magnetic material for hard disk drive heads. Since returning to MIT in June of 1996, he has mostly concentrated on leaving.

Rob is the founder and president of Cystic Fibrosis Online Resources, a non-profit organization that runs a web site for people with cystic fibrosis. Elizabeth and Rob currently live in North Cambridge with their fish, their neglected garden, and too many books and computers. Elizabeth plans to enter academia; Rob does not, but has few definitive near-term plans other than getting his wisdom teeth extracted.

Readers with questions or comments about the thesis work should feel free to write to him at `rcalhoun@alum.mit.edu`.

Colophon

Experimental Notes

Microscopy. All optical microscopy work was done on a Zeiss Axioskop using a 1.25 NA Plan-Neofluar oil-immersion objective, a 1.30 oil-immersion condenser, and monochromatic (green) illumination. Zeiss microscopes are widely regarded as the best in the world and the many hundreds of hours spent using this instrument comprised the only truly enjoyable part of the thesis work. Because of the wide field of view, the fine image quality and the smooth focus action on the Zeiss, it is feasible to sort out fairly complicated dislocation structures when sitting at the microscope. Conversely, it is nearly impossible to capture the experience of the microscopist on film; in any one two-dimensional image, dislocations move in and out of the picture, and interpretation of the image much more difficult. I relied heavily on drawings made at the time of observation when later interpreting photographs.

Photography and Imaging. I used two kinds of imaging technology: traditional silver halide film and a CCD (video) camera. All film photographs were taken on the Zeiss using a Canon A-1 35mm body with an autowinder and cable release. I used Kodak TMAX-100, a fine-grained black and white film. The contrast of decorated dislocations is low, and I was never able to make really high contrast negatives. Professor Lechtman suggested using orthochromic (process) film but I was unable to find it in 35mm rolls.

After exposure, 35mm negatives were developed either in the lab or commercially and transferred to Kodak PhotoCD format. I have mixed feelings about the PhotoCDs; while I like having both the 35mm negatives and high-quality digital scans (nearly 23 pixels per μm at 1000$\times$) stored on CD-ROM, Kodak's support for black and white photography in this medium is poor. All images opened with Kodak's software are flat and lacking in contrast and dynamic range.

Much better contrast was obtained with the Dage-MTI CCD-72 camera. At 8 pixels per μm, the CCD images are coarser than the PhotoCDs but the contrast is much better; 10 bits of gray scale could be obtained by image summation. The ability to adjust the gain and black level of the camera in real time is a significant advantage. These images were digitized by summing six consecutive frames in IPLab using a Perceptics PixelBuffer frame grabber and stored on Zip disks.

Image Processing. IPlab was used for most image processing work, with the obligatory bounces in and out of Photoshop for file conversion, sizing, and adding micron markers. IPLab is a good, stable program which handles very large files exceptionally gracefully. The scripting feature is very mouse and menu oriented, which means it is fast but occasionally aggravating. A free alternative image analysis program for the Macintosh is NIH Image. Both IPLab and Image can use Photoshop plug-ins for image acquisition, which means most hardware is supported.

Calculations. Mathematica 2.2.2 was used for symbolic computations and a combination of Mathematica, Excel, KaleidaGraph and Statview for numerical computations. Statview is inflexible and often useless; many computations required extensive exporting and reimporting of data to make up for its lack of relational capabilities. Most statistical tests such as p-values were, in the end, computed in Mathematica.

Thesis Notes

This thesis was typeset in Donald Knuth's computer modern family using the LaTeX typesetting system. The document style is vanilla AMS-book format. Textures, a fast and beautiful implementation of TeX, was used for compiling the LaTeX code, previewing, and printing. All writing was done with Pete Keleher's great shareware editor Alpha. Alpha lets you rebind any keystroke to any command, comes work-saving LaTeX macros, and much more. Line drawings were made in Canvas 3.5; EndNote was used for managing references.

Text munging (such as rearranging data for Statview or bludgeoning EndNote and LaTeX to work together) was performed with Larry Wall and Matthias Neeracher's MacPerl. The index was produced with MakeIndex and LaTeX.

This thesis was written on an Apple Power Macintosh 8500. Black and white pages were printed on a Hewlett-Packard LaserJet 5MP printer on Xerox Image Elite and Hammermill Bond papers. Black and white and color photographs were RIPed on a Fiery ColorPass 4000+ processor for printing on a Canon Color Laser Copier model CLC 700.

Supplier Information

Suppliers of software and other items used in the thesis can be contacted as follows:

Supplier	Product	Phone #	Web address
Abacus Concepts	Statview	510-540-1949	www.statview.com
Adobe	Photoshop	800-833-6687	www.adobe.com
Alpha CD Imaging	Kodak PhotoCD	650-325-4877	www.alphacd.com
Apple Computer	Macintoshes	800-795-1000	www.apple.com
Bicron (Harshaw)	silver chloride	800-472-5656	www.bicron.com
Blue Sky Research	Textures	800-622-8398	www.bluesky.com
Dage-MTI	CCD-72 camera		(various suppliers)
ESPI	tungsten sheet	800-638-2581	www.jeffnet.org/espi
Iomega	Zip disks		www.iomega.com
Mo-Sci	glass microspheres	573-364-2338	
National Instruments	LabVIEW	800-433-3488	www.labview.com
Niles & Associates	EndNote	510-559-8592	www.niles.com
Perceptics	Frame grabber	423-966-9200	www.perceptics.com
Pete Keleher	Alpha (editor)		www.cs.umd.edu/~keleher/alpha
Quartz Plus	quartz tubing	508-371-1715	
Signal Analytics	IPLab	703-208-2230	www.iplab.com
Strem Chemical	cuprous chloride	508-462-3191	
Synergy Software	Kaleidagraph	610-779-0522	www.synergy.com
Wall/Neeracher	MacPerl		www.perl.org
Wolfram Research	Mathematica	800-965-3726	www.wri.com
Wok 'N Roll	Chinese take-out	617-497-8638	
Carl Zeiss	Microscope	800-233-2343	www.zeiss.com

Index